

Pathologies of the Large- N Limit for RP^{N-1} , CP^{N-1} , QP^{N-1} and Mixed Isovector/Isotensor σ -Models

Alan D. Sokal
Andrei O. Starinets
Department of Physics
New York University
4 Washington Place
New York, NY 10003 USA

Internet: SOKAL@NYU.EDU, AOS2839@SCIRES.NYU.EDU

November 6, 2000

Abstract

We compute the phase diagram in the $N \rightarrow \infty$ limit for lattice RP^{N-1} , CP^{N-1} and QP^{N-1} σ -models with the quartic action, and more generally for mixed isovector/isotensor models. We show that the $N = \infty$ limit exhibits phase transitions that are forbidden for any finite N . We clarify the origin of these pathologies by examining the exact solution of the one-dimensional model: we find that there are complex zeros of the partition function that tend to the real axis as $N \rightarrow \infty$. We conjecture the correct phase diagram for finite N as a function of the spatial dimension d . Along the way, we prove some new correlation inequalities for a class of N -component σ -models, and we obtain some new results concerning the complex zeros of confluent hypergeometric functions.

PACS CODES: 11.15.Pg, 02.30.Gp, 05.50.+q, 11.10.Kk, 11.15.Ex, 64.60.Cn, 64.70.Md, 75.10.Hk.

KEY WORDS: RP^{N-1} model; CP^{N-1} model; QP^{N-1} model; N -vector model; mixed isovector/isotensor model; nonlinear σ -model; nematic liquid crystal; $N \rightarrow \infty$ limit; $1/N$ expansion; confluent hypergeometric function; correlation inequalities.

Contents

1	Introduction	3
2	$N \rightarrow \infty$ Limit for Mixed Isovector/Isotensor Models: General Theory	5
3	$N \rightarrow \infty$ Limit for Mixed Isovector/Isotensor Models: Translation-Invariant Case	9
3.1	Basic Definitions	9
3.2	Direct Approach	10
3.3	Parametric Approach	13
4	Behavior of Solutions for $\tilde{\beta}_V = 0$	15
4.1	Overview	15
4.2	Direct Approach	15
4.3	Parametric Approach	18
4.4	One-Dimensional Case	21
5	Behavior of Solutions for $\tilde{\beta}_V \neq 0$	22
5.1	Overview	22
5.2	Direct Approach	23
5.3	Parametric Approach	23
5.4	One-Dimensional Case	27
6	One-Dimensional Case: Pure RP^{N-1}, CP^{N-1} and QP^{N-1} Models	28
6.1	General N	29
6.2	$N \rightarrow \infty$ Limit	31
7	One-Dimensional Case: Mixed Isovector/Isotensor Models	31
7.1	General N	32
7.2	$N \rightarrow \infty$ Limit in Mixed Models with Various Scalings	34
8	Conclusions	35
A	The Lattice Propagator and Free Energy	38
A.1	Formulae	38
A.2	Numerical Calculation of $f_d(\gamma)$ and its Derivatives	42
B	Confluent Hypergeometric Function ${}_1F_1(a; b; b\xi)$ in the Limit $b \rightarrow \infty$	44
B.1	Asymptotic Expansion in Powers of $1/b$ at Fixed ξ	44
B.2	Complex Zeros of ${}_1F_1(a; b; b\xi)$ as $b \rightarrow \infty$	47
B.3	Asymptotic Expansion when $\xi = 1 + b^{-1/2}\zeta$	49
C	Correlation Inequalities	50
C.1	Tools #1: Griffiths Inequalities for the Ising Model	51
C.2	Tools #2: Ginibre Inequalities for the XY Model	51
C.3	Correlation Inequalities for S^{N-1} σ -Models	52

1 Introduction

Over the past decade there has been much interest in two-dimensional lattice σ -models taking values in the real projective space RP^{N-1} [1, 2, 3, 4, 5, 6, 7, 8, 9, 10, 11, 12, 13, 14, 15, 16], the complex projective space CP^{N-1} [1, 17, 4, 18, 19, 20, 21, 22, 23, 24] or the quaternionic projective space QP^{N-1} [25].¹ These models are good laboratories for investigating asymptotic freedom, topological phenomena and universality; they are intermediate in complexity between two-dimensional N -vector models (σ -models taking values in the sphere S^{N-1}) and four-dimensional non-abelian gauge theories.²

In three dimensions, the RP^2 lattice theory has long been employed as a model of nematic liquid crystals [32, 33, 34]. In addition, a mixed isovector/isotensor model generalizing the RP^2 theory has been proposed as a model of orientational transitions in crystals [35] and of uniaxial liquid crystals exhibiting various kinds of head-tail asymmetry [36, 37, 38]; and a mixed isovector/isotensor model generalizing the RP^{N-1} theory arose in a study of N -component ferromagnets with annealed random couplings [39, 40].

The $N \rightarrow \infty$ limit of the RP^{N-1} and CP^{N-1} σ -models has been studied by several groups [1, 17, 2, 4, 3, 7]; and Oku and Abe [39, 40], Magnoli and Ravanini [2] and Ohno *et al.* [3] have studied the $N \rightarrow \infty$ limit of a mixed isovector/isotensor model that generalizes the RP^{N-1} model.³ The result (in lattice dimension $d = 2$) is that there is a first-order phase transition in the RP^{N-1} and CP^{N-1} models at $\tilde{\beta}_c \approx 0.956$. The question is whether the phase transition observed *at* $N = \infty$ occurs also at large but finite N .

The $N = \infty$ phase transition of the RP^{N-1} and CP^{N-1} models has two curious features [17, 41, 3]:

- (a) It occurs in all lattice dimensions, including $d = 1$. Indeed, it occurs even for a lattice consisting of only two sites! (However, in dimension $d \leq 3/2$ the transition is second-order rather than first-order [3].)
- (b) It is associated with the spontaneous breaking of the Z_2 or $U(1)$ local gauge invariance. That is, in the mixed isovector/isotensor model for $\tilde{\beta}_T > \tilde{\beta}_c$, the free energy has *unequal* left and right derivatives with respect to $\tilde{\beta}_V$ at $\tilde{\beta}_V = 0$. (Equivalently, the isovector energy E_V is a discontinuous function of $\tilde{\beta}_V$ at $\tilde{\beta}_V = 0$.)

Both of these features are, however, rigorously forbidden at finite N : in any short-range one-dimensional model (and of course on a finite lattice), the free energy and all expectation values are real-analytic functions of the parameters in the Hamiltonian⁴; and spontaneous

¹ There is also, of course, an enormous literature on the continuum versions of these models, which we refrain from citing. Our point of view is that the continuum model can be given a *meaning* only by defining it properly as a continuum limit of ultraviolet-cutoff models (such as lattice models); and in order to define such a continuum limit, one must first investigate the phase diagram of the cutoff models and search for critical points.

² These models are also good laboratories for the development and application of new collective-mode Monte Carlo algorithms, such as multigrid [26, 18, 27] and cluster algorithms [28, 29, 30, 9, 31].

³ We have also profited from consulting an unpublished manuscript on this problem that Sergio Caracciolo and Andrea Pelissetto have kindly shared with us [12].

⁴ See [42, 43] and [44, Theorem II.5.3 and Remark 1 following it].

breaking of a local gauge symmetry cannot occur under any conditions [45]. Thus, it seems unlikely that such a transition can survive to finite N .

In this paper we propose to clarify this behavior, by comparing to the exact solution in the one-dimensional case.⁵ We shall see that, in $d = 1$, the phase transitions in the RP^{N-1} , CP^{N-1} and QP^{N-1} models (and more generally in the mixed isovector/isotensor model) are artifacts of the $N \rightarrow \infty$ limit, arising from complex zeros of the partition function that tend to the real axis as $N \rightarrow \infty$. There is no phase transition for any finite N .⁶ We conjecture that the same is true in all lattice dimensions $d \leq 2$.

By contrast, in dimension $d > 2$ there is a transition from the isotropic phase to a phase with nematic long-range order [52, 53, 54]; this transition is expected to be first-order for all $N > 2$ [34, 55, 56]. In this paper we shall compute the location and properties of this transition in the $N \rightarrow \infty$ limit.

The RP^{N-1} , CP^{N-1} and QP^{N-1} models to be considered here are defined by the lattice Hamiltonian

$$H = -\frac{\beta}{2} \sum_{\langle xy \rangle} |\boldsymbol{\sigma}_x^* \cdot \boldsymbol{\sigma}_y|^2, \quad (1.1)$$

where the sum runs over all nearest-neighbor pairs $\langle xy \rangle$ (each pair counted once), and each spin $\boldsymbol{\sigma}_x$ is a unit vector in \mathbb{R}^N , \mathbb{C}^N or \mathbb{Q}^N , respectively (in the real case, the complex conjugation and absolute value are of course redundant). The *a priori* measure for each spin $\boldsymbol{\sigma}_x$ is normalized uniform measure on the appropriate unit sphere, which we shall denote $d\Omega(\boldsymbol{\sigma}_x)$. This model has a global symmetry group $G = O(N)$, $U(N)$ or $U(N, \mathbb{Q})$ as well as a local gauge group $G_{loc} = Z_2$, $U(1)$ or $U(1, \mathbb{Q})$ [$\simeq SU(2)$]. In order to treat all three cases in parallel, it is convenient to write $\mathbb{K} = \mathbb{R}$, \mathbb{C} or \mathbb{Q} , with corresponding real dimension $k = 1$, 2 or 4.

More generally, we shall consider the mixed isovector/isotensor model defined by the Hamiltonian

$$H = -\sum_{\langle xy \rangle} \left[\beta_V \boldsymbol{\sigma}_x \cdot \boldsymbol{\sigma}_y + \frac{\beta_T}{2} (\boldsymbol{\sigma}_x \cdot \boldsymbol{\sigma}_y)^2 \right], \quad (1.2)$$

where each spin $\boldsymbol{\sigma}_x$ is a unit vector in \mathbb{R}^N . The pure RP^{N-1} model corresponds to $\beta_V = 0$. We shall restrict attention to the case $\beta_T \geq 0$. For simplicity, we refrain from considering in this paper the mixed models based on CP^{N-1} and QP^{N-1} . The central goal of this paper is to compute the phase diagram of the model (1.2) in the $N \rightarrow \infty$ limit — it turns out to be surprisingly intricate and dimension-dependent — and to discuss how much of this phase diagram should be expected to survive to finite N .

⁵ The one-dimensional RP^{N-1} and mixed isovector/isotensor models have been studied previously by Liu and Joseph [46], Thorpe and Blume [47], Kohring and Shrock [34], Cucchieri *et al.* [48], Seiler and Yildirim [49], and Hasenbusch and Horgan [50].

⁶ This phenomenon, in which a phase transition that is forbidden for all finite N nevertheless occurs at $N = \infty$, was observed nearly two decades ago by Celmaster and Green [51]. They noted that the one-dimensional $SU(N)$ and $U(N)$ principal chiral models at $N = \infty$ show spontaneous breaking of a continuous global symmetry, and that the two-dimensional $SU(N)$ and $U(N)$ lattice gauge theories at $N = \infty$ show spontaneous breaking of the local gauge symmetry — transitions that are of course forbidden at finite N . They concluded that these examples “illustrate the possible pitfalls of investigating symmetry breaking at $N \rightarrow \infty$.”

The plan of this paper is as follows: In Section 2 we show how to obtain the $N \rightarrow \infty$ limit (and the $1/N$ expansion) for the mixed isovector/isotensor model (1.2), paying particular attention to conceptual questions (the order of integration, how to determine which saddle point is dominant, ...). In Section 3 we specialize to the translation-invariant nearest-neighbor case, and give two complementary methods for computing the $N \rightarrow \infty$ limit: a direct method and a parametric method. In Sections 4 and 5 we carry out these calculations in detail for $\beta_V = 0$ and $\beta_V \neq 0$, respectively; our main goal is to determine the phase diagram in the (β_V, β_T) -plane as a function of the spatial dimension d (which we treat as a continuous variable). Some of the results in these sections are known from previous work [2, 3], but most of them are new. In Sections 6 and 7 we solve the one-dimensional model and extract the $N \rightarrow \infty$ limit; we clarify the origin of the phase transition at $N = \infty$, and explain why it does *not* occur for any finite N . In Section 8 we draw some conclusions, and conjecture the phase diagram in the (β_V, β_T) -plane for finite N . In Appendix A we collect some formulae concerning the lattice propagator and free energy in general dimension d . In Appendix B we prove some asymptotic expansions for confluent hypergeometric functions and their zeros; these appear to be new. In Appendix C we prove some new correlation inequalities for a class of N -component σ -models that includes the mixed isovector/isotensor model.

2 $N \rightarrow \infty$ Limit for Mixed Isovector/Isotensor Models: General Theory

Let us begin by considering the mixed isovector/isotensor model on an arbitrary *finite* lattice \mathcal{L} having V sites. The Hamiltonian is

$$H = - \sum_{\langle xy \rangle} \left[J_{xy} \boldsymbol{\sigma}_x \cdot \boldsymbol{\sigma}_y + \frac{K_{xy}}{2} (\boldsymbol{\sigma}_x \cdot \boldsymbol{\sigma}_y)^2 \right], \quad (2.1)$$

where the sum runs over all unordered pairs $\langle xy \rangle$ of sites in \mathcal{L} (each pair counted once). We shall assume that $K_{xy} = K_{yx} \geq 0$, while $J_{xy} = J_{yx}$ may have either sign. Without loss of generality we assume $J_{xx} = K_{xx} = 0$. The *a priori* measure for each spin $\boldsymbol{\sigma}_x$ is normalized uniform measure on the unit sphere in \mathbb{R}^N :

$$d\Omega(\boldsymbol{\sigma}_x) = \frac{\Gamma(N/2)}{\pi^{N/2}} \delta(\boldsymbol{\sigma}_x^2 - 1) d^N \boldsymbol{\sigma}_x. \quad (2.2)$$

The partition function is therefore

$$Z = \left(\frac{\Gamma(N/2)}{\pi^{N/2}} \right)^V \int \exp \left\{ \sum_{\langle xy \rangle} \left[J_{xy} \boldsymbol{\sigma}_x \cdot \boldsymbol{\sigma}_y + \frac{K_{xy}}{2} (\boldsymbol{\sigma}_x \cdot \boldsymbol{\sigma}_y)^2 \right] \right\} \prod_x \delta(\boldsymbol{\sigma}_x^2 - 1) d^N \boldsymbol{\sigma}_x. \quad (2.3)$$

Our main goal is to compute the leading term in the large- N expansion of the free energy $-\log Z$, namely the limiting free energy per component

$$F = - \lim_{N \rightarrow \infty} \frac{1}{N} \log Z. \quad (2.4)$$

We also want to compute the leading term in the large- N expansion of the n -point correlation functions $\langle \sigma_{x_1}^{(\alpha_1)} \cdots \sigma_{x_n}^{(\alpha_n)} \rangle$, the most important of which are the isovector and isotensor correlation functions

$$G_V(x, y) = \langle \boldsymbol{\sigma}_x \cdot \boldsymbol{\sigma}_y \rangle \quad (2.5)$$

$$\begin{aligned} G_T(x, y) &= \langle \mathbf{T}_x \cdot \mathbf{T}_y \rangle \equiv \sum_{\alpha, \beta=1}^N \langle T_x^{(\alpha\beta)} T_y^{(\alpha\beta)} \rangle \\ &= \langle (\boldsymbol{\sigma}_x \cdot \boldsymbol{\sigma}_y)^2 \rangle - \frac{1}{N} \end{aligned} \quad (2.6)$$

where we have defined the symmetric traceless isotensor field

$$T_x^{(\alpha\beta)} = \sigma_x^{(\alpha)} \sigma_x^{(\beta)} - \frac{1}{N} \delta^{\alpha\beta}. \quad (2.7)$$

We begin by introducing auxiliary variables μ_{xy} so as to ‘‘Gaussianize’’ the isotensor part of the Boltzmann weight:

$$\exp \left[\frac{K_{xy}}{2} (\boldsymbol{\sigma}_x \cdot \boldsymbol{\sigma}_y)^2 \right] = (2\pi K_{xy})^{-1/2} \int_{-\infty}^{\infty} \exp \left[-\frac{\mu_{xy}^2}{2K_{xy}} + \mu_{xy} \boldsymbol{\sigma}_x \cdot \boldsymbol{\sigma}_y \right] d\mu_{xy}. \quad (2.8)$$

[When $K_{xy} = 0$, the Gaussian $(2\pi K_{xy})^{-1/2} \exp[-\mu_{xy}^2/2K_{xy}]$ is of course interpreted as $\delta(\mu_{xy})$.] It follows that the partition function (2.3) of the mixed isovector/isotensor model can be rewritten as that of a pure N -vector model with annealed random couplings $J_{xy} + \mu_{xy}$, where the μ_{xy} are Gaussian-distributed with mean zero and variance K_{xy} .⁷

Next we introduce auxiliary variables $\{\alpha_x\}$ in the standard way to ‘‘Gaussianize’’ the *a priori* measure:

$$\delta(\boldsymbol{\sigma}_x^2 - 1) = \frac{1}{2\pi i} \int_{c_x - i\infty}^{c_x + i\infty} e^{-\alpha_x (\boldsymbol{\sigma}_x^2 - 1)} d\alpha_x \quad (2.9)$$

where $c_x = c_x(\{\mu\})$ is a real constant chosen large enough to make the integral over $\{\boldsymbol{\sigma}\}$ absolutely convergent. We then get

$$\begin{aligned} Z &= \left(\frac{1}{2\pi i} \right)^V \left(\frac{\Gamma(N/2)}{\pi^{N/2}} \right)^V \int_{-\infty}^{\infty} \prod_{\langle xy \rangle} (2\pi K_{xy})^{-1/2} d\mu_{xy} \int_{c_x - i\infty}^{c_x + i\infty} \prod_x d\alpha_x \int_{\mathbb{R}^N} \prod_x d^N \boldsymbol{\sigma}_x \\ &\quad \exp \left[\sum_x \alpha_x - \sum_{\langle xy \rangle} \frac{\mu_{xy}^2}{2K_{xy}} - \frac{1}{2} (\boldsymbol{\sigma}, B\boldsymbol{\sigma}) \right] \end{aligned} \quad (2.10)$$

where

$$B_{xy} = 2\alpha_x \delta_{xy} - (J_{xy} + \mu_{xy}). \quad (2.11)$$

⁷ This equivalence was noted almost two decades ago by Oku and Abe [39], who started from the N -vector model with annealed random couplings and showed its equivalence with the mixed isovector/isotensor model (1.2).

Note that the order of integration here is crucial, as the $\{c_x\}$ must be chosen in a $\{\mu\}$ -dependent way so that $\text{Re } B$ is positive definite.

We can now perform the Gaussian integral over $\{\sigma\}$. For convenience let us introduce new variables $\tilde{J}_{xy} = J_{xy}/N$, $\tilde{K}_{xy} = K_{xy}/N$, $\tilde{\mu}_{xy} = \mu_{xy}/N$, $\tilde{\alpha}_x = \alpha_x/N$ and hence $\tilde{B}_{xy} = B_{xy}/N$. We get

$$Z = \left(\frac{N}{2\pi i}\right)^V \left(\frac{\Gamma(N/2)}{\pi^{N/2}} e^{N/2}\right)^V \left(\frac{2\pi}{N}\right)^{NV/2} \int_{-\infty}^{\infty} \prod_{\langle xy \rangle} \left(\frac{N}{2\pi \tilde{K}_{xy}}\right)^{1/2} d\tilde{\mu}_{xy} \int_{\tilde{c}_x - i\infty}^{\tilde{c}_x + i\infty} \prod_x d\tilde{\alpha}_x \exp[-N\mathcal{F}(\tilde{\mu}, \tilde{\alpha})] \quad (2.12)$$

where

$$\mathcal{F}(\tilde{\mu}, \tilde{\alpha}) = -\sum_x \tilde{\alpha}_x + \sum_{\langle xy \rangle} \frac{\tilde{\mu}_{xy}^2}{2\tilde{K}_{xy}} + \frac{1}{2} \text{tr} \log \tilde{B} + \frac{V}{2}. \quad (2.13)$$

Let us now perform the $\{\tilde{\alpha}\}$ integrals by the saddle-point method. The saddle-point equations are

$$\frac{\partial \mathcal{F}}{\partial \tilde{\alpha}_x} = (\tilde{B}^{-1})_{xx} - 1 = 0 \quad \text{for all } x. \quad (2.14)$$

It can be proven [57] that there exists a unique *real* saddle point $\tilde{\alpha}_* = \tilde{\alpha}_*(\tilde{\mu})$ in the region where \tilde{B} is positive-definite; we conjecture (but have not proven) that this is the *only* saddle point, real or complex, in the region where $\text{Re } \tilde{B}$ is positive-definite. For the purposes of calculating the leading $N \rightarrow \infty$ contribution, it suffices to replace $\tilde{\alpha}$ by its saddle-point value⁸:

$$\hat{\mathcal{F}}(\tilde{\mu}) \equiv \mathcal{F}(\tilde{\mu}, \tilde{\alpha}_*(\tilde{\mu})). \quad (2.15)$$

We then perform the integral over $\{\tilde{\mu}\}$ by Laplace's method: it is dominated by the configuration(s) of $\{\tilde{\mu}\}$ that make $\hat{\mathcal{F}}(\tilde{\mu})$ an absolute minimum, and so we have

$$F = \inf_{\{\tilde{\mu}\}} \hat{\mathcal{F}}(\tilde{\mu}) \quad (2.16)$$

(the prefactors cancel to leading order).

The stationary points of $\hat{\mathcal{F}}(\tilde{\mu})$ are given by

$$\frac{\partial \hat{\mathcal{F}}}{\partial \tilde{\mu}_{xy}} = \frac{\partial \mathcal{F}}{\partial \tilde{\mu}_{xy}} \Big|_{\tilde{\alpha}=\tilde{\alpha}_*(\tilde{\mu})} = \frac{\tilde{\mu}_{xy}}{\tilde{K}_{xy}} - (\tilde{B}^{-1})_{xy} = 0 \quad \text{for all } x, y. \quad (2.17)$$

In general, $\hat{\mathcal{F}}$ has *many* stationary points. Indeed, for a pure RP^{N-1} model ($J \equiv 0$), any gauge transform $\tilde{\mu}_{xy} \rightarrow \eta_x \eta_y \tilde{\mu}_{xy}$ ($\eta = \pm 1$) of a stationary point is also a stationary point with the same value of \mathcal{F} , so in particular there are many degenerate absolute minima. If $J_{xy} \neq 0$, there is no longer a gauge invariance, but at least for small J_{xy} all of the foregoing stationary points survive (and move slightly). We conjecture that if $J_{xy} \geq 0$ for all x, y ("ferromagnetism"), then one of the absolute minima has $\tilde{\mu}_{xy} \geq 0$ for all x, y , and moreover

⁸ In principle one should prove that the limit $N \rightarrow \infty$ and the integration over $\{\tilde{\mu}\}$ can be interchanged. Unfortunately, we have no rigorous proof, though it seems eminently reasonable.

there is a unique absolute minimum with this property; but we have, as yet, no proof. Let us also remark that if $J \equiv 0$, then $\tilde{\mu} \equiv 0$ is always a stationary point (with $\tilde{\alpha}_{*x} = \frac{1}{2}$ for all x), but this is the dominant saddle point only for K sufficiently small (see Section 4.2).

By expanding (2.12)/(2.13) around the saddle point, one can obtain a systematic expansion in powers of $1/N$. Examination of this expansion could potentially shed alternative light on the reliability of the large- N limit; but we shall not pursue this approach here.

The saddle-point method also provides a $1/N$ expansion of the correlation functions. At leading order in $1/N$, the fields $\boldsymbol{\sigma} = \{\sigma_x^{(\alpha)}\}_{x \in \mathcal{L}, 1 \leq \alpha \leq N}$ are Gaussian with mean zero and covariance matrix

$$\langle \sigma_x^{(\alpha)} \sigma_y^{(\beta)} \rangle = \frac{\delta^{\alpha\beta}}{N} \left[(\tilde{B}_*^{-1})_{xy} + O(1/N) \right] \quad (2.18)$$

where

$$\tilde{B}_{*xy} = 2\tilde{\alpha}_{*x}\delta_{xy} - (\tilde{J}_{xy} + \tilde{\mu}_{xy}) . \quad (2.19)$$

Thus,

$$G_V(x, y) \equiv \langle \boldsymbol{\sigma}_x \cdot \boldsymbol{\sigma}_y \rangle = (\tilde{B}_*^{-1})_{xy} + O(1/N) , \quad (2.20)$$

where the saddle-point equation (2.14) ensures consistency when $x = y$ (since $\boldsymbol{\sigma}_x \cdot \boldsymbol{\sigma}_x = 1$). Moreover, higher-point correlation functions are given by sums of products of \tilde{B}_*^{-1} : for example,

$$\langle \sigma_{x_1}^{(\alpha_1)} \sigma_{x_2}^{(\alpha_2)} \sigma_{x_3}^{(\alpha_3)} \sigma_{x_4}^{(\alpha_4)} \rangle = \frac{\delta^{\alpha_1\alpha_2} \delta^{\alpha_3\alpha_4}}{N^2} (\tilde{B}_*^{-1})_{x_1x_2} (\tilde{B}_*^{-1})_{x_3x_4} + \text{two permutations} + O(1/N) \quad (2.21)$$

and likewise for all $2n$ -point correlation functions. One useful consequence is that, to leading order in $1/N$, correlations involving products of $O(N)$ -invariant combinations *factorize* [58]:

$$\left\langle \prod_{i=1}^n \boldsymbol{\sigma}_{x_i} \cdot \boldsymbol{\sigma}_{y_i} \right\rangle = \prod_{i=1}^n \langle \boldsymbol{\sigma}_{x_i} \cdot \boldsymbol{\sigma}_{y_i} \rangle + O(1/N) . \quad (2.22)$$

In particular,

$$G_T(x, y) \equiv \langle (\boldsymbol{\sigma}_x \cdot \boldsymbol{\sigma}_y)^2 \rangle - \frac{1}{N} = (\tilde{B}_*^{-1})_{xy}^2 + O(1/N) . \quad (2.23)$$

For the pure RP^{N-1} model, the factorization (2.22) should be understood as applying to the symmetry-broken measure $\langle \cdot \rangle_{SB}$ obtained by letting $\tilde{\beta}_V \downarrow 0$. Alternatively, for Z_2 -gauge-invariant correlations — that is, those for which each lattice site occurs an *even* number of times in the sequence $x_1, \dots, x_n, y_1, \dots, y_n$ — we have (to leading order in $1/N$)

$$\left\langle \prod_{i=1}^n \boldsymbol{\sigma}_{x_i} \cdot \boldsymbol{\sigma}_{y_i} \right\rangle = \prod_{i=1}^n \langle \boldsymbol{\sigma}_{x_i} \cdot \boldsymbol{\sigma}_{y_i} \rangle_{SB} = \prod_{i=1}^n \langle (\boldsymbol{\sigma}_{x_i} \cdot \boldsymbol{\sigma}_{y_i})^2 \rangle^{1/2} , \quad (2.24)$$

where $\langle \cdot \rangle$ denotes expectation in the Z_2 -gauge-invariant Gibbs measure.

3 $N \rightarrow \infty$ Limit for Mixed Isovector/Isotensor Models: Translation-Invariant Case

3.1 Basic Definitions

Let us now restrict attention to the case where \mathcal{L} is a d -dimensional cube of side L with periodic boundary conditions, and the couplings are translation-invariant and nearest-neighbor: $J_{xy} = \tilde{\beta}_V \delta_{xy}^{\text{NN}}$, $K_{xy} = \tilde{\beta}_T \delta_{xy}^{\text{NN}}$ with $\tilde{\beta}_T > 0$. Let us also restrict attention to solutions for $\{\tilde{\alpha}\}$ and $\{\tilde{\mu}\}$ that are translation-invariant and for which $\tilde{\mu}$ is the same in all lattice directions. (In principle we should *prove* that these are the dominant saddle points; but since we are unable to do so, we shall simply *assume* that they are, like all previous workers!) We thus have

$$\tilde{B}_{xy} = 2\tilde{\alpha}\delta_{xy} - (\tilde{\beta}_V + \tilde{\mu})\delta_{xy}^{\text{NN}}, \quad (3.1)$$

or in Fourier space

$$\tilde{B}(p) = 2\tilde{\alpha} \left[1 - \gamma \sum_{i=1}^d \cos p_i \right] \quad (3.2)$$

where

$$\gamma \equiv \frac{\tilde{\beta}_V + \tilde{\mu}}{\tilde{\alpha}}. \quad (3.3)$$

Let us introduce the fundamental quantities

$$f_{d,L}(\gamma) = L^{-d} \sum_p \left[1 - \gamma \sum_{i=1}^d \cos p_i \right]^{-1} \quad (3.4)$$

$$g_{d,L}(\gamma) = L^{-d} \sum_p \log \left[1 - \gamma \sum_{i=1}^d \cos p_i \right] \quad (3.5)$$

where the sum runs over momenta with components $p_i = 2\pi k_i/L$ ($k_i = 0, 1, \dots, L-1$). These quantities are well-defined for $|\gamma| < 1/d$; they are strictly increasing functions of $|\gamma|$, and diverge as $|\gamma| \uparrow 1/d$. They satisfy

$$\frac{dg_{d,L}(\gamma)}{d\gamma} = -\frac{f_{d,L}(\gamma) - 1}{\gamma}. \quad (3.6)$$

We then have

$$(\tilde{B}^{-1})_{xx} = \frac{1}{2\tilde{\alpha}} f_{d,L}(\gamma) \quad (3.7a)$$

$$(\tilde{B}^{-1})_{xy} = \frac{1}{2d\tilde{\alpha}\gamma} [f_{d,L}(\gamma) - 1] \quad \text{for } |x - y| = 1 \quad (3.7b)$$

where of course the right-hand side of (3.7b) must be interpreted as zero when $\gamma = 0$. After passing to the infinite-volume limit, the correlation function $(\tilde{B}^{-1})_{xy}$ exhibits exponential decay

$$(\tilde{B}^{-1})_{xy} \sim e^{-m|x-y|} \quad \text{as } |x - y| \rightarrow \infty \quad (3.8)$$

with mass gap

$$m = \operatorname{arccosh} \left[\frac{1}{\gamma} - (d-1) \right]. \quad (3.9)$$

Our goal is to compute the free energy per unit volume

$$\bar{F} \equiv L^{-d} F \quad (3.10)$$

in the infinite-volume limit $L \rightarrow \infty$. We shall do this in two ways: a direct approach (Section 3.2) and a parametric approach (Section 3.3). These two approaches have complementary advantages, and together they give added insight into the phase diagram. The parametric approach has been used previously by Magnoli and Ravanini [2], while the direct approach appears to be new.

3.2 Direct Approach

We implement the method set forth in Section 2: namely, we compute the function $\widehat{\mathcal{F}}(\tilde{\mu}) \equiv \mathcal{F}(\tilde{\mu}, \tilde{\alpha}_*(\tilde{\mu}))$ and then find its absolute minimum. The first step is to fix $\tilde{\mu}$ and solve the saddle-point equation (2.14) for $\tilde{\alpha}$: from (3.7a) we have

$$2\tilde{\alpha}_* = f_{d,L}(\gamma_*) \equiv f_{d,L} \left(\frac{\tilde{\beta}_V + \tilde{\mu}}{\tilde{\alpha}_*} \right). \quad (3.11)$$

It is not hard to see that γ_* goes monotonically from $-1/d$ to $1/d$ as $\tilde{\mu}$ goes from $-\infty$ to ∞ .⁹ So we can use γ_* (henceforth denoted simply by γ) as an independent variable in place of $\tilde{\mu}$. The free energy per unit volume $\overline{\mathcal{F}}(\tilde{\mu}) \equiv L^{-d} \widehat{\mathcal{F}}(\tilde{\mu})$, written as a function of γ , is

$$\overline{\mathcal{F}}(\gamma) = \frac{1}{2} \left[1 - f_{d,L}(\gamma) + \frac{d}{\tilde{\beta}_T} \left(\frac{\gamma f_{d,L}(\gamma)}{2} - \tilde{\beta}_V \right)^2 + \log f_{d,L}(\gamma) + g_{d,L}(\gamma) \right]. \quad (3.12)$$

Let us write it as

$$\overline{\mathcal{F}}(\gamma) = \mathcal{F}_0(\gamma) + \tilde{\beta}_V \mathcal{F}_1(\gamma) + \frac{d}{2\tilde{\beta}_T} \tilde{\beta}_V^2, \quad (3.13)$$

where $\mathcal{F}_0(\gamma)$ [resp. $\mathcal{F}_1(\gamma)$] is an even (resp. odd) function of γ :

$$\mathcal{F}_0(\gamma) = \frac{1}{2} \left[1 - f_{d,L}(\gamma) + \frac{d}{4\tilde{\beta}_T} \gamma^2 f_{d,L}(\gamma)^2 + \log f_{d,L}(\gamma) + g_{d,L}(\gamma) \right] \quad (3.14)$$

$$\mathcal{F}_1(\gamma) = -\frac{d}{2\tilde{\beta}_T} \gamma f_{d,L}(\gamma) \quad (3.15)$$

The free energy per unit volume is then

$$\bar{F} = \inf_{\gamma} \overline{\mathcal{F}}(\gamma). \quad (3.16)$$

⁹ This is easiest seen in reverse: write $\tilde{\mu} = \frac{1}{2}\gamma_* f_{d,L}(\gamma_*) - \tilde{\beta}_V$. It follows from the properties of $f_{d,L}$ that $\tilde{\mu}$ goes monotonically from $-\infty$ to ∞ as γ_* goes from $-1/d$ to $1/d$.

Since $\mathcal{F}_1(\gamma)/\gamma < 0$ for all γ , it follows that when $\tilde{\beta}_V > 0$ (resp. $\tilde{\beta}_V < 0$) the absolute minimum of $\bar{\mathcal{F}}$ lies at $\gamma > 0$ (resp. $\gamma < 0$). Of course, when $\tilde{\beta}_V = 0$, $\bar{\mathcal{F}}$ is an even function of γ , so the sign of γ is irrelevant.

Note also that $f_{d,L}(\gamma)$ goes monotonically from 1 to $+\infty$ as $|\gamma|$ goes from 0 to $1/d$. So we can use $f \equiv f_{d,L}(\gamma)$ and $\text{sgn } \gamma$ as independent variables in place of γ , if we prefer. As we shall see, this is sometimes convenient.

Note, finally, that we can read off from the $\tilde{\beta}_V = 0$ solution the qualitative behavior of the free energy for small but nonzero $\tilde{\beta}_V$. Indeed, suppose that the absolute minima of $\mathcal{F}_0(\gamma)$ lie at $\pm\gamma_1, \dots, \pm\gamma_n$, with common minimum value $\mathcal{F}_0(\pm\gamma_i) = \bar{F}_0$. Then, for small $\tilde{\beta}_V$, we have from (3.13)

$$\bar{F} \equiv \inf_{\gamma} \bar{\mathcal{F}}(\gamma) = \bar{F}_0 - |\tilde{\beta}_V| \max_{1 \leq i \leq n} |\mathcal{F}_1(\gamma_i)| + O(\tilde{\beta}_V^2). \quad (3.17)$$

Thus, if the unique absolute minimum of $\mathcal{F}_0(\gamma)$ lies at $\gamma = 0$, we have $\bar{F} = \bar{F}_0 + O(\tilde{\beta}_V^2)$; but if there is any absolute minimum of $\mathcal{F}_0(\gamma)$ at $\gamma \neq 0$, we have $\bar{F} = \bar{F}_0 - O(|\tilde{\beta}_V|)$ and hence a first-order phase transition as $\tilde{\beta}_V$ passes through 0. Surprisingly, this happens even in finite volume ($L < \infty$). Note also that the isovector energy $E_V \sim \partial \bar{F} / \partial \tilde{\beta}_V$ is discontinuous at such a first-order transition, indicating that the Z_2 gauge invariance of the $\tilde{\beta}_V = 0$ theory is spontaneously broken. Both these features are manifestly artifacts of the $N \rightarrow \infty$ limit, as they are rigorously forbidden at any finite N .

Let us now consider the infinite-volume limit $L \rightarrow \infty$. *Formally* we can pass to the infinite-volume limit in (3.4) and (3.5), yielding

$$f_d(\gamma) \equiv \lim_{L \rightarrow \infty} f_{d,L}(\gamma) = \int \frac{d^d p}{(2\pi)^d} \left[1 - \gamma \sum_{i=1}^d \cos p_i \right]^{-1} \quad (3.18)$$

$$g_d(\gamma) \equiv \lim_{L \rightarrow \infty} g_{d,L}(\gamma) = \int \frac{d^d p}{(2\pi)^d} \log \left[1 - \gamma \sum_{i=1}^d \cos p_i \right] \quad (3.19)$$

where the integral runs over the Brillouin zone $[-\pi, \pi]^d$. This substitution gives the correct answer in dimension $d \leq 2$. However, in dimension $d > 2$ we must be a bit more careful, because the infinite-volume quantity $f_d(\gamma)$ tends to a finite value f_* as $\gamma \uparrow 1/d$ even though the finite-volume quantity $f_{d,L}(\gamma)$ diverges due to the contribution of the $p = 0$ mode.¹⁰ In particular, the equation $f_{d,L}(\gamma) = f$ has a solution for arbitrarily large f , which satisfies $\gamma = 1/d - O(L^{-d})$. In infinite volume, we can think of all these solutions with $f \geq f_*$ as arising from $\gamma = 1/d$; we shall refer to these solutions as the “condensate phase”, and use f to parametrize them rather than γ . It is important to note that when $f = 2\tilde{\alpha}_*$ exceeds f_* , the finite-lattice Green’s function $\tilde{B}_*(p)^{-1}$ defined by (3.2), which consists of delta functions located at the momenta with components $p_i = 2\pi k_i/L$, converges in distribution as $L \rightarrow \infty$ *not* to the corresponding infinite-lattice Green’s function $\tilde{B}_*(p)^{-1}$, but rather to

$$\tilde{B}_*(p)^{-1} + (2\pi)^d \left(1 - \frac{f_*}{f} \right) \delta(p). \quad (3.20)$$

¹⁰ The same happens as $\gamma \downarrow -1/d$, due to the contribution of the $p = (\pi, \dots, \pi)$ mode.

Here the delta-function contribution at $p = 0$ corresponds to the long-range order

$$\lim_{|x-y| \rightarrow \infty} (\tilde{B}_\star^{-1})_{xy} = 1 - \frac{f_\star}{f}. \quad (3.21)$$

Note also that the zero mode does *not* contribute to $g_{d,L}$ in the infinite-volume limit at fixed $f \geq f_\star$, since $1/d - |\gamma| \gtrsim L^{-d}$ and $\lim_{L \rightarrow \infty} (\log L^d)/L^d = 0$; therefore we should consider $g_{d,L}(\gamma)$ to be fixed at the value $g_\star \equiv g_d(1/d)$.

In summary, in dimension $d > 2$ we should consider the additional branches

$$\overline{\mathcal{F}}_\pm(f) = \mathcal{F}_{0\star}(f) \pm \tilde{\beta}_V \mathcal{F}_{1\star}(f) + \frac{d}{2\tilde{\beta}_T} \tilde{\beta}_V^2, \quad (3.22)$$

(corresponding to $\gamma = \pm 1/d$) as a function of the variable $f \in [f_\star, \infty)$, where

$$\mathcal{F}_{0\star}(f) = \frac{1}{2} \left[1 - f + \frac{f^2}{4d\tilde{\beta}_T} + \log f + g_\star \right] \quad (3.23)$$

$$\mathcal{F}_{1\star}(f) = -\frac{f}{2\tilde{\beta}_T} \quad (3.24)$$

and we should then minimize over both (3.13) and (3.22). Since $\mathcal{F}_{1\star}(f) < 0$, the optimal choice of sign in (3.22) is clearly $\text{sgn } \gamma = \text{sgn } \tilde{\beta}_V$. Whenever the absolute minimum of the free energy is found in the condensate phase $f > f_\star$ at $\gamma = 1/d$, the correlation functions at $N = \infty$ exhibit both ferromagnetic and nematic long-range order¹¹:

$$\lim_{|x-y| \rightarrow \infty} G_V(x, y) = 1 - \frac{f_\star}{f} \quad (3.25)$$

$$\lim_{|x-y| \rightarrow \infty} G_T(x, y) = \left(1 - \frac{f_\star}{f} \right)^2 \quad (3.26)$$

In Appendix A we collect some results concerning the behavior of the functions $f_d(\gamma)$ and $g_d(\gamma)$. In particular, we show how these quantities have a natural analytic continuation in the parameter d , which allows us to discuss noninteger dimensions $d > 0$; the ability to treat d as a continuous variable is very useful. The small- γ Taylor expansions of $f_d(\gamma)$ and $g_d(\gamma)$ are given in (A.13) and (A.14), respectively. It follows that $\mathcal{F}_0(\gamma)$ and $\mathcal{F}_1(\gamma)$ have the following small- γ expansions:

$$\begin{aligned} \mathcal{F}_0(\gamma) &= \frac{d}{8} \left(\frac{1}{\tilde{\beta}_T} - 1 \right) \gamma^2 + \frac{d}{64} \left(\frac{8d}{\tilde{\beta}_T} + (3 - 10d) \right) \gamma^4 \\ &\quad + \frac{d}{192} \left(\frac{6d(7d - 3)}{\tilde{\beta}_T} - (62d^2 - 63d + 20) \right) \gamma^6 + \dots \end{aligned} \quad (3.27)$$

$$\mathcal{F}_1(\gamma) = -\frac{d}{2\tilde{\beta}_T} \gamma - \frac{d^2}{4\tilde{\beta}_T} \gamma^3 - \frac{3d^2(2d - 1)}{16\tilde{\beta}_T} \gamma^5 + \dots \quad (3.28)$$

The behavior of $f_d(\gamma)$ and $g_d(\gamma)$ as $\gamma \uparrow 1/d$ is discussed at the end of Appendix A.1.

¹¹ In the antiferromagnetic case $\gamma = -1/d$, one has instead $\lim_{|x-y| \rightarrow \infty} (-1)^{|x-y|} G_V(x, y) = 1 - f_\star/f$.

3.3 Parametric Approach

Thus far we have been analyzing the phase diagram by searching directly for the absolute minimum of $\overline{\mathcal{F}}(\tilde{\mu})$, without bothering to use the stationarity equation $\overline{\mathcal{F}}'(\tilde{\mu}) = 0$. On the other hand, in searching for the absolute minimum we have the *right* to restrict attention to such stationary points if we so choose. As we shall see, this alternate approach has some advantages: in particular, it will allow us to visualize the phase diagram simultaneously for all $\tilde{\beta}_T > 0$ (at any fixed value of $\tilde{\beta}_V$).

We proceed as follows: The stationarity equation (2.17) for $\tilde{\mu}$, when combined with (3.3)/(3.7b) and the saddle-point equation (3.11) for $\tilde{\alpha}$, yields¹²

$$\frac{1}{2}\gamma f_{d,L}(\gamma) - \tilde{\beta}_V \equiv \tilde{\mu} = \frac{f_{d,L}(\gamma) - 1}{d\gamma f_{d,L}(\gamma)} \tilde{\beta}_T. \quad (3.29)$$

If we restrict attention to solutions of (3.29), then the free energy (3.12) can be rewritten so as to eliminate reference to either $\tilde{\beta}_V$ or $\tilde{\beta}_T$:

$$\overline{\mathcal{F}} = \frac{1}{2} \left[1 - f_{d,L}(\gamma) + \log f_{d,L}(\gamma) + g_{d,L}(\gamma) + \frac{\tilde{\beta}_T}{d} \left(\frac{f_{d,L}(\gamma) - 1}{\gamma f_{d,L}(\gamma)} \right)^2 \right] \quad (3.30a)$$

$$= \frac{1}{2} \left[\frac{1 - f_{d,L}(\gamma)}{2} + \log f_{d,L}(\gamma) + g_{d,L}(\gamma) - \tilde{\beta}_V \frac{f_{d,L}(\gamma) - 1}{\gamma f_{d,L}(\gamma)} \right]. \quad (3.30b)$$

The solutions to (3.29) come in two types:

(a) $\gamma = 0$ is a solution to (3.29) if and only if $\tilde{\beta}_V = 0$ (i.e. the pure RP^{N-1} model); the corresponding free energy is $\overline{\mathcal{F}} = 0$.¹³

(b) If $\gamma \neq 0$, we can solve (3.29) for $\tilde{\beta}_T$:

$$\tilde{\beta}_T = \frac{d\gamma^2 f_{d,L}(\gamma)^2}{2[f_{d,L}(\gamma) - 1]} - \frac{d\gamma f_{d,L}(\gamma)}{f_{d,L}(\gamma) - 1} \tilde{\beta}_V. \quad (3.31)$$

For each fixed $\tilde{\beta}_V$, equations (3.31) and (3.30b) give $\tilde{\beta}_T$ and $\overline{\mathcal{F}}$ parametrically as a function of $\gamma \in (-1/d, 1/d)$. We must trace out this curve in the $(\tilde{\beta}_T, \overline{\mathcal{F}})$ -plane, and then take the smallest value of $\overline{\mathcal{F}}$ for each $\tilde{\beta}_T$.¹⁴

In Sections 4 and 5 we will carry out this procedure (in the limit $L \rightarrow \infty$) and discuss the qualitative properties of the solution as a function of the lattice dimension d . As preparation,

¹² Alternatively, this same equation can be obtained by differentiating (3.13) with respect to γ , using (3.6), and setting the result equal to zero. Miraculously, the derivative of $f_{d,L}$ enters here only through the overall factor $\gamma f_{d,L} + f'_{d,L}$ [which never vanishes, see e.g. (A.10)], so the solution does not involve $f'_{d,L}$ at all.

¹³ We remark that Magnoli and Ravanini [2, equation (3)] made the mistake of multiplying equation (3.29) by γ , thereby introducing a spurious $\gamma = 0$ solution also for $\tilde{\beta}_V \neq 0$. Fortunately, this error had no effect on their final results, because the purported $\gamma = 0$ solution was never the dominant saddle point anyway.

¹⁴ Alternatively we can fix $\tilde{\beta}_T$ and then use equations (3.31) and (3.30a) to give $\tilde{\beta}_V$ and $\overline{\mathcal{F}}$ parametrically as a function of γ . Yet another variant was employed by Magnoli and Ravanini [2], who fixed $\rho \equiv \tilde{\beta}_T/\tilde{\beta}_V$ and computed $\tilde{\beta} \equiv \tilde{\beta}_V + \tilde{\beta}_T$ and $\overline{\mathcal{F}}$ parametrically as a function of γ .

let us compute, using (3.6)/(A.8), the derivatives with respect to γ of (3.30b) and (3.31):

$$\frac{d\bar{\mathcal{F}}}{d\gamma} = -\frac{\gamma(f-2)f' + 2f(f-1)}{4\gamma f} - \tilde{\beta}_V \frac{f-f^2 + \gamma f'}{2\gamma^2 f^2} \quad (3.32)$$

$$\frac{d\tilde{\beta}_T}{d\gamma} = \frac{d\gamma f[\gamma(f-2)f' + 2f(f-1)]}{2(f-1)^2} + \tilde{\beta}_V \frac{d(f-f^2 + \gamma f')}{(f-1)^2} \quad (3.33)$$

$$\begin{aligned} \frac{d^2\tilde{\beta}_T}{d\gamma^2} &= \frac{d\gamma(2\tilde{\beta}_V - 2\gamma f + \gamma f^2)}{2(f-1)^2} f'' + \frac{\gamma d(\gamma - 2\tilde{\beta}_V)}{(f-1)^3} f'^2 \\ &\quad + \frac{2d(\tilde{\beta}_V - 2\gamma f + \gamma f^2)}{(f-1)^2} f' + \frac{df^2}{f-1} \end{aligned} \quad (3.34)$$

where $f' \equiv df/d\gamma$; these equations hold both in finite volume and in the infinite-volume limit. In particular, we have

$$\frac{d\bar{\mathcal{F}}}{d\tilde{\beta}_T} = -\frac{(f-1)^2}{2d\gamma^2 f^2} \leq 0. \quad (3.35)$$

It is a curious fact that the derivative $d\bar{\mathcal{F}}/d\tilde{\beta}_T$ does not depend on $\tilde{\beta}_V$. Note also that $d\bar{\mathcal{F}}/d\tilde{\beta}_T$ becomes more negative $|\gamma|$ grows (in all dimensions $d > 0$): this strict monotonicity follows from inequality (A.10).

In the infinite-volume theory in dimension $d > 2$, we need to consider also the ‘‘condensate phase’’ parametrized by $f \in [f_*, \infty)$ with $\gamma \equiv (1/d) \operatorname{sgn} \tilde{\beta}_V$ and $g \equiv g_*$. Here (3.30) is replaced by

$$\bar{\mathcal{F}} = \frac{1}{2} \left[1 - f + \log f + g_* + d\tilde{\beta}_T \left(\frac{f-1}{f} \right)^2 \right] \quad (3.36a)$$

$$= \frac{1}{2} \left[\frac{1-f}{2} + \log f + g_* - d|\tilde{\beta}_V| \frac{f-1}{f} \right] \quad (3.36b)$$

while (3.31) is replaced by

$$\tilde{\beta}_T = \frac{f^2}{2d(f-1)} - \frac{f}{f-1} |\tilde{\beta}_V|. \quad (3.37)$$

The derivatives of (3.36b) and (3.37) with respect to f are

$$\frac{d\bar{\mathcal{F}}}{df} = -\frac{f^2 - 2f + 2d|\tilde{\beta}_V|}{4f^2} \quad (3.38)$$

$$\frac{d\tilde{\beta}_T}{df} = \frac{f^2 - 2f + 2d|\tilde{\beta}_V|}{2d(f-1)^2} \quad (3.39)$$

and hence

$$\frac{d\bar{\mathcal{F}}}{d\tilde{\beta}_T} = -\frac{d(f-1)^2}{2f^2} < 0. \quad (3.40)$$

Once again, $d\bar{\mathcal{F}}/d\tilde{\beta}_T$ is independent of $\tilde{\beta}_V$. Moreover, (3.35) and (3.40) coincide in the condensate phase $|\gamma| = 1/d$.¹⁵ In particular, they coincide at their joining point $|\gamma| = 1/d$, $f = f_*$; this means that any phase transition between these two branches must be of second (or higher) order. Note also that $d\bar{\mathcal{F}}/d\tilde{\beta}_T$ is a monotonic function of f : it becomes more negative as f grows.

For $d > 2$ it is convenient to use f as the independent variable in *both* the “normal phase” ($|\gamma| < 1/d$) and the condensate phase: see e.g. Figure 3 below. In particular, equations (3.32)/(3.33) for the normal phase can be converted to yield $d\bar{\mathcal{F}}/df$ and $d\tilde{\beta}_T/df$ by dividing them by $f'(\gamma)$. It is curious to note that in dimensions $2 < d \leq 4$, where $f_*(d) \equiv \lim_{\gamma \uparrow 1/d} df_d(\gamma)/d\gamma$ is infinite, the limiting slopes $d\bar{\mathcal{F}}/df$ and $d\tilde{\beta}_T/df$ for $\gamma \uparrow 1/d$ in the normal phase coincide with the values (3.38)/(3.39) obtained for $f \downarrow f_*$ in the condensate phase (this matching of slopes is seen e.g. in Figure 3). On the other hand, for $d > 4$ this matching of slopes does not occur.

4 Behavior of Solutions for $\tilde{\beta}_V = 0$

4.1 Overview

Our conclusions concerning the phase diagram of the $N = \infty RP^{N-1}$ model, as a function of the spatial dimension d (treated as a real variable), are summarized in Figure 1. There are three possible phases: a white-noise phase ($\gamma = 0$) in which the isotensor correlation length is zero; an isotropic phase ($0 < |\gamma| < 1/d$) in which the isotensor correlation length is finite but nonzero; and a nematic ordered phase ($|\gamma| = 1/d$) in which the isotensor correlation function exhibits long-range order. For $0 < d \leq 3/2$, there is a second-order transition at $\tilde{\beta}_T = 1$ from the white-noise phase to the isotropic phase. For $3/2 < d < d_* \approx 2.38403$, this transition is first-order and takes place at a dimension-dependent $\tilde{\beta}_{T,c} < 1$. For $2 < d < d_*$, there is a subsequent second-order transition from the isotropic phase to a nematic ordered phase at a dimension-dependent $\tilde{\beta}_{T,c'} \equiv f_*^2/[2d(f_* - 1)] < \infty$. At $d = d_*$ the two transitions collide at $\tilde{\beta}_{T,*} \approx 0.873264$, and for $d > d_*$ there is only a first-order transition from the white-noise phase directly into the nematic ordered phase, at a dimension-dependent $\tilde{\beta}_{T,c''} < 1$.¹⁶

Let us now show how these conclusions can be derived using either the direct or the parametric approach.

4.2 Direct Approach

For $\tilde{\beta}_V = 0$, the free energy is given simply by $\mathcal{F}_0(\gamma)$. Since \mathcal{F}_0 is an even function of γ , one of its stationary points is always $\gamma = 0$. To learn about other possible stationary points, we begin by examining the Taylor expansion (3.27) of $\mathcal{F}_0(\gamma)$ near $\gamma = 0$. The coefficient

¹⁵ Both these properties follow alternatively from the fact that (3.35) holds also in finite volume.

¹⁶ Ohno *et al.* [3] were the first to note the existence of the special dimension d_* ; but they did not attempt to determine it numerically, stating only that $2 < d_* < 3$. Caracciolo and Pelissetto, in an unpublished manuscript [12], found essentially the same value of d_* as we report here.

of γ^2 is positive for $\tilde{\beta}_T < 1$ and negative for $\tilde{\beta}_T > 1$. The coefficient of γ^4 is positive for $\tilde{\beta}_T < 8d/\max(10d-3, 0)$ and negative for $\tilde{\beta}_T > 8d/\max(10d-3, 0)$. It follows that the local behavior near $\gamma = 0$ falls into three cases:

- (a) $0 < d < 3/2$: The coefficient of γ^4 is positive when $\tilde{\beta}_T = 1$. Thus, as $\tilde{\beta}_T$ passes through 1, the local minimum at $\gamma = 0$ turns into a local maximum, and a pair of degenerate minima at $\gamma = \pm\gamma_0(\tilde{\beta}_T)$ bifurcates off it. These minima satisfy the equation

$$\tilde{\beta}_T = \frac{d\gamma_0^2 f_d(\gamma_0)^2}{2[f_d(\gamma_0) - 1]}. \quad (4.1)$$

As $\tilde{\beta}_T \downarrow 1$ we have

$$\begin{aligned} \gamma_0(\tilde{\beta}_T) &= \left(\frac{2}{\frac{3}{2}-d}\right)^{1/2} (\tilde{\beta}_T - 1)^{1/2} \times \\ &\quad \left[1 + \frac{20d^2 - 54d + 31}{4(\frac{3}{2}-d)^2}(\tilde{\beta}_T - 1) + O((\tilde{\beta}_T - 1)^2)\right] \end{aligned} \quad (4.2)$$

$$\begin{aligned} \mathcal{F}_0(\gamma_0(\tilde{\beta}_T), \tilde{\beta}_T) &= -\frac{d}{8(\frac{3}{2}-d)}(\tilde{\beta}_T - 1)^2 - \frac{d(4d^2 - 18d + 13)}{48(\frac{3}{2}-d)^3}(\tilde{\beta}_T - 1)^3 \\ &\quad + O((\tilde{\beta}_T - 1)^4) \end{aligned} \quad (4.3)$$

- (b) $d = 3/2$: The coefficient of γ^4 is zero when $\tilde{\beta}_T = 1$, but the coefficient of γ^6 is positive. Therefore, the qualitative behavior is the same as for $d < 3/2$, but the powers are changed:

$$\gamma_0(\tilde{\beta}_T) = \frac{2}{5^{1/4}}(\tilde{\beta}_T - 1)^{1/4} - \frac{3}{10 \cdot 5^{3/4}}(\tilde{\beta}_T - 1)^{3/4} + O((\tilde{\beta}_T - 1)^{5/4}) \quad (4.4)$$

$$\mathcal{F}_0(\gamma_0(\tilde{\beta}_T), \tilde{\beta}_T) = -\frac{1}{2\sqrt{5}}(\tilde{\beta}_T - 1)^{3/2} - \frac{9}{10}(\tilde{\beta}_T - 1)^2 + O((\tilde{\beta}_T - 1)^{5/2}) \quad (4.5)$$

- (c) $d > 3/2$: The coefficient of γ^4 is negative when $\tilde{\beta}_T = 1$. The behavior for $\tilde{\beta}_T \approx 1$ and $\gamma \approx 0$ will turn out to be irrelevant, as a first-order phase transition occurs *before* $\tilde{\beta}_T = 1$, at a γ far away from 0.

The local behavior near $\gamma = 0$ does not, of course, necessarily determine the global behavior of $\mathcal{F}_0(\gamma)$.¹⁷ But our numerical computations confirm — although we have been unable to prove it analytically — that $\mathcal{F}_0(\gamma)$ always has at most one pair of local minima $\gamma = \pm\gamma_0(\tilde{\beta}_T) \neq 0$, and that:

¹⁷ This point was overlooked by Hikami and Maskawa [1, Appendix], who asserted (incorrectly) that there is a phase transition at $\tilde{\beta}_T = 1$ in all dimensions d .

- (a) $0 < d < 3/2$: For $\tilde{\beta}_T \leq 1$, the unique absolute minimum of $\mathcal{F}_0(\gamma)$ lies at $\gamma = 0$. For $\tilde{\beta}_T > 1$, $\mathcal{F}_0(\gamma)$ has precisely two degenerate absolute minima, at $\gamma = \pm\gamma_0(\tilde{\beta}_T)$ satisfying (4.2). The free energy \bar{F} therefore equals 0 for $\tilde{\beta}_T \leq 1$, and it satisfies (4.3) for $\tilde{\beta}_T > 1$. There is thus a second-order phase transition at $\tilde{\beta}_T = 1$, in which the specific heat $C_H \sim \partial^2 \bar{F} / \partial \tilde{\beta}_T^2$ has a jump discontinuity (see Figure 2a).
- (b) $d = 3/2$: The qualitative behavior is the same as for $d < 3/2$, but $\gamma_0(\tilde{\beta}_T)$ satisfies (4.4), and the free energy for $\tilde{\beta}_T > 1$ satisfies (4.5). There is thus a second-order phase transition at $\tilde{\beta}_T = 1$, in which the specific heat has a $(\tilde{\beta}_T - 1)^{-1/2}$ singularity as $\tilde{\beta}_T \downarrow 1$ (see Figure 2b).
- (c) $3/2 < d \leq 2$: For $\tilde{\beta}_T < \tilde{\beta}_{T,c}(d) < 1$, the unique absolute minimum of $\mathcal{F}_0(\gamma)$ lies at $\gamma = 0$. For $\tilde{\beta}_T > \tilde{\beta}_{T,c}(d)$, $\mathcal{F}_0(\gamma)$ has precisely two degenerate absolute minima, at $\gamma = \pm\gamma_0(\tilde{\beta}_T)$, where

$$\gamma_0(\tilde{\beta}_T) \rightarrow \begin{cases} \gamma_c > 0 & \text{as } \tilde{\beta}_T \downarrow \tilde{\beta}_{T,c} \\ 1/d & \text{as } \tilde{\beta}_T \rightarrow +\infty \end{cases} \quad (4.6)$$

There is thus a first-order phase transition at a dimension-dependent $\tilde{\beta}_{T,c}(d) < 1$ (see Figure 2c for the case $d = 2$).¹⁸ We have

$$\tilde{\beta}_{T,c} = 1 - \frac{3}{20}(d - \frac{3}{2})^2 - \frac{63}{100}(d - \frac{3}{2})^3 + O\left((d - \frac{3}{2})^4\right) \quad (4.7)$$

$$\gamma_c = \sqrt{\frac{6}{5}} \left[(d - \frac{3}{2})^{1/2} + \frac{51}{20}(d - \frac{3}{2})^{3/2} + O\left((d - \frac{3}{2})^{5/2}\right) \right] \quad (4.8)$$

as $d \downarrow 3/2$.

For $d > 2$ we need to consider also the ‘‘condensate phase’’ (3.23) parametrized by $f \geq f_*$ at $\gamma = 1/d$ and $g = g_*$. For convenience we use f as the independent variable in the plots also in the ‘‘ordinary phase’’ $0 < \gamma < 1/d$. We have:

- (d) $2 < d < d_* \approx 2.38403$: The qualitative behavior near the first-order transition point $\tilde{\beta}_{T,c}$ is the same as for $d \leq 2$. However, beyond this point the behavior is different: $\gamma_0(\tilde{\beta}_T)$ now reaches $1/d$ when $\tilde{\beta}_T$ reaches the *finite* value

$$\tilde{\beta}_{T,c'}(d) \equiv \frac{f_*^2}{2d(f_* - 1)}. \quad (4.9)$$

For $\tilde{\beta}_T > \tilde{\beta}_{T,c'}$, the function $\mathcal{F}_0(\gamma)$ is strictly decreasing on the interval $[0, 1/d]$, and the absolute minimum of the free energy is found in the condensate phase at

$$f = d\tilde{\beta}_T \left[1 + \left(1 - \frac{2}{d\tilde{\beta}_T} \right)^{1/2} \right] > f_* \quad (4.10)$$

$$\mathcal{F}_0 = -\frac{f-1}{4} + \frac{\log f + g_*}{2} < 0 \quad (4.11)$$

¹⁸ For $d = 2$, the transition at $\tilde{\beta}_{T,c} \approx 0.956$ was found previously by Magnoli and Ravanini [2], using the parametric approach (see Section 4.3 below).

There is a second-order isotropic-to-nematic phase transition at $\tilde{\beta}_T = \tilde{\beta}_{T,c'}$ (see Figure 3a). The two transitions $\tilde{\beta}_{T,c} < \tilde{\beta}_{T,c'}$ come closer together as d grows, and they collide at the dimension d_* where γ_c reaches $1/d$ (see Figure 4). Equivalently, d_* is defined by the condition

$$\mathcal{F}_* \equiv -\frac{f_* - 1}{4} + \frac{\log f_* + g_*}{2} \begin{cases} < 0 & \text{for } 2 < d < d_* \\ = 0 & \text{for } d = d_* \\ > 0 & \text{for } d > d_* \end{cases} \quad (4.12)$$

(see Figure 5).

- (e) $d = d_*$: The two transitions coincide: $\tilde{\beta}_{T,c} = \tilde{\beta}_{T,c'} = \tilde{\beta}_{T,*} \approx 0.873264$. Thus, for $\tilde{\beta}_T < \tilde{\beta}_{T,*}$, the unique minimum lies at $\gamma = 0$; for $\tilde{\beta}_T = \tilde{\beta}_{T,*}$, it lies exactly at $\gamma = 1/d$ with $f = f_*$; for $\tilde{\beta}_T > \tilde{\beta}_{T,*}$, it lies in the condensate phase $\gamma = 1/d$ at the value (4.10). There is a first-order phase transition as $\tilde{\beta}_T$ passes through $\tilde{\beta}_{T,*}$ (see Figure 3b).
- (f) $d > d_*$: For $\tilde{\beta}_T \leq f_*^2/[2d(f_* - 1)]$, $\mathcal{F}_0(\gamma)$ is a strictly increasing function of γ on $[0, 1/d]$; for $f_*^2/[2d(f_* - 1)] < \tilde{\beta}_T < 1$, it first increases and then decreases; for $\tilde{\beta}_T \geq 1$, it is strictly decreasing. In all three cases, $\mathcal{F}_0(\gamma)$ never has a local minimum in the interval $0 < \gamma \leq 1/d$. Therefore, the absolute minimum is either at $\gamma = 0$ or else in the condensate phase at (4.10)/(4.11). There is a $\tilde{\beta}_{T,c''}(d)$ such that the former behavior occurs for $\tilde{\beta}_T < \tilde{\beta}_{T,c''}(d)$ and the latter for $\tilde{\beta}_T > \tilde{\beta}_{T,c''}(d)$ (see Figure 3c): it is given by

$$\tilde{\beta}_{T,c''}(d) \equiv \frac{f_{c''}^2}{2d(f_{c''} - 1)} \quad (4.13)$$

where $f_{c''}$ is the unique solution of $\log f + g_* = (f - 1)/2$ satisfying $f > f_*$.¹⁹ As $d \rightarrow \infty$, we have $f_{c''} = f_\infty + O(d^{-1})$ and $\tilde{\beta}_{T,c''} = f_\infty^2/[2(f_\infty - 1)]d^{-1} + O(d^{-2})$, where $f_\infty \approx 3.512863$ is the unique solution of $\log f = (f - 1)/2$ on $f > 1$.

4.3 Parametric Approach

Since $\overline{\mathcal{F}}$ and $\tilde{\beta}_T$ are *even* functions of γ when $\tilde{\beta}_V = 0$, it suffices to consider $\gamma \geq 0$. From (3.31) we have

$$\tilde{\beta}_T = \frac{d\gamma^2 f^2}{2(f - 1)} = 1 + \frac{3 - 2d}{4}\gamma^2 - \frac{20d^2 - 54d + 31}{16}\gamma^4 + \dots \quad (4.14)$$

In Figure 6 we plot $\tilde{\beta}_T$ versus γ for dimensions $d = 1, 3/2, 2, 9/4, d_*, 3$. Moreover, for $d > 2$ we need to consider the ‘‘condensate phase’’

$$\tilde{\beta}_T = \frac{f^2}{2d(f - 1)} \quad (4.15)$$

parametrized by $f \in [f_*, \infty)$.

The following assertions appear to be true:

¹⁹ Since $-(f - 1)/4 + (\log f + g_*)/2$ is a concave function of f that is > 0 at $f = f_*$ and tends to $-\infty$ as $f \rightarrow +\infty$, it has a unique zero in the interval (f_*, ∞) .

- (a) For $0 < d \leq 3/2$, $\tilde{\beta}_T$ is a strictly increasing function of γ on $[0, 1/d]$. It tends to $+\infty$ as $\gamma \uparrow 1/d$.
- (b) For $3/2 < d < \bar{d} \approx 2.55391$, there exists $\gamma_{cusp}(d) \in (0, 1/d)$ such that $\tilde{\beta}_T$ is a strictly decreasing function of γ on $[0, \gamma_{cusp}]$ and a strictly increasing function of γ on $[\gamma_{cusp}, 1/d]$. The value of γ_{cusp} is determined by the condition $\gamma = 2f(f-1)/[(2-f)f']$. Moreover, $d\gamma_{cusp}$ is an increasing function of d : it moves from $\gamma_{cusp} = 0$ at $d = 3/2$ to $\gamma_{cusp} = 1/d$ at $d = \bar{d}$. The value of \bar{d} is determined by the condition $f_*(\bar{d}) = 2$.
- (b₁) For $3/2 < d \leq 2$, $\tilde{\beta}_T$ tends to $+\infty$ as $\gamma \uparrow 1/d$.
- (b₂) For $2 < d < \bar{d}$, $\tilde{\beta}_T$ tends to a *finite* value $f_*^2/[2d(f_* - 1)]$ as $\gamma \uparrow 1/d$. However, the slope $d\tilde{\beta}_T/d\gamma$ at this point is $+\infty$. In the condensate phase $f \geq f_*$, $\tilde{\beta}_T$ is a strictly increasing function of f .
- (c) For $d \geq \bar{d}$, $\tilde{\beta}_T$ is a strictly decreasing function of γ on $[0, 1/d]$. It tends to a *finite* value $f_*^2/[2d(f_* - 1)] < 1$ as $\gamma \uparrow 1/d$.
- (c₁) For $\bar{d} \leq d \leq 4$, the slope $d\tilde{\beta}_T/d\gamma$ is $-\infty$ at $\gamma = 1/d$.
- (c₂) For $d > 4$, the slope is a finite negative number.

In either case, in the condensate phase $f \geq f_*$, $\tilde{\beta}_T$ at first decreases and then increases; it reaches its absolute minimum at $f = 2$ and $\beta_T = 2/d$.

The assertions about the behavior as $\gamma \uparrow 1/d$ are simple rigorous consequences of known facts about $f_d(\gamma)$ [see Appendix A], and the assertions about the condensate phase are trivial calculus. But we have been unable to demonstrate analytically the observed monotonicity properties of $\tilde{\beta}_T(\gamma)$.

Let us next look at the free energy $\overline{\mathcal{F}}(\gamma)$ defined by (3.30b) with $\tilde{\beta}_V = 0$:

$$\overline{\mathcal{F}} = -\frac{f-1}{4} + \frac{\log f + g}{2} = \frac{d(2d-3)}{64}\gamma^4 + \frac{d(7d^2-18d+10)}{48}\gamma^6 + \dots \quad (4.16)$$

From (3.35) it follows that $\overline{\mathcal{F}}$ is decreasing wherever $\tilde{\beta}_T$ is increasing, and conversely. As $\gamma \uparrow 1/d$, $\overline{\mathcal{F}}$ tends to $-\infty$ [resp. to a finite number $\mathcal{F}_* = -(f_* - 1)/4 + (\log f_* + g_*)/2$] in dimension $d \leq 2$ (resp. $d > 2$). In dimension $d > 2$, we need to consider also the condensate phase $f \geq f_*$, in which $\overline{\mathcal{F}}$ is given by (3.36b). Again we have to distinguish $2 < d \leq \bar{d}$ (corresponding to $f_* \geq 2$) from $d > \bar{d}$ (corresponding to $f_* < 2$). In the former case, $\overline{\mathcal{F}}$ decreases monotonically from \mathcal{F}_* to $-\infty$ as f rises from f_* to $+\infty$. In the latter case, $\overline{\mathcal{F}}$ first rises from \mathcal{F}_* to $(2 \log 2 - 1)/4 + g_*/2$ as f rises from f_* to 2, then decreases monotonically to $-\infty$ as f rises from 2 to $+\infty$. We refrain from showing the plots of $\overline{\mathcal{F}}$ versus γ .

We are now ready to plot $\overline{\mathcal{F}}$ parametrically versus $\tilde{\beta}_T$. As in Section 4.2, six cases need to be distinguished (see Figure 7):

Case (a), $0 < d < 3/2$: As γ increases from 0, $\tilde{\beta}_T$ increases smoothly from 1, with an initial correction of order γ^2 , while $\overline{\mathcal{F}}$ decreases smoothly from 0, with an initial correction of order γ^4 . It follows that $\overline{\mathcal{F}}$ is a smooth and decreasing function of $\tilde{\beta}_T$ in the regime $\tilde{\beta}_T \geq 1$; from (4.14) and (4.16) we reobtain the expansion (4.3) as $\tilde{\beta}_T \downarrow 1$. This of course beats the

$\gamma = 0$ solution $\overline{\mathcal{F}} = 0$ whenever $\tilde{\beta}_T > 1$. On the other hand, for $\tilde{\beta}_T \leq 1$ the only solution is given by $\gamma = 0$ and $\overline{\mathcal{F}} = 0$. We therefore have a second-order phase transition at $\tilde{\beta}_T = 1$ (see Figure 7a). [In Section 4.4 we give explicit formulae for the case $d = 1$.]

Case (b), $d = 3/2$: The parametric plot $\overline{\mathcal{F}}(\tilde{\beta}_T)$ is qualitatively like that for $d < 3/2$, but since $\tilde{\beta}_T - 1 \sim \gamma^4$ while $\overline{\mathcal{F}} \sim \gamma^6$, the expansion as $\tilde{\beta}_T \downarrow 1$ has fractional powers $\overline{\mathcal{F}} \sim (\tilde{\beta}_T - 1)^{3/2}$, as already seen in (4.5). There is again a second-order phase transition at $\tilde{\beta}_T = 1$ (see Figure 7b).

Case (c), $3/2 < d \leq 2$: A typical parametric plot $\overline{\mathcal{F}}(\tilde{\beta}_T)$ is shown in Figure 7c. As γ increases from 0, $\tilde{\beta}_T$ initially *decreases* from 1, while $\overline{\mathcal{F}}$ initially *increases* from 0; the dependence $\overline{\mathcal{F}}(\tilde{\beta}_T)$ is thus initially backward-bending. At $\gamma = \gamma_{cusp}$, both $d\tilde{\beta}_T/d\gamma$ and $d\overline{\mathcal{F}}/d\gamma$ pass through zero, so the parametric plot exhibits a cusp. After this, $\tilde{\beta}_T$ increases and $\overline{\mathcal{F}}$ decreases, with the curve staying below the $\gamma < \gamma_{cusp}$ curve [the latter property follows from the monotonicity of the slope (3.35)]; $\tilde{\beta}_T$ tends to $+\infty$ and $\overline{\mathcal{F}}$ tends to $-\infty$ as $\gamma \uparrow 1/d$. Of course, the $\gamma = 0$ solution $\overline{\mathcal{F}} = 0$ is also present for all $\tilde{\beta}_T$. Since the stable phase is the one with the minimal $\overline{\mathcal{F}}$, the point where the ‘‘cusped branch’’ crosses the $\overline{\mathcal{F}} = 0$ solution corresponds to a first-order phase transition with a d -dependent critical inverse temperature $\tilde{\beta}_{T,c} < 1$. This value can be located numerically by solving $\overline{\mathcal{F}}(\gamma) = 0$ for γ using (3.30b), and then substituting into (3.31) to find $\tilde{\beta}_T$. For d slightly greater than $3/2$ it is given by (4.7)/(4.8).

Cases (d–f), $d > 2$: These cases are qualitatively similar to case (c). The only difference is that for $d > 2$, $\tilde{\beta}_T$ reaches a finite value at $\gamma = 1/d$; beyond this point we must consider the condensate phase parametrized by $f \geq f_*$ at $\gamma = 1/d$ and $g = g_*$. From (3.37) and (3.36b) this branch is given by

$$\tilde{\beta}_T = \frac{f^2}{2d(f-1)} \quad (4.17)$$

$$\overline{\mathcal{F}} = -\frac{f-1}{4} + \frac{\log f + g_*}{2} \quad (4.18)$$

(shown as dashed lines in Figures 7d–f). The condensate phase may begin after the cusp ($d < \bar{d} \approx 2.55391$), at the cusp ($d = \bar{d}$) or before the cusp ($d > \bar{d}$); this distinction is, however, of little interest. What *does* matter is where the cusped branch crosses the $\overline{\mathcal{F}} = 0$ solution: for $d < d_* \approx 2.38403$ this crossing occurs within the ‘‘ordinary branch’’ $0 < \gamma < 1/d$ (Figure 7d), while for $d > d_*$ it occurs within the ‘‘condensate branch’’ $f > f_*$ at $\gamma = 1/d$ (Figure 7f); for $d = d_*$ it occurs precisely at the joining point $f = f_*$ (Figure 7e). For $d < d_*$, this crossing corresponds to the first-order white-noise-to-isotropic transition; we solve numerically for the corresponding $\tilde{\beta}_{T,c}$ in the same manner as in case (c). For these dimensions there is also a subsequent second-order isotropic-to-nematic transition where the ordinary and condensate branches join: this occurs at $\tilde{\beta}_{T,c'} \equiv f_*^2/[2d(f_* - 1)]$. For $d > d_*$, the crossing corresponds to the first-order white-noise-to-nematic transition; we solve numerically for $\tilde{\beta}_{T,c''}$ by solving $\overline{\mathcal{F}}(f) = 0$ for f using (4.18) [taking only the solution with $f > f_*$] and then substituting into (4.17). We have, for example, $\tilde{\beta}_{T,c''}(3) \approx 0.734865$, $\tilde{\beta}_{T,c''}(4) \approx 0.572931$, $\tilde{\beta}_{T,c''}(5) \approx 0.466744$ and $\tilde{\beta}_{T,c''}(6) \approx 0.393066$. As $d \rightarrow \infty$, we have $\tilde{\beta}_{T,c''} = f_\infty^2/[2(f_\infty - 1)]d^{-1} + O(d^{-2})$, where $f_\infty \approx 3.512863$ is the unique solution of $\log f = (f - 1)/2$ on $f > 1$.

4.4 One-Dimensional Case

For the special case $d = 1$, we have available the exact formulae (A.11)/(A.12) for $f(\gamma)$ and $g(\gamma)$:

$$f(\gamma) = (1 - \gamma^2)^{-1/2} \quad (4.19)$$

$$g(\gamma) = \log\left(\frac{1 + (1 - \gamma^2)^{1/2}}{2}\right) \quad (4.20)$$

It is convenient to introduce a new variable $s \in [0, 1)$ via

$$\gamma = \frac{2s}{1 + s^2} \quad (4.21)$$

$$f = \frac{1 + s^2}{1 - s^2} \quad (4.22)$$

[From (3.9) we see that $s = e^{-m}$ where m is the isovector mass gap.] Using the direct approach (3.12), we find

$$\bar{\mathcal{F}}(s) = \mathcal{F}_0(s) = \frac{1}{2} \left[\frac{-2s^2}{1 - s^2} + \frac{s^2}{\tilde{\beta}_T(1 - s^2)^2} - \log(1 - s^2) \right]. \quad (4.23)$$

The derivative of (4.23) with respect to s^2 is

$$\frac{d\mathcal{F}_0}{d(s^2)} = \frac{1 + s^2}{2(1 - s^2)} \left[\frac{1}{\tilde{\beta}_T} - 1 + s^2 \right]. \quad (4.24)$$

It follows then that for $\tilde{\beta}_T \leq 1$, \mathcal{F}_0 is a strictly increasing function of s^2 on $[0, 1)$, so the absolute minimum lies at $s_\star = 0$ ($\gamma = 0$) and has $\mathcal{F}_0 = 0$. For $\tilde{\beta}_T \geq 1$, \mathcal{F}_0 has a unique local minimum at $s_\star^2 = 1 - 1/\tilde{\beta}_T$, which is of course its absolute minimum. We therefore have

$$\bar{F} \equiv \inf_{0 \leq s < 1} \mathcal{F}_0(s) = \begin{cases} 0 & \text{for } 0 \leq \tilde{\beta}_T \leq 1 \\ -\frac{1}{2}(\tilde{\beta}_T - 1 - \log \tilde{\beta}_T) & \text{for } \tilde{\beta}_T \geq 1 \end{cases} \quad (4.25)$$

exhibiting a second-order phase transition at $\tilde{\beta}_T = 1$.

Finally, let us compute the correlation functions. Recalling that in $d = 1$ the free propagator is a pure exponential

$$(\tilde{B}^{-1})_{xy} = e^{-m|x-y|} = s^{|x-y|}, \quad (4.26)$$

we find from (2.20) and (2.23) the isovector and isotensor correlation functions

$$G_V(x, y) = s_\star^{|x-y|} \quad (4.27)$$

$$G_T(x, y) = s_\star^{2|x-y|} \quad (4.28)$$

Of course, the result for G_V reflects the (spurious) spontaneous breaking of Z_2 gauge invariance at $\tilde{\beta}_T > 1$, when $N = \infty$.

In Section 6 we will confirm these results by computing the $N \rightarrow \infty$ limit of the exact finite- N solution.

5 Behavior of Solutions for $\tilde{\beta}_V \neq 0$

5.1 Overview

We begin by summarizing our conclusions concerning the phase diagram of the $N = \infty$ mixed isovector/isotensor model. The complete phase diagram is a two-dimensional surface in the space of parameters $\tilde{\beta}_V, \tilde{\beta}_T, d$. In Figures 8–13 we show the qualitative phase diagrams in the $(\tilde{\beta}_V, \tilde{\beta}_T)$ -plane for different ranges of spatial dimension d : first-order transitions are shown in solid lines, and second-order transitions in dashed lines.

There is always a line of first-order transitions at $\tilde{\beta}_V = 0, \tilde{\beta}_T > \tilde{\beta}_{T,c}(d)$. The remaining features of the phase diagram depend on the spatial dimension:

- (a) $0 < d \leq 3/2$: There are no phase transitions other than the second-order transition at $(\tilde{\beta}_V, \tilde{\beta}_T) = (0, 1)$ and the first-order line at $\tilde{\beta}_V = 0, \tilde{\beta}_T > 1$ (Figure 8).
- (b) $3/2 < d \leq 2$: Three curves of first-order transitions meet at the point $(\tilde{\beta}_V, \tilde{\beta}_T) = (0, \tilde{\beta}_{T,c})$: the first-order line at $\tilde{\beta}_V = 0, \tilde{\beta}_T > \tilde{\beta}_{T,c}$; and a pair of symmetrical curves $\tilde{\beta}_{T,c}(\tilde{\beta}_V)$. Second-order phase transitions occur at the endpoints $(\tilde{\beta}_V, \tilde{\beta}_T) = (\pm\tilde{\beta}_{V,e}, \tilde{\beta}_{T,e})$ of the latter curves (Figure 9).
- (c) $2 < d < d_* \approx 2.38403$: In addition to the transitions present for $3/2 < d \leq 2$, there is an additional pair of second-order transition lines located at

$$\tilde{\beta}_{T,c'} = \frac{f_*^2}{2d(f_* - 1)} - \frac{f_*}{f_* - 1}|\tilde{\beta}_V| \quad (5.1)$$

(Figure 10).²⁰ The intersection of these lines with the $\tilde{\beta}_V = 0$ axis at $\tilde{\beta}_{T,c'} = f_*^2/[2d(f_* - 1)]$ corresponds to the isotropic-to-nematic transition of the RP^{N-1} model, while their intersections with the $\tilde{\beta}_T = 0$ axis at $\tilde{\beta}_V = \pm f_*/2d$ correspond to the paramagnetic-to-ferromagnetic ($\tilde{\beta}_V > 0$) and paramagnetic-to-antiferromagnetic ($\tilde{\beta}_V < 0$) transitions of the N -vector model.

- (d) $d = d_*$: The two transitions of the RP^{N-1} model (at $\tilde{\beta}_{T,c}$ and $\tilde{\beta}_{T,c'}$) coincide. For $\tilde{\beta}_V \neq 0$, the second-order transition lines (5.1) remain above the first-order curves (Figure 11).
- (e) $d_* < d < d_{**} = 3$: Second-order transitions occur on that part of (5.1) where they lie above the first-order curves (Figure 12).
- (f) $d \geq 3$: The second-order transition lines (5.1) join onto the endpoints $(\pm\tilde{\beta}_{V,e}, \tilde{\beta}_{T,e})$ of the first-order transition curves (Figure 13).

²⁰ Equation (10) of [40] contains an error: where Oku writes \tilde{K} (= our $\tilde{\beta}_T$) he should have written \tilde{K}/\tilde{K}^2 (= our $\tilde{\beta}_T/\tilde{\beta}_V^2$); with this change, the equation agrees with our (5.1). This error can be traced back to a notational confusion in an earlier paper of the same group [39, p. 125], where the authors say “here we have scaled a as $a \rightarrow \tilde{K}a$ ” but without explicitly defining a new symbol; they then presumably confused the scaled and unscaled meanings of a . We have been unable to understand where equation (11) of [40] comes from.

The dependence of $\tilde{\beta}_{T,e}$ and $\tilde{\beta}_{V,e}$ on d is shown in Figures 14 and 15. Together with Figure 1, which illustrates the dependence of $\tilde{\beta}_{T,c}$ on d at $\tilde{\beta}_V = 0$, these plots describe the principal features of the phase diagram.

Let us now show how these conclusions can be derived using either the direct or the parametric approach.

5.2 Direct Approach

We now have to look at the entire free energy $\overline{\mathcal{F}}(\gamma) = \mathcal{F}_0(\gamma) + \tilde{\beta}_V \mathcal{F}_1(\gamma) + \text{const.}$ Since $\mathcal{F}_1(\gamma)/\gamma < 0$ for all γ , it follows immediately that the absolute minimum of $\overline{\mathcal{F}}(\gamma)$ lies in the region $\text{sgn } \gamma = \text{sgn } \tilde{\beta}_V$. In what follows, we restrict attention without loss of generality to $\tilde{\beta}_V > 0$ and $\gamma > 0$.

The plots for $\tilde{\beta}_V = 0$ (Figures 2 and 3) get smoothly perturbed as we turn on $\tilde{\beta}_V > 0$. In particular, for $d \leq 3/2$ we observe empirically (though we have been unable to prove it analytically) that $\overline{\mathcal{F}}(\gamma)$ has a *unique* local minimum in the region $\gamma > 0$; it is of course the absolute minimum. Moreover, it varies smoothly with $\tilde{\beta}_T > 0$ and $\tilde{\beta}_V > 0$. Therefore, there are no phase transitions at $\beta_T \neq 0$.

For $d > 3/2$ the story is more complicated. The local minima lying for $\tilde{\beta}_V = 0$ at $\gamma = 0$ and at $\gamma = \gamma_0(\tilde{\beta}_T)$ both move smoothly as a small $\tilde{\beta}_V > 0$ is turned on. Let us call the resulting minima $\gamma_a(\tilde{\beta}_V, \tilde{\beta}_T)$ and $\gamma_b(\tilde{\beta}_V, \tilde{\beta}_T)$, respectively. Three nontrivial things can then happen:

- (a) A first-order phase transition can occur when the two minima become degenerate [$\overline{\mathcal{F}}(\gamma_a) = \overline{\mathcal{F}}(\gamma_b)$ with $\gamma_a \neq \gamma_b$].
- (b) A second-order phase transition can occur when the two minima collide ($\gamma_a = \gamma_b$).
- (c) A second-order phase transition to a phase with long-range order can occur when γ_b reaches $1/d$, provided that it is the absolute minimum [$\gamma_b = 1/d$ with $\overline{\mathcal{F}}(\gamma_b) \leq \overline{\mathcal{F}}(\gamma_a)$].

These correspond, respectively, to the first-order curve $\tilde{\beta}_{T,c}(\tilde{\beta}_V)$, the critical endpoints $(\pm \tilde{\beta}_{V,e}, \tilde{\beta}_{T,e})$, and the second-order lines $\tilde{\beta}_{T,c'}(\tilde{\beta}_V)$ given by (5.1).

One could now construct plots of $\overline{\mathcal{F}}$ versus γ (or versus f for the condensate phase) for various values of $\tilde{\beta}_V$ and $\tilde{\beta}_T$. For example, one could look at “slices” at fixed $\tilde{\beta}_V$ and show how the shape of $\overline{\mathcal{F}}(\gamma)$ curves is deformed as $\tilde{\beta}_T$ increases (analogous to Figures 2 and 3 for $\tilde{\beta}_V = 0$). One would then see the behavior (a), (b) and (c) corresponding to the first-order transition curve, the critical endpoint and the second-order transition line. Rather than pursuing this approach in detail, however, we turn to the parametric approach, in which the same features can be observed more efficiently because one studies *all* $\tilde{\beta}_T$ in a single plot, for each fixed $\tilde{\beta}_V$.

5.3 Parametric Approach

We know that the absolute minimum of the free energy lies in the region $\text{sgn } \gamma = \text{sgn } \tilde{\beta}_V$. We therefore restrict attention to $\tilde{\beta}_V > 0$ and consider only $\gamma > 0$. For each fixed $\tilde{\beta}_V$, we

plot $\tilde{\beta}_T$ and $\overline{\mathcal{F}}$ parametrically as a function of γ , using (3.31) and (3.30b). Since $f_d(\gamma)$ is a monotonically increasing function of γ on $[0, 1/d]$, we can (and do) alternatively use f as an independent parameter in place of γ ; this has the advantage of allowing us to treat normal and condensate phases using the same independent parameter f for both of them. We use (3.31)/(3.30b) for the normal phase $1 \leq f < f_*$, and (3.37)/(3.36b) for the condensate phase $f \geq f_*$.

Figure 16 contains a “notations guide” illustrating various features of the parametric plots of $\overline{\mathcal{F}}$ versus $\tilde{\beta}_T$, to be discussed presently. In particular, points c and c' correspond, respectively, to the first-order curve $\tilde{\beta}_{T,c}(\tilde{\beta}_V)$ and the second-order lines $\tilde{\beta}_{T,c'}(\tilde{\beta}_V)$ given by (5.1). The condensate phase $f \geq f_*$ is shown (both here and in subsequent figures) as a dashed line.

In Figures 17–23 we plot $\tilde{\beta}_T$ versus f , and $\overline{\mathcal{F}}$ versus $\tilde{\beta}_T$, at different values of $\tilde{\beta}_V$ in various ranges of dimension d . Two qualitatively different cases need to be distinguished:

Case (a), $0 < d \leq 3/2$: Here $\tilde{\beta}_T$ is a strictly increasing function of f on $[1, \infty)$ for any value of $\tilde{\beta}_V$; it tends to $+\infty$ as $f \rightarrow +\infty$ ($\gamma \uparrow 1/d$). Then $\overline{\mathcal{F}}$ is a smooth function of $\tilde{\beta}_T$ for any $\tilde{\beta}_V \neq 0$. In particular, no phase transition occurs for nonzero $\tilde{\beta}_V$. The complete phase diagram is schematically shown in Figure 8. (We refrain from showing here the parametric plots, as they are so boring.)

Cases (b–f), $d > 3/2$: For $d > 3/2$, the generic behavior $\tilde{\beta}_T(f)$ is the following: For $0 < \tilde{\beta}_V < \tilde{\beta}_{V,e}$ there exist $f_1, f_2 \in [1, \infty)$ such that $\tilde{\beta}_T$ is a strictly increasing function of f for $1 \leq f \leq f_1$, a strictly decreasing function for $f_1 \leq f \leq f_2$, and a strictly increasing function for $f_2 \leq f < \infty$. As $\tilde{\beta}_V$ increases, the maximum at f_1 and the minimum at f_2 come closer together, and they finally collide at $f = f_e$ (or equivalently $\gamma = \gamma_e$) when $\tilde{\beta}_V = \tilde{\beta}_{V,e}$. This point is given by the solution of the simultaneous equations $d\tilde{\beta}_T/d\gamma = 0$ and $d^2\tilde{\beta}_T/d\gamma^2 = 0$ (see Figure 24 for a plot of γ_e versus d). Beyond this point, $\tilde{\beta}_T$ is a strictly increasing function of f on the entire domain $1 \leq f < \infty$.

This behavior of $\tilde{\beta}_T(f)$ is reflected in the parametric plot $\overline{\mathcal{F}}(\tilde{\beta}_T)$, where the values f_1 and f_2 correspond to the cusp singularities “1” and “2” of the triangle-shaped structure shown schematically in Figure 16. This is exemplified in Figure 17, which shows the $d = 2$ case. The “triangle” becomes smaller as $\tilde{\beta}_V$ increases (Figure 17a,b,c) and disappears as $\tilde{\beta}_V \uparrow \tilde{\beta}_{V,e}$ (Figure 17d).

For $3/2 < d \leq 2$, a first-order phase transition occurs at the point of self-intersection (point c in Figure 16) for all $0 < \tilde{\beta}_V < \tilde{\beta}_{V,e}$. The coordinates $\tilde{\beta}_{T,c}(\tilde{\beta}_V)$ of this transition are found by solving the system $\tilde{\beta}_T(\gamma_1, d, \tilde{\beta}_V) = \tilde{\beta}_T(\gamma_2, d, \tilde{\beta}_V)$ and $\overline{\mathcal{F}}(\gamma_1, d, \tilde{\beta}_V) = \overline{\mathcal{F}}(\gamma_2, d, \tilde{\beta}_V)$. They form two symmetric slightly convex branches on the phase diagram, as shown in Figure 9 for the case $d = 2$.²¹ The triple point $\tilde{\beta}_{T,c}(0)$ is a slightly decreasing function of d , as shown in Figure 1.

For $d > 2$, we need to consider also the branch coming from the condensate phase $f \geq f_*$ with $\gamma = 1/d$ (shown by a dashed line in Figures 16–23). The beginning of this branch

²¹ Magnoli and Ravanini [2, Figure 2] correctly found the endpoint $(\tilde{\beta}_{V,e}, \tilde{\beta}_{T,e}) \approx (0.0134, 0.905)$ with $\gamma_e \approx 0.411$, but incorrectly drew the transition curve as concave and as smooth at $\tilde{\beta}_V = 0$. They also failed to notice the first-order transition curve at $\tilde{\beta}_V = 0$, $\tilde{\beta}_T > \tilde{\beta}_{T,c}$.

at point c' (Figure 16) corresponds to $f = f_*$. A key role is played by the position of c' relative to the points c , 2 and 1 (and therefore to the internal structure of the “triangle”); this depends on d and on $\tilde{\beta}_V$. We have to distinguish several cases:

Case (c), $2 < d < d_* \approx 2.38403$: The evolution of $\tilde{\beta}_T(f)$ follows the generic pattern described earlier for $d > 3/2$. For small values of $\tilde{\beta}_V$ (Figure 18a,b,c,d) there are two phase transitions: a first-order transition at point c of the “triangle”, and a normal-to-condensate second-order transition at point c' , which lies *outside* the “triangle”. These correspond on the phase diagram (Figure 10) to the first-order curve $\tilde{\beta}_{T,c}(\tilde{\beta}_V)$ and the second-order lines $\tilde{\beta}_{T,c'}(\tilde{\beta}_V)$, respectively. As we increase $\tilde{\beta}_V$, the “triangle” shrinks and finally disappears at the point $(\tilde{\beta}_{V,e}, \tilde{\beta}_{T,e})$, shown as a dot in Figure 18e. This point corresponds to the endpoint of the solid curve in Figure 10, and is a second-order phase transition. Its evolution as a function of d is shown in Figures 14 and 15. For $\tilde{\beta}_V > \tilde{\beta}_{V,e}$, only the transition at point c' remains (dashed line in Figure 10).

Case (d), $d = d_* \approx 2.38403$: As d increases, the first-order transition curve $\tilde{\beta}_{T,c}(\tilde{\beta}_V)$ and the second-order transition lines $\tilde{\beta}_{T,c'}(\tilde{\beta}_V)$ come closer together; at $d = d_*$ they collide at $\tilde{\beta}_V = 0$, $\tilde{\beta}_{T,c} = \tilde{\beta}_{T,c'} = \tilde{\beta}_{T,*} \approx 0.873264$ (Figures 1 and 11). In terms of the parametric plot, points c and c' collide when $\tilde{\beta}_V = 0$ (Figure 7e). For all $\tilde{\beta}_V > 0$, point c' continues to lie *outside* the “triangle”, so that the rest of the scenario has the same features as the case $2 < d < d_*$ considered above.

Case (e₁), $d_* < d < \bar{d} \approx 2.55391$: At small $\tilde{\beta}_V$, the point c' lies *inside* the “triangle”, between points 2 and c ; the first-order phase transition at point c thus corresponds to a passage directly into the condensate phase (Figure 19a,b). As $\tilde{\beta}_V$ increases, the condensate branch gradually gets “expelled” from the “triangle”; we define $\tilde{\beta}_{V,cc'}$ to be the value of $\tilde{\beta}_V$ at which points c and c' coincide (Figure 19c). In Figure 25 we plot $\tilde{\beta}_{V,cc'}$ as a function of d . For $\tilde{\beta}_V > \tilde{\beta}_{V,cc'}$, the point c' lies outside the “triangle” (Figure 19d), so that the first-order transition at point c is a transition within the normal phase (just as in the case $2 < d < d_*$); there is a subsequent second-order transition at point c' to the condensate phase. Finally, at $\tilde{\beta}_V = \tilde{\beta}_{V,e}$, the “triangle” disappears (Figure 19e); this occurs within the normal phase. For $\tilde{\beta}_V > \tilde{\beta}_{V,e}$ the only phase transition is the second-order transition to the condensate phase at point c' . The complete phase diagram is shown in Figure 12.

Case (e₂), $d = \bar{d} \approx 2.55391$: The dimension \bar{d} is, by definition, the one in which point c' coincides with point 2 of the “triangle” when $\tilde{\beta}_V = 0$. For any $\tilde{\beta}_V > 0$, the description is identical to the one given above for the case $d_* < d < \bar{d}$.

Case (e₃), $\bar{d} < d < d_{} = 3$:** At $\tilde{\beta}_V = 0$, the start of the condensate branch (point c') lies between points 2 and 1 of the “triangle” (Figure 20a,b). As $\tilde{\beta}_V$ increases, point c' is gradually expelled from the “triangle”: first it reaches point 2 when $\tilde{\beta}_V$ equals

$$\tilde{\beta}_{V,2} = \frac{f_*(2 - f_*)}{2d}, \quad (5.2)$$

where (3.39) vanishes at $f = f_*$; then it reaches point c at $\tilde{\beta}_V = \tilde{\beta}_{V,cc'}$. Finally, the “triangle” disappears at $\tilde{\beta}_V = \tilde{\beta}_{V,e}$; it does so in the normal phase (since point c' has already been expelled from the “triangle”), so that $\gamma_e < 1/d$ (see Figure 24). This evolution is shown in detail in Figure 21a–c for the case $d = 2.75$. For $\tilde{\beta}_V > \tilde{\beta}_{V,e}$, the only remaining transition is the normal-to-condensate transition at point c' (Figure 20f). The phase diagram is identical to that for $d_* < d < \bar{d}$. In Figure 25 we plot $\tilde{\beta}_{V,2} < \tilde{\beta}_{V,cc'} < \tilde{\beta}_{V,e}$ as a function of d .

Case (f), $d \geq d_{} = 3$:** The three points $\tilde{\beta}_{V,2}$, $\tilde{\beta}_{V,cc'}$ and $\tilde{\beta}_{V,e}$ all merge at $d = d_{**} = 3$ (we demonstrate this analytically below). For $d \geq 3$, point c' stays inside the “triangle” until the “triangle” disappears at $\tilde{\beta}_V = \tilde{\beta}_{V,e}$ (see Figure 22 for $d = 3$ and Figure 23 for $d = 5$). The phase diagram for $d \geq 3$ is shown in Figure 13. The dimension $d_{**} = 3$ is equivalently characterized by noting that γ_e reaches $1/d$ as $d \uparrow 3$ (see Figure 24).²²

A curious thing happens in dimensions $d > 4$, where $f'_* \equiv f'_d(1/d)$ is finite. Then $d\tilde{\beta}_T/d\gamma$ for the normal phase, given by (3.33), can vanish at $\gamma = 1/d$: this happens when $\tilde{\beta}_V$ equals

$$\tilde{\beta}_{V,1} = \frac{f_*}{2d} \left[2 - \frac{f_*}{1 - df_*(f_* - 1)/f'_*} \right], \quad (5.3)$$

which lies strictly below $\tilde{\beta}_{V,2}$ (since $f_* > 1$ and $f'_* < \infty$) and corresponds to point c' coinciding with point 1 of the “triangle”. Indeed, this coincidence occurs for all $\tilde{\beta}_V$ in the range $\tilde{\beta}_{V,1} \leq \tilde{\beta}_V \leq \tilde{\beta}_{V,2} = \tilde{\beta}_{V,e}$; it ends only when the “triangle” disappears. See Figures 23c,d,e for an illustration of this phenomenon in $d = 5$.

Let us now prove that $d_{**} = 3$. Using the asymptotic expansion (A.15) for $f_d(\gamma)$ as $\gamma \uparrow 1/d$, we obtain

$$\frac{d\tilde{\beta}_T}{df} = p_1(d) \epsilon^{\frac{d}{2}-1} + p_2(d, \tilde{\beta}_V) \epsilon^{2-\frac{d}{2}} + O(\epsilon), \quad (5.4)$$

where $\epsilon = 1 - \gamma d > 0$ and

$$p_1(d) = \left(\frac{d}{2\pi} \right)^{d/2} \frac{\Gamma(1 - d/2)}{d(f_* - 1)} \quad (5.5)$$

$$p_2(d, \tilde{\beta}_V) = \left(\frac{2\pi}{d} \right)^{d/2} \frac{f_*(f_* - d\tilde{\beta}_V)}{(f_* - 1) \Gamma(2 - d/2)} \quad (5.6)$$

Alternatively, we can write (5.4) as a function of $f_* - f$ as $f \uparrow f_*$:

$$\frac{d\tilde{\beta}_T}{df} = -\frac{f_* - f}{d(f_* - 1)} + p_2(d, \tilde{\beta}_V) \left(\frac{-2\pi}{d \Gamma(1 - d/2)} \right)^{\frac{4-d}{d-2}} (f_* - f)^{\frac{4-d}{d-2}} + O\left((f_* - f)^{\frac{2}{d-2}} \right). \quad (5.7)$$

Let us now fix $\tilde{\beta}_V$ to the value $\tilde{\beta}_{V,2} = f_*(2 - f_*)/(2d)$ where point c' coincides with point 2 of the “triangle”. At $\tilde{\beta}_V = \tilde{\beta}_{V,2}$ the coefficient p_2 becomes

$$p_2(d, \tilde{\beta}_{V,2}) = \left(\frac{2\pi}{d} \right)^{d/2} \frac{f_*^3}{2(f_* - 1) \Gamma(2 - d/2)}. \quad (5.8)$$

²² The existence of the special dimension d_{**} , as well as the fact that $d_{**} = 3$, were found independently by Caracciolo and Pelissetto [12].

As $\epsilon \downarrow 0$ (i.e. $f \uparrow f_*$), the first term in (5.4)/(5.7) [which is negative for $2 < d < 4$] dominates for $d < 3$, while the second term (which is positive for $0 \leq d < 4$) dominates for $d > 3$; at $d = 3$ both terms are of the order $\epsilon^{1/2}$, with net coefficient $p_1(3) + p_2(3, \tilde{\beta}_{V,2}(3)) > 0$. Therefore, for any $2 < d < 3$, we have $d\tilde{\beta}_T/df < 0$ for sufficiently small $\epsilon > 0$ (i.e. for f slightly less than f_*). The condition $d\tilde{\beta}_T/df < 0$ corresponds to the existence of the back-bending branch of the “triangle” (between points 1 and 2). It means that the point $\tilde{\beta}_{V,e}$ where the “triangle” disappears is strictly larger than $\tilde{\beta}_{V,2}$. By contrast, for $d \geq 3$, we have $d\tilde{\beta}_T/df > 0$ for sufficiently small $\epsilon > 0$. This means that there is no “triangle” structure for any $\tilde{\beta}_V > \tilde{\beta}_{V,2}$; rather, the “triangle” disappears exactly at $\tilde{\beta}_V = \tilde{\beta}_{V,2}$. That is, the points $\tilde{\beta}_{V,2}$, $\tilde{\beta}_{V,cc'}$ and $\tilde{\beta}_{V,e}$ all coincide for $d \geq d_{**} = 3$.

Finally, as $d \rightarrow \infty$, we have the following asymptotic expressions for the endpoints $\tilde{\beta}_{T,e}$ and $\tilde{\beta}_{V,e}$:

$$\tilde{\beta}_{T,e} = \frac{1}{2d} + \frac{1}{2d^2} + \frac{7}{8d^3} + \frac{15}{8d^4} + \frac{153}{32d^5} + \frac{451}{32d^6} + \dots \quad (5.9)$$

$$\tilde{\beta}_{V,e} = \frac{1}{2d} - \frac{1}{8d^3} - \frac{3}{8d^4} - \frac{33}{32d^5} - \frac{3}{d^6} - \dots \quad (5.10)$$

5.4 One-Dimensional Case

The free energy in the direct approach is given by (3.12). We use the explicit expressions (A.11)/(A.12) to eliminate γ , $f(\gamma)$ and $g(\gamma)$ in favor of the variable s defined in (4.21)/(4.22):

$$\bar{\mathcal{F}}(s) = \frac{1}{2} \left[\frac{-2s^2}{1-s^2} + \frac{s^2}{\tilde{\beta}_T(1-s^2)^2} - \log(1-s^2) - \frac{\tilde{\beta}_V}{\tilde{\beta}_T} \frac{2s}{1-s^2} + \frac{\tilde{\beta}_V^2}{\tilde{\beta}_T} \right] \quad (5.11)$$

The derivative of (5.11) with respect to s is

$$\frac{d\bar{\mathcal{F}}}{ds} = \frac{(1+s^2)}{\tilde{\beta}_T(1-s^2)^3} \left[s + \tilde{\beta}_T \left(s + \frac{\tilde{\beta}_V}{\tilde{\beta}_T} \right) (s^2 - 1) \right] \quad (5.12)$$

and therefore the extremum s_* satisfies the cubic equation

$$s^3 + vs^2 - (1-r)s - v = 0, \quad (5.13)$$

where $v = \tilde{\beta}_V/\tilde{\beta}_T$ and $r = 1/\tilde{\beta}_T$. For $\tilde{\beta}_V > 0$ this cubic is strictly convex on $s > 0$, negative at $s = 0$ and positive at $s = 1$; it therefore has exactly one root $s_* \geq 0$, which is simple and lies in $0 < s_* < 1$; moreover, s_* is a real-analytic function of $\tilde{\beta}_V, \tilde{\beta}_T > 0$. For $\tilde{\beta}_V < 0$, the relevant solution is obtained by noting that (5.13) is invariant under the combined substitution $\tilde{\beta}_V \rightarrow -\tilde{\beta}_V$, $s \rightarrow -s$. There is thus no phase transition when $\tilde{\beta}_V \neq 0$. Note also that when $0 < \tilde{\beta}_T < 1$, the root $s = 0$ when $v = 0$ is simple, so that s_* is a real-analytic function of $\tilde{\beta}_V$ also at $\tilde{\beta}_V = 0$. So there is no phase transition when $\tilde{\beta}_V = 0$ and $0 < \tilde{\beta}_T < 1$. (The same obviously holds also for $\tilde{\beta}_T = 0$ and in fact also for $\tilde{\beta}_T < 0$.)

For small $\tilde{\beta}_V > 0$ we have:

1) For $\tilde{\beta}_T < 1$:

$$s_\star = \frac{\tilde{\beta}_V}{1 - \tilde{\beta}_T} + O(\tilde{\beta}_V^3) \quad (5.14)$$

$$\bar{F}(\tilde{\beta}_V, \tilde{\beta}_T) = -\frac{\tilde{\beta}_V^2}{2(1 - \tilde{\beta}_T)} + O(\tilde{\beta}_V^4) \quad (5.15)$$

2) For $\tilde{\beta}_T = 1$:

$$s_\star = |\tilde{\beta}_V|^{1/3} - \frac{|\tilde{\beta}_V|}{3} + \frac{|\tilde{\beta}_V|^{5/3}}{9} + O(|\tilde{\beta}_V|^{7/3}) \quad (5.16)$$

$$\bar{F}(\tilde{\beta}_V, \tilde{\beta}_T) = -\frac{3}{4}|\tilde{\beta}_V|^{4/3} + \frac{|\tilde{\beta}_V|^2}{6} + O(|\tilde{\beta}_V|^{8/3}) \quad (5.17)$$

3) For $\tilde{\beta}_T > 1$:

$$s_\star = \left(1 - \frac{1}{\tilde{\beta}_T}\right)^{1/2} + \frac{\tilde{\beta}_V}{2\tilde{\beta}_T(\tilde{\beta}_T - 1)} + O(\tilde{\beta}_V^2) \quad (5.18)$$

$$\bar{F}(\tilde{\beta}_V, \tilde{\beta}_T) = -\frac{1}{2}(\tilde{\beta}_T - 1 - \log \tilde{\beta}_T) - |\tilde{\beta}_V| \left(1 - \frac{1}{\tilde{\beta}_T}\right)^{1/2} + O(\tilde{\beta}_V^2) \quad (5.19)$$

We conclude that for $\tilde{\beta}_T > 1$ there is a first-order phase transition as $\tilde{\beta}_V$ passes through 0: the free energy has an absolute-value cusp, and the isovector energy E_V has a jump discontinuity. In particular, at $\tilde{\beta}_V = 0$ the Z_2 gauge symmetry is spontaneously broken. Of course, this is an artifact of the $N \rightarrow \infty$ limit, and does not occur for any finite N .

Remark. To obtain the free energy in the parametric approach, we plug this s_\star into either (3.30a) or (3.30b), using the explicit expressions (A.11)/(A.12) to eliminate both γ and g in favor of f and hence s :

$$\bar{\mathcal{F}} = \frac{1}{2} \left[\frac{-2s^2}{1-s^2} - \log(1-s^2) + \tilde{\beta}_T s^2 \right] \quad (5.20a)$$

$$= \frac{1}{2} \left[\frac{-s^2}{1-s^2} - \log(1-s^2) - \tilde{\beta}_V s \right] \quad (5.20b)$$

Finally, by the same reasoning as in Section 4.4 the correlation functions are

$$G_V(x, y) = s_\star^{|x-y|} \quad (5.21)$$

$$G_T(x, y) = s_\star^{2|x-y|} \quad (5.22)$$

6 One-Dimensional Case: Pure RP^{N-1} , CP^{N-1} and QP^{N-1} Models

In this section we compute the exact finite- N solution for the one-dimensional RP^{N-1} , CP^{N-1} and QP^{N-1} models and discuss the behavior as $N \rightarrow \infty$. We reproduce the $N = \infty$

phase transition at $\tilde{\beta}_T = 1$ found in Section 4.4, and we explain why it is an artifact of the $N \rightarrow \infty$ limit.

6.1 General N

Note first that the one-link integral

$$\mathcal{Z}_N(\beta) = \int \exp \left[\frac{\beta}{2} |\boldsymbol{\sigma}_1^* \cdot \boldsymbol{\sigma}_2|^2 \right] d\Omega(\boldsymbol{\sigma}_2) \quad (6.1)$$

is independent of the unit vector $\boldsymbol{\sigma}_1$ [since by G -invariance $\boldsymbol{\sigma}_1$ can be rotated to $(1, 0, \dots, 0)$]. It follows that for a one-dimensional *open* chain — or more generally, for any lattice which has no closed cycles (i.e. is a *forest*) — the partition function factorizes as

$$Z = \mathcal{Z}_N(\beta)^\ell \quad (6.2)$$

where ℓ is the number of links in the lattice. In particular, the infinite-volume free energy in one dimension (which is independent of boundary conditions and can thus be computed using an open chain) is

$$\bar{F}_N(\beta) = \lim_{L \rightarrow \infty} \left[-\frac{1}{L} \log \mathcal{Z}_N(\beta)^{L-1} \right] = -\log \mathcal{Z}_N(\beta). \quad (6.3)$$

So it suffices to study the one-link integral $\mathcal{Z}_N(\beta)$.

Let us study the more general integral

$$\tilde{\mathcal{Z}}_n(M) = \int e^{\mathbf{x} \cdot M \mathbf{x}} d\Omega(\mathbf{x}) \quad (6.4)$$

where M is an $n \times n$ symmetric real matrix and $d\Omega$ is normalized uniform measure on the unit sphere in \mathbb{R}^n . It is easy to see that $\mathcal{Z}_N(\beta)$ equals $\tilde{\mathcal{Z}}_{kN}(M)$ where $k = 1, 2, 4$ for $\mathbb{K} = \mathbb{R}, \mathbb{C}, \mathbb{Q}$ provided we take M to have k eigenvalues equal to $\beta/2$ and $k(N-1)$ eigenvalues equal to 0.

Diagonalizing M and then making the change of variables $\lambda_j = x_j^2$ in (6.4), we obtain

$$\tilde{\mathcal{Z}}_n(M) = c_n \int_0^\infty \left(\prod_{j=1}^n \frac{d\lambda_j}{\lambda_j^{1/2}} \right) \delta \left(\sum_{j=1}^n \lambda_j - 1 \right) \exp \left[\sum_{j=1}^n \mu_j \lambda_j \right], \quad (6.5)$$

where μ_1, \dots, μ_n are the eigenvalues of M ; here $c_n = \Gamma(n/2)/2\pi^{n/2}$ since $\tilde{\mathcal{Z}}_n(0) = 1$. Specializing now to the case $\mu_1 = \dots = \mu_k = \beta/2$ and $\mu_{k+1} = \dots = \mu_n = 0$, we change variables to $t = \lambda_1 + \dots + \lambda_k$ and obtain

$$\mathcal{Z}_N(\beta) = \frac{\Gamma(\frac{n}{2})}{\Gamma(\frac{k}{2})\Gamma(\frac{n-k}{2})} \int_0^1 e^{\beta t/2} t^{\frac{k}{2}-1} (1-t)^{\frac{n-k}{2}-1} dt \quad (6.6a)$$

$$= {}_1F_1 \left(\frac{k}{2}; \frac{n}{2}; \frac{\beta}{2} \right) \quad (6.6b)$$

where $n = kN$ and

$${}_1F_1(a; c; z) = 1 + \frac{a}{c}z + \frac{a(a+1)}{c(c+1)}\frac{z^2}{2!} + \dots \quad (6.7a)$$

$$= \frac{\Gamma(c)}{\Gamma(a)\Gamma(c-a)} \int_0^1 e^{zt} t^{a-1} (1-t)^{c-a-1} dt \quad [\text{for } \text{Re } c > \text{Re } a > 0] \quad (6.7b)$$

is the confluent hypergeometric function [59, 60, 61]. Thus,

$$\mathcal{Z}_N(\beta) = \begin{cases} {}_1F_1(\frac{1}{2}; \frac{N}{2}; \frac{\beta}{2}) & \text{for } RP^{N-1} \\ {}_1F_1(1; N; \frac{\beta}{2}) & \text{for } CP^{N-1} \\ {}_1F_1(2; 2N; \frac{\beta}{2}) & \text{for } QP^{N-1} \end{cases} \quad (6.8)$$

We remark that the CP^{N-1} case can be written in terms of elementary functions:

$${}_1F_1\left(1; N; \frac{\beta}{2}\right) = \frac{(N-1)!}{(\beta/2)^{N-1}} \left[e^{\beta/2} - \sum_{j=0}^{N-2} \frac{(\beta/2)^j}{j!} \right]. \quad (6.9)$$

(A slightly more complicated derivation of the CP^{N-1} result has been given by DiVecchia *et al.* [17, Appendix B.2]. The RP^{N-1} result is also well known [46, 34, 3].)

Finally, let us discuss the correlation functions, restricting attention for simplicity to the RP^{N-1} model. For the isovector correlation function we have

$$G_V(x, y) \equiv \langle \boldsymbol{\sigma}_x \cdot \boldsymbol{\sigma}_y \rangle = \delta_{xy}; \quad (6.10)$$

it vanishes for $x \neq y$ as a consequence of Z_2 gauge invariance. The isotensor correlation function can be computed using standard results on one-dimensional $O(N)$ -invariant σ -models²³; the result is

$$G_T(x, y) \equiv \langle \mathbf{T}_x \cdot \mathbf{T}_y \rangle \equiv \langle (\boldsymbol{\sigma}_x \cdot \boldsymbol{\sigma}_y)^2 \rangle - \frac{1}{N} = \left(1 - \frac{1}{N}\right) v_{N,2}^{|x-y|} \quad (6.11)$$

where

$$v_{N,2} = \frac{\beta}{N(N+2)} \frac{{}_1F_1(\frac{3}{2}; \frac{N}{2} + 2; \frac{\beta}{2})}{{}_1F_1(\frac{1}{2}; \frac{N}{2}; \frac{\beta}{2})} \quad (6.12a)$$

$$= \frac{1}{N-1} \left(\frac{{}_1F_1(\frac{3}{2}; \frac{N}{2} + 1; \frac{\beta}{2})}{{}_1F_1(\frac{1}{2}; \frac{N}{2}; \frac{\beta}{2})} - 1 \right) \quad (6.12b)$$

$$= \frac{N}{(N-1)\beta} \frac{{}_1F_1(\frac{3}{2}; \frac{N}{2}; \frac{\beta}{2})}{{}_1F_1(\frac{1}{2}; \frac{N}{2}; \frac{\beta}{2})} + \frac{1}{N-1} \left(\frac{N}{\beta} + 1 \right) \quad (6.12c)$$

(the equalities being proven by standard recurrence formulae for ${}_1F_1$).

²³ See e.g. [48, equations (2.33), (3.16) and (3.19)].

6.2 $N \rightarrow \infty$ Limit

The large- N limit is obtained by taking $N \rightarrow \infty$ with $\tilde{\beta} \equiv \beta/kN$ fixed.²⁴ For the free energy, this limit can be read off by applying Laplace's method to the integral (6.6a):

$$\bar{F}(\tilde{\beta}) = - \lim_{N \rightarrow \infty} \frac{1}{kN} \log \mathcal{Z}_N(kN\tilde{\beta}) = - \sup_{0 \leq t \leq 1} \frac{1}{2} [\tilde{\beta}t + \log(1-t)] \quad (6.13a)$$

$$= \begin{cases} 0 & \text{for } \tilde{\beta} \leq 1 \\ -\frac{1}{2}(\tilde{\beta} - 1 - \log \tilde{\beta}) & \text{for } \tilde{\beta} \geq 1 \end{cases} \quad (6.13b)$$

in agreement with (4.25). Thus, in the $N = \infty$ limit, the free energy exhibits a second-order phase transition at $\tilde{\beta} = 1$: the specific heat $C_H \sim \partial^2 \bar{F} / \partial \tilde{\beta}^2$ has a jump discontinuity.

On the other hand, we know that such a phase transition is impossible for any finite N . Indeed, from the integral (6.6a), it is clear that $\mathcal{Z}_N(\beta)$ is an entire analytic function of β ; and since $\mathcal{Z}_N(\beta) > 0$ for β real, it follows that $\log \mathcal{Z}_N(\beta)$ is a real-analytic function of β (see Figure 26a). How, then, can the nonanalyticity at $\tilde{\beta} = 1$ arise in the limit $N \rightarrow \infty$? The answer is that a limit of real-analytic functions need not be real-analytic: singularities can come in from the complex plane and pinch the real axis. Since $\mathcal{Z}_N(\beta)$ is analytic, the only singularities of $\log \mathcal{Z}_N(\beta)$ are at the (complex) zeros of $\mathcal{Z}_N(\beta)$. So there must be zeros of $\mathcal{Z}_N(\beta)$ very close to $\tilde{\beta} = 1$:

Theorem 6.1 *Fix $a > 0$. Then there exist, for all sufficiently large $c > 0$, complex numbers z_c^* satisfying ${}_1F_1(a; c; z_c^*) = 0$ and $\lim_{c \rightarrow \infty} (z_c^*/c) = 1$.*

In Appendix B we give two proofs of this theorem: a “soft” proof based on a direct transcription of the intuition just sketched (Appendix B.2), and a “hard” proof that provides an explicit asymptotic expansion for z_c^* in powers of $c^{-1/2}$ (Appendix B.3). Surprisingly, we have been unable to find this result anywhere in the extensive mathematical literature on confluent hypergeometric functions.

For the isotensor correlation function (6.11)/(6.12), we can apply Theorem B.1 to (6.12c) to obtain

$$\lim_{N \rightarrow \infty} v_{N,2}(N\tilde{\beta}) = \begin{cases} 0 & \text{for } \tilde{\beta} \leq 1 \\ 1 - 1/\tilde{\beta} & \text{for } \tilde{\beta} \geq 1 \end{cases} \quad (6.14)$$

in agreement with (4.28). The approach to the $N \rightarrow \infty$ limit is shown in Figure 26b.

7 One-Dimensional Case: Mixed Isovector/Isotensor Models

Let us now generalize these one-dimensional results to the mixed isovector/isotensor model (1.2).

²⁴ Some authors define $\tilde{\beta} = \beta/N$. But the present definition is more suited to treating the RP^{N-1} , CP^{N-1} and QP^{N-1} cases in a unified manner.

7.1 General N

Consider the mixed isovector/isotensor Hamiltonian

$$H = - \sum_{\langle xy \rangle} \left[\beta_V \boldsymbol{\sigma}_x \cdot \boldsymbol{\sigma}_y + \frac{\beta_T}{2} (\boldsymbol{\sigma}_x \cdot \boldsymbol{\sigma}_y)^2 \right] \quad (7.1)$$

with $\boldsymbol{\sigma}_x \in S^{N-1}$, on a one-dimensional lattice of L sites with free boundary conditions. We obtain immediately the partition function

$$Z = \mathcal{Z}_N(\beta_V, \beta_T)^\ell, \quad (7.2)$$

where $\ell = L - 1$ is the number of links and

$$\mathcal{Z}_N(\beta_V, \beta_T) = \int \exp \left[\beta_V \boldsymbol{\sigma}_1 \cdot \boldsymbol{\sigma}_2 + \frac{\beta_T}{2} (\boldsymbol{\sigma}_1 \cdot \boldsymbol{\sigma}_2)^2 \right] d\Omega(\boldsymbol{\sigma}_2) \quad (7.3)$$

is the one-link integral. The free energy is

$$\bar{F}_N(\beta_V, \beta_T) = \lim_{L \rightarrow \infty} \left[-\frac{1}{L} \log \mathcal{Z}_N(\beta_V, \beta_T)^{L-1} \right] = -\log \mathcal{Z}_N(\beta_V, \beta_T). \quad (7.4)$$

To evaluate the one-link integral (7.3), let us fix $\boldsymbol{\sigma}_1 = (1, 0, \dots, 0)$ and write $\boldsymbol{\sigma}_2 = (s_1, \dots, s_N)$, so that

$$\mathcal{Z}_N(\beta_V, \beta_T) = \frac{\Gamma(N/2)}{2\pi^{N/2}} \int \delta(s_1^2 + \dots + s_N^2 - 1) e^{\beta_V s_1 + (\beta_T/2) s_1^2} ds_1 \dots ds_N \quad (7.5a)$$

$$= \frac{\Gamma(\frac{N}{2})}{\Gamma(\frac{1}{2})\Gamma(\frac{N-1}{2})} \int_{-1}^1 (1-s^2)^{(N-3)/2} \exp \left[\beta_V s + \frac{\beta_T}{2} s^2 \right] ds. \quad (7.5b)$$

In the two limiting cases $\beta_T = 0$ and $\beta_V = 0$, we have

$$\mathcal{Z}_N(\beta_V, 0) = \Gamma(N/2) \left(\frac{2}{\beta_V} \right)^{(N-2)/2} I_{(N-2)/2}(\beta_V) \quad (7.6)$$

$$\mathcal{Z}_N(0, \beta_T) = {}_1F_1 \left(\frac{1}{2}; \frac{N}{2}; \frac{\beta_T}{2} \right) \quad (7.7)$$

where I_ν is a modified Bessel function. Expanding (7.5b) in powers of either β_T or β_V , we get the series representations

$$\mathcal{Z}_N(\beta_V, \beta_T) = \sum_{k=0}^{\infty} \frac{(\beta_T/2)^k}{k!} \frac{(1/2)_k}{(N/2)_k} {}_1F_2 \left(k + \frac{1}{2}; \frac{1}{2}; \frac{N}{2} + k; \frac{\beta_V^2}{4} \right) \quad (7.8)$$

and

$$\mathcal{Z}_N(\beta_V, \beta_T) = \sum_{k=0}^{\infty} \frac{\beta_V^{2k}}{(2k)!} \frac{(1/2)_k}{(N/2)_k} {}_1F_1 \left(k + \frac{1}{2}; \frac{N}{2} + k; \frac{\beta_T}{2} \right) \quad (7.9a)$$

$$= \sum_{k=0}^{\infty} \frac{(\beta_V/2)^{2k}}{k!} \frac{1}{(N/2)_k} {}_1F_1 \left(k + \frac{1}{2}; \frac{N}{2} + k; \frac{\beta_T}{2} \right) \quad (7.9b)$$

where $(a)_n = \Gamma(a+n)/\Gamma(a)$ is Pochhammer's symbol. Or we can have the double series

$$\mathcal{Z}_N(\beta_V, \beta_T) = \sum_{k,l=0}^{\infty} \frac{(1/2)_{k+l}}{(N/2)_{k+l} (1/2)_l} \frac{(\beta_T/2)^k (\beta_V^2/4)^l}{k! l!}, \quad (7.10)$$

which is a special case of the Kampé de Fériet double hypergeometric series [62, p. 150, equation 29] [63, Section 1.5] [64, pp. 26–27].

It is worth remarking that $\mathcal{Z}_N(\beta_V, \beta_T)$ has a kind of “Lee-Yang property”: for all $N \geq 1$ (not necessarily integer) and all $\beta_T \geq 0$, the zeros of $\mathcal{Z}_N(\beta_V, \beta_T)$ in the complex β_V -plane all lie on the imaginary axis. Indeed, for $\beta_T = 0$ this is a well-known property of the Bessel functions (7.6)²⁵; while for $\beta_T > 0$ it follows from the formula

$$\mathcal{Z}_N(\beta_V, \beta_T) = \exp\left(\frac{\beta_T}{2} \frac{\partial^2}{\partial \beta_V^2}\right) \mathcal{Z}_N(\beta_V, 0) \quad (7.11)$$

combined with the fact that the operator $\exp[(\beta_T/2) (\partial^2/\partial \beta_V^2)]$ preserves the Lee-Yang property [66]. This Lee-Yang property fails for sufficiently negative β_T , except when $N = 1$ [67].

Let us now compute the isovector and isotensor correlation functions. Standard results on one-dimensional $O(N)$ -invariant σ -models [48] yield

$$G_V(x, y) \equiv \langle \boldsymbol{\sigma}_x \cdot \boldsymbol{\sigma}_y \rangle = v_{N,1}^{|x-y|} \quad (7.12a)$$

$$G_T(x, y) \equiv \langle \mathbf{T}_x \cdot \mathbf{T}_y \rangle \equiv \langle (\boldsymbol{\sigma}_x \cdot \boldsymbol{\sigma}_y)^2 \rangle - \frac{1}{N} = \left(1 - \frac{1}{N}\right) v_{N,2}^{|x-y|} \quad (7.12b)$$

where

$$v_{N,1} = \frac{\int_{-1}^1 s (1-s^2)^{(N-3)/2} e^{\beta_V s + (\beta_T/2)s^2} ds}{\int_{-1}^1 (1-s^2)^{(N-3)/2} e^{\beta_V s + (\beta_T/2)s^2} ds} \quad (7.13a)$$

$$v_{N,2} = \frac{\int_{-1}^1 \frac{s^2-1/N}{1-1/N} (1-s^2)^{(N-3)/2} e^{\beta_V s + (\beta_T/2)s^2} ds}{\int_{-1}^1 (1-s^2)^{(N-3)/2} e^{\beta_V s + (\beta_T/2)s^2} ds} \quad (7.13b)$$

For the N -vector model ($\beta_T = 0$) we recover the well-known result

$$v_{N,k} = \frac{I_{(N/2)+k-1}(\beta_V)}{I_{(N/2)-1}(\beta_V)}, \quad (7.14)$$

while for the pure RP^{N-1} model ($\beta_V = 0$) we recover (6.12).

²⁵ The zeros of I_ν are pure imaginary for all $\nu > -1$ [65, section 15.27], so the right-hand side of (7.6) has the Lee-Yang property for all $N > 0$. But the integral (7.5b) is convergent only for $N > 1$ (or, by a limiting process, also for $N = 1$).

7.2 $N \rightarrow \infty$ Limit in Mixed Models with Various Scalings

Let us now consider the limit $N \rightarrow \infty$ with β_V and β_T scaled as

$$\beta_V = N^\varepsilon \tilde{\beta}_V \quad (7.15a)$$

$$\beta_T = N \tilde{\beta}_T \quad (7.15b)$$

where $0 \leq \varepsilon \leq 1$. We apply Laplace's method to the integral (7.5b), which can be written in the form

$$\mathcal{Z}_N(\beta_V, \beta_T) = \frac{\Gamma(\frac{N}{2})}{\Gamma(\frac{1}{2})\Gamma(\frac{N-1}{2})} \int_{-1}^1 (1-s^2)^{-3/2} e^{-N\mathcal{F}(s)} ds \quad (7.16)$$

where

$$\mathcal{F}(s) = -\frac{1}{2} \log(1-s^2) - \frac{\tilde{\beta}_T}{2} s^2 - N^{\varepsilon-1} \tilde{\beta}_V s. \quad (7.17)$$

If $0 \leq \varepsilon < 1$, the behavior at $N = \infty$ is exactly as in the pure RP^{N-1} model ($\tilde{\beta}_V = 0$): for $\tilde{\beta}_T \leq 1$, $\mathcal{F}(s)$ has an absolute minimum at $s = 0$; while for $\tilde{\beta}_T > 1$, $\mathcal{F}(s)$ has a local maximum at $s = 0$ and absolute minima at $s = \pm s_0$, where

$$s_0 = \left(1 - \frac{1}{\tilde{\beta}_T}\right)^{1/2}. \quad (7.18)$$

There is therefore a second-order phase transition for $\tilde{\beta}_T = 1$, and the value of $\tilde{\beta}_V$ plays no role.

However, for $\varepsilon = 1$ the situation is very different. The stationary points of the function $\mathcal{F}(s)$ are the solutions of the cubic equation

$$s^3 + vs^2 - (1-r)s - v = 0, \quad (7.19)$$

where $v = \tilde{\beta}_V/\tilde{\beta}_T$ and $r = 1/\tilde{\beta}_T$. The absolute minimum of \mathcal{F} is given by the unique root s_* of (7.19) lying in the interval $0 \leq (\text{sgn } \tilde{\beta}_V)s \leq 1$.²⁶ This is exactly the same cubic equation (5.13) found in Section 5.4, even though the free energy is different [compare (5.11) with (7.17)].²⁷ We therefore draw the same conclusions: there is no phase transition when $\tilde{\beta}_V \neq 0$ or $0 \leq \tilde{\beta}_T < 1$; but for $\tilde{\beta}_T > 1$ (resp. $\tilde{\beta}_T = 1$) there is a first-order (resp. second-order) phase transition as $\tilde{\beta}_V$ passes through 0.

The phase transition observed as $\tilde{\beta}_V$ passes through 0 when $\tilde{\beta}_T \geq 1$ can be understood as arising from pure-imaginary zeros of $\mathcal{Z}_N(\beta_V, \beta_T)$ in the complex $\tilde{\beta}_V$ -plane that approach the origin as $N \rightarrow \infty$. Indeed, Laplace's method applied to (7.5b) immediately yields

$$\lim_{N \rightarrow \infty} \frac{\mathcal{Z}_N(\beta_V, N\tilde{\beta}_T)}{\mathcal{Z}_N(0, N\tilde{\beta}_T)} = \cosh(\beta_V s_0) \quad (7.20)$$

²⁶ Using elementary monotonicity arguments one can show that for any $\tilde{\beta}_T$ and nonzero $\tilde{\beta}_V$, equation (7.19) always has a unique real root in the interval $0 \leq (\text{sgn } \tilde{\beta}_V)s \leq 1$.

²⁷ We remark that (7.17) = 2(5.20b) - (5.20a).

where

$$s_0 = \begin{cases} 0 & \text{for } \tilde{\beta}_T \leq 1 \\ \left(1 - \frac{1}{\tilde{\beta}_T}\right)^{1/2} & \text{for } \tilde{\beta}_T \geq 1 \end{cases} \quad (7.21)$$

It follows that if $\tilde{\beta}_T > 1$, $\mathcal{Z}_N(\beta_V, N\tilde{\beta}_T)$ has (for all sufficiently large N) zeros in the complex β_V -plane that tend to $\pm(2k+1)\pi i/2s_0$ as $N \rightarrow \infty$. (As mentioned previously, we know that these zeros lie on the imaginary axis for all N .) In the variable $\tilde{\beta}_V \equiv \beta_V/N$, these zeros tend to the origin at a rate $1/N$, producing a phase transition in the limit. For $0 \leq \tilde{\beta}_T < 1$, by contrast, the zeros in the β_V -plane scale with N and thus stay a finite distance away from the origin in the $\tilde{\beta}_V$ -plane. Indeed, the closest zeros to the origin lie on the imaginary axis at the $\tilde{\beta}_V$ value where two saddle points given by (7.19) collide, namely

$$\tilde{\beta}_V = \pm \frac{(r - 4 + \sqrt{r^2 + 8r}) \sqrt{r + 2 - \sqrt{r^2 + 8r}}}{4\sqrt{2}r} \quad (7.22)$$

where $r = 1/\tilde{\beta}_T > 1$; this goes monotonically from $\pm i/2$ at $\tilde{\beta}_T = 0$ to zero at $\tilde{\beta}_T = 1$ (see Figure 27).²⁸ The corrections to (7.22) are presumably of order $N^{-2/3}$, as they are at $\tilde{\beta}_T = 0$.²⁹ For $\tilde{\beta}_T = 1$, the zeros in the β_V -plane presumably scale as a fractional power of N ; empirically we find that they scale like $N^{1/3}$, exactly like the leading correction term for $0 \leq \tilde{\beta}_T < 1$ (see Figure 28).

Let us conclude by considering the correlation functions (7.12)/(7.13) in the limit $N \rightarrow \infty$ with $\tilde{\beta}_V, \tilde{\beta}_T$ fixed. In this limit, the integrals in both numerator and denominator of (7.13) are dominated by s_* , so we obtain

$$\lim_{N \rightarrow \infty} v_{N,k}(N\tilde{\beta}) = s_*^k \quad (7.23)$$

for $k = 1, 2$, in complete agreement with (5.21)/(5.22). We thus verify by explicit calculation the factorization (2.23) in the $N \rightarrow \infty$ limit. Of course, this solution exhibits the (spurious) spontaneous breaking of Z_2 gauge invariance at $\tilde{\beta}_V = 0$ and $\tilde{\beta}_T > 1$, when $N = \infty$.

8 Conclusions

What is the phase diagram of the mixed isovector/isotensor model (1.2) for large but finite N ? We know some things for sure:

²⁸ With a bit more work one can presumably show that the free energy $\bar{F} = -\lim_{N \rightarrow \infty} (1/N) \log \mathcal{Z}_N(N\tilde{\beta}_V, N\tilde{\beta}_T)$ has a branch cut on the imaginary axis starting at the points (7.22). From this it would follow, by the methods of Appendix B.2, that zeros of $\mathcal{Z}_N(N\tilde{\beta}_V, N\tilde{\beta}_T)$ accumulate densely on this cut as $N \rightarrow \infty$.

²⁹ At $\tilde{\beta}_T = 0$ we have $\mathcal{Z}_N(\beta_V, 0) \sim I_{(N-2)/2}(\beta_V)$, and the first root of $I_\nu(z)$ is given by $z = \pm i j_{\nu,1}$ where

$$j_{\nu,1} \simeq \nu + 1.85575\nu^{1/3} + 1.03315\nu^{-1/3} - 0.00397\nu^{-1} + \dots$$

[65, section 15.8] [68, equation 9.5.14]. We have no proof that this same scaling of the correction terms persists for $0 < \tilde{\beta}_T < 1$, but it seems plausible and is consistent with our numerical calculations.

- (a) In dimension $d \leq 1$, no phase transitions of any kind are possible in the finite (β_V, β_T) -plane [42, 43, 44].
- (b) In dimension $d \leq 2$, no spontaneous breaking of the $SO(N)$ global symmetry is possible in the finite (β_V, β_T) -plane [69, 70, 71]. In particular, magnetic and nematic long-range order are impossible, and all correlation functions decay at least as an inverse power of the distance [72, 53].
- (c) No spontaneous breaking of the Z_2 gauge invariance at $\beta_V = 0$ is possible in any dimension [45].

In addition, some properties of the phase diagram in dimension $d > 2$ are known rigorously:

- (d) All correlation functions $\langle (\boldsymbol{\sigma}_{x_1} \cdot \boldsymbol{\sigma}_{y_1}) \cdots (\boldsymbol{\sigma}_{x_n} \cdot \boldsymbol{\sigma}_{y_n}) \rangle$ in the mixed isovector/isotensor model at (β_V, β_T) are bounded above by the corresponding Ising-model correlation functions $\langle \varepsilon_{x_1} \varepsilon_{y_1} \cdots \varepsilon_{x_n} \varepsilon_{y_n} \rangle$ at $\beta = |\beta_V|$: we prove this in Appendix C (Theorem C.5 and Corollary C.6). In particular, for $|\beta_V| \leq \beta_{c,Ising}$ there is no ferromagnetic or antiferromagnetic long-range order.
- (e) For $\beta_V > Nf_*/(2d)$ there is ferromagnetic long-range order [53, 54]. Likewise, for $\beta_V < -Nf_*/(2d)$ there is antiferromagnetic long-range order.
- (f) For $\beta_T > \frac{N^2(N+1)f_*}{2(N-1)2d}$ there is nematic long-range order [52, 53, 54].

Facts (e) and (f) are proven by the method of infrared bounds [73, 74, 75]. It is noteworthy that (e) is asymptotically sharp as $N \rightarrow \infty$ when $\beta_T = 0$: it captures the leading large- N behavior (5.1) of the pure N -vector model. By contrast, (f) is a very poor bound for large N : it behaves as N^2 while the true critical point is presumably of order N .

One of the most striking aspects of the $N = \infty$ solution is that it violates fact (c): spontaneous breaking of the Z_2 gauge invariance occurs at $N = \infty$ whenever the absolute minimum of the free energy in the pure RP^{N-1} model is located at $\gamma \neq 0$ [cf. the discussion surrounding (3.17)]. But the distinction at $N = \infty$ between the white-noise phase ($\gamma = 0$) and the isotropic phase ($0 < \gamma < 1/d$) does not survive to finite N . Indeed, at finite N the correlation functions *never* have the white-noise form (except of course at $\beta_T = 0$). Rather, the white-noise “phase” $0 < \tilde{\beta}_T < \tilde{\beta}_{T,c}$ (or $0 < \tilde{\beta}_T < \tilde{\beta}_{T,c''}$ in dimensions $d > d_*$) simply corresponds to the region where γ is of order $1/N$ [and hence the mass gap (3.9) is of order $\log N$] when $N \rightarrow \infty$ at fixed $\tilde{\beta}_T$, while the isotropic “phase” corresponds to the region where γ and the mass gap are of order 1 when $N \rightarrow \infty$ at fixed $\tilde{\beta}_T$. There is no sharp distinction between these two regions at any finite N ; rather, for each finite N , the white-noise and isotropic “phases” both belong to a single paramagnetic phase in which the isotensor mass gap m_T is finite and nonzero. This behavior is seen explicitly in the $d = 1$ solution (6.11)/(6.12)/(6.14) [see Figure 26b]; we conjecture that it constitutes the correct interpretation of the “white-noise-to-isotropic (pseudo)transition” in all dimensions. Likewise, the spontaneous breaking of the Z_2 gauge invariance in the isotropic “phase” at $N = \infty$, arising from the absolute-value cusp in the free energy $\bar{F} = \bar{F}_0 - O(|\beta_V|)$ as $\tilde{\beta}_V$ passes through 0, cannot survive to finite N ; the behavior at small β_V *must* be smooth [45]. Rather, we can understand the white-noise “phase” $0 < \tilde{\beta}_T < \tilde{\beta}_{T,c}$ (or $0 < \tilde{\beta}_T < \tilde{\beta}_{T,c''}$) as

corresponding to the region where this rounding takes place over a β_V interval of order N , while the isotropic “phase” $\tilde{\beta}_T > \tilde{\beta}_{T,c}$ (or $\tilde{\beta}_T > \tilde{\beta}_{T,c''}$) corresponds to the region where this rounding takes place over a β_V interval of order $o(N)$. Once again, this behavior is seen explicitly in the $d = 1$ solution, where the rounding in the isotropic “phase” takes place over a β_V interval of order 1 [cf. the discussion surrounding (7.20)/(7.21)]; we conjecture that this constitutes the correct interpretation of the “spontaneous breaking of Z_2 gauge invariance” in all dimensions.

Putting facts (a)–(f) together with our analysis of the large- N limit — and its pathologies in $d = 1$ — we are led to conjecture the phase diagram shown in Figure 29 for the finite- N mixed isovector/isotensor model in dimensions $d > 2$. When both β_T and $|\beta_V|$ are small, there is a paramagnetic phase in which both the isovector and isotensor correlation functions decay exponentially; in particular, there is no long-range order of any kind. Along the $\beta_T = 0$ axis (pure N -vector model), there is a second-order paramagnetic-to-ferromagnetic transition at $\beta_V = \beta_{c,N\text{-vector}}$, and a second-order paramagnetic-to-antiferromagnetic transition at $\beta_V = -\beta_{c,N\text{-vector}}$; for large N we have $\beta_{c,N\text{-vector}} = Nf_*/(2d) + O(1)$. At the opposite extreme $\beta_T = +\infty$, the spins are forced to point up or down along a single axis, so the $O(N)$ -invariant correlations are those of an Ising model with coupling β_V ; therefore, there is a second-order paramagnetic-to-ferromagnetic transition at $\beta_V = \beta_{c,Ising}$ and a second-order paramagnetic-to-antiferromagnetic transition at $\beta_V = -\beta_{c,Ising}$ (independent of N). It is reasonable to conjecture that the paramagnetic-to-ferromagnetic transitions at $\beta_T = 0$ and $\beta_T = +\infty$ are the endpoints of a continuous curve of paramagnetic-to-ferromagnetic transitions; moreover, this curve $\beta_{V,c}(\beta_T)$ should be monotone decreasing (since β_V and β_T both promote ferromagnetic ordering). In the entire region to the right of this curve, there is ferromagnetic long-range order. It is also reasonable to conjecture, though this is much less certain, that the transition remains second-order everywhere along this curve. There is, of course, a symmetrical paramagnetic-to-antiferromagnetic transition curve in the half-plane $\beta_V < 0$.

Finally, along the $\beta_V = 0$ axis (pure RP^{N-1} model), there is a paramagnetic-to-nematic transition at $\beta_T = \beta_{c,RP^{N-1}}$. On the basis of mean-field theory [34, 3, 55, 56] and Monte Carlo simulations (for $d = 3$, $N = 3, 4, 5$) [34], this transition is expected to be first-order for all $N > 2$, at least in dimensions $d \geq 3$.³⁰ (Perhaps the transition is second-order for $2 < d < d_*$.³¹) We expect that $\beta_{c,RP^{N-1}}$ scales for large N proportional to N ; we predict (but with less confidence) that the limiting proportionality constant is $\tilde{\beta}_{T,c'}$ [defined by (4.9)] when $2 < d < d_*$, and $\tilde{\beta}_{T,c''}$ [defined by (4.13)] when $d \geq d_*$.

What about the first-order transition curve $\tilde{\beta}_{T,c}(\tilde{\beta}_V)$ found at $N = \infty$ in dimensions $d > 3/2$ (Figures 9–13) — does it survive to finite N ? We doubt it: this transition is the extension to $\tilde{\beta}_V \neq 0$ of the “white-noise-to-isotropic transition” of the RP^{N-1} model, which we have argued is an artifact of the $N = \infty$ limit. Moreover, extensive Monte Carlo

³⁰ By contrast, for $N = 2$ the RP^{N-1} model is equivalent, via the change of variables $\theta' = 2\theta$, to the standard XY model, so the transition is second-order.

³¹ Of course, it is far from clear what noninteger dimensions d should be taken to *mean* nonperturbatively. But one can also study the 2-dimensional model with power-law-decaying long-range interaction $K_{xy} \sim |x - y|^{-(d+2-\sigma)}$ ($\sigma > 0$ small), which should behave qualitatively like the putative short-range model in dimension $d = 2 + \sigma$.

simulations of the two-dimensional mixed isovector/isotensor model for $N = 3$, along with preliminary simulations of the two-dimensional RP^{N-1} models for $N = 4, 6, 8$, showed no sign of any first-order transition [16].

One plausible scenario is the following: All transitions (whether first-order or second-order) within the “normal phase” $|\gamma| < 1/d$ are artifacts of the $N = \infty$ limit, but transitions (whether first-order or second-order) into the “condensate phase” $|\gamma| = 1/d$ do survive to finite N . In this scenario, the transition curve in the limit $N \rightarrow \infty$ would be given by the upper envelope of the transitions shown in Figures 10–13: namely, by the line $\tilde{\beta}_{T,c'}(\tilde{\beta}_V)$ defined by (5.1) for $2 < d \leq d_*$, and by $\max[\tilde{\beta}_{T,c}(\tilde{\beta}_V), \tilde{\beta}_{T,c'}(\tilde{\beta}_V)]$ for $d > d_*$. Most likely, this curve corresponds to the part TF–F1 of the paramagnetic-to-ferromagnetic transition curve. In particular, point TF would lie at a β_V value that is $o(N)$ [e.g. most likely of order 1] and a β_T value that is close to $N\tilde{\beta}_{T,c'}$ [resp. $N\tilde{\beta}_{T,c}$] for $2 < d \leq d_*$ [resp. $d > d_*$], so that as $N \rightarrow \infty$ the whole curve N–TF is compressed to the point $\tilde{\beta}_V = 0$, $\tilde{\beta}_T = \tilde{\beta}_{T,c'}$ [resp. $\tilde{\beta}_T = \tilde{\beta}_{T,c}$]. Moreover, the whole nematic region (bounded by AF2–TA–N–TF–F2) is compressed at $N = \infty$ to the line $\tilde{\beta}_V = 0$, $\tilde{\beta}_T \geq \tilde{\beta}_{T,c'}$ [resp. $\tilde{\beta}_T \geq \tilde{\beta}_{T,c}$]; this compression is what produces the spurious first-order transition as this line is crossed. It would be useful to test these predictions by Monte Carlo simulation of the 3-dimensional mixed isovector/isotensor model for various values of N .

In dimensions $d \leq 2$ we expect that there are no phase transitions of any kind in the finite (β_V, β_T) -plane. However, for $1 < d \leq 2$ there is an Ising-like phase transition at $\beta_T = +\infty$, $\beta_V = \beta_{c,Ising}$; and it is at present unclear whether “new” continuum limits — that is, continuum theories whose isotensor correlation functions differ from those of the continuum limit of the pure N -vector model — can be obtained by approaching this point [11, 13, 14, 15] (see also [48, 49, 50] for the analogous problem in $d = 1$).

A The Lattice Propagator and Free Energy

A.1 Formulae

In this appendix we record some needed formulae concerning the lattice propagator and free energy

$$f_d(\gamma) = \int \frac{d^d p}{(2\pi)^d} \left[1 - \gamma \sum_{i=1}^d \cos p_i \right]^{-1} \quad (\text{A.1})$$

$$g_d(\gamma) = \int \frac{d^d p}{(2\pi)^d} \log \left[1 - \gamma \sum_{i=1}^d \cos p_i \right] \quad (\text{A.2})$$

which are well-defined for $|\gamma| \leq 1/d$ [with $f_d(\pm 1/d) = \infty$ for $d \leq 2$]. Inserting the integral representations

$$\frac{1}{z} = \int_0^\infty e^{-tz} dt \quad (\text{A.3})$$

$$\log z = \int_0^{\infty} \frac{e^{-t} - e^{-tz}}{t} dt \quad (\text{A.4})$$

and performing the momentum-space integrals, we obtain

$$f_d(\gamma) = \int_0^{\infty} e^{-t} I_0(\gamma t)^d dt \quad (\text{A.5})$$

$$g_d(\gamma) = \int_0^{\infty} \frac{e^{-t}}{t} [1 - I_0(\gamma t)^d] dt \quad (\text{A.6})$$

where I_0 is a modified Bessel function. This defines an analytic continuation to non-integer d .

Note also the relations

$$\frac{df_d(\gamma)}{d\gamma} = \frac{1}{\gamma} \int_0^{\infty} (t-1) e^{-t} I_0(\gamma t)^d dt \quad (\text{A.7})$$

$$\frac{dg_d(\gamma)}{d\gamma} = -\frac{f_d(\gamma) - 1}{\gamma} \quad (\text{A.8})$$

which can be obtained by writing

$$\frac{d}{d\gamma} I_0(\gamma t)^d = \frac{t}{\gamma} \frac{d}{dt} I_0(\gamma t)^d \quad (\text{A.9})$$

and integrating by parts. In particular, we have

$$\begin{aligned} \gamma f'_d(\gamma) + f_d(\gamma) &= \int_0^{\infty} t e^{-t} I_0(\gamma t)^d dt \\ &= \int_0^{\infty} dt_1 \int_0^{\infty} dt_2 e^{-t_1-t_2} I_0(\gamma(t_1+t_2))^d \\ &\geq \int_0^{\infty} dt_1 \int_0^{\infty} dt_2 e^{-t_1-t_2} I_0(\gamma t_1)^d I_0(\gamma t_2)^d \\ &= f_d(\gamma)^2 \end{aligned} \quad (\text{A.10})$$

for all $d \geq 0$ (with strict inequality for $d > 0$), since $\log I_0$ is a convex function and satisfies $\log I_0(0) = 0$.³² It follows that $(f_d - 1)/\gamma f_d$ is an increasing function of γ .

³² The convexity of $\log I_0$ follows easily from Hölder's inequality applied to the integral representation

$$I_0(t) = \int_{-\pi}^{\pi} \frac{dp}{2\pi} e^{t \cos p}$$

The cases $d = 1, 2$ can be expressed in terms of standard functions:

$$f_d(\gamma) = \begin{cases} (1 - \gamma^2)^{-1/2} & \text{for } d = 1 \\ \frac{2}{\pi} K(2\gamma) & \text{for } d = 2 \end{cases} \quad (\text{A.11})$$

where K is a complete elliptic integral of the first kind. The case $d = 3$ can also be expressed in terms of the elliptic integral K , but the result is a god-awful mess [77, 78, 79]. Similarly we have³³

$$g_d(\gamma) = \begin{cases} \log\left(\frac{1 + \sqrt{1 - \gamma^2}}{2}\right) & \text{for } d = 1 \\ -\frac{\gamma^2}{2} {}_4F_3\left(1, \frac{3}{2}, \frac{3}{2}, 1; 2, 2, 2; 4\gamma^2\right) & \text{for } d = 2 \end{cases} \quad (\text{A.12})$$

In general dimension we have the expansions for small γ :

$$\begin{aligned} f_d(\gamma) = & 1 + \frac{d}{2}\gamma^2 + \frac{3d(2d-1)}{8}\gamma^4 + \frac{5d(6d^2-9d+4)}{16}\gamma^6 \\ & + \frac{35d(24d^3-72d^2+82d-33)}{128}\gamma^8 + \frac{63d(120d^4-600d^3+1250d^2-1225d+456)}{256}\gamma^{10} \\ & + \frac{231d(720d^5-5400d^4+17700d^3-30600d^2+27041d-9460)}{1024}\gamma^{12} \\ & + \frac{429d(5040d^6-52920d^5+249900d^4-661500d^3+1011017d^2-826336d+274800)}{2048}\gamma^{14} + \dots \end{aligned} \quad (\text{A.13})$$

$$\begin{aligned} g_d(\gamma) = & -\frac{d}{4}\gamma^2 - \frac{3d(2d-1)}{32}\gamma^4 - \frac{5d(6d^2-9d+4)}{96}\gamma^6 \\ & - \frac{35d(24d^3-72d^2+82d-33)}{1024}\gamma^8 - \frac{63d(120d^4-600d^3+1250d^2-1225d+456)}{2560}\gamma^{10} \\ & - \frac{77d(720d^5-5400d^4+17700d^3-30600d^2+27041d-9460)}{4096}\gamma^{12} \\ & - \frac{429d(5040d^6-52920d^5+249900d^4-661500d^3+1011017d^2-826336d+274800)}{28672}\gamma^{14} - \dots \end{aligned} \quad (\text{A.14})$$

We remark that for *integer* $d \geq 1$, the Taylor coefficients of f_d and $-g_d$ are all positive, as can be seen by expanding (A.1) and (A.2). But our numerical computations of the expansions (A.13)/(A.14) up to order γ^{22} suggest that this property holds *only* for integer d (that is, for every noninteger d , at least one of the Taylor coefficients is negative).

(see e.g. [76, Theorem I.2.3]). Note also that for *integer* $d \geq 1$, the inequality (A.10) can be proven directly from (A.1), using the Schwarz inequality.

³³ The explicit expression for $g_2(\gamma)$ is obtained by taking the limit $g_2(\gamma) = \lim_{\epsilon \rightarrow 0} [\Gamma(\epsilon) - R(\epsilon, \gamma)]$, where $R(\epsilon, \gamma) = \int_0^\infty t^{\epsilon-1} e^{-t} I_0^2(\gamma t) dt = \Gamma(\epsilon) {}_4F_3\left(\frac{1}{2}, \frac{3}{2}, \frac{\epsilon}{2}, \frac{\epsilon+1}{2}; 1, 1, 1; 4\gamma^2\right) = \Gamma(\epsilon) F_4\left(\frac{\epsilon}{2}, \frac{\epsilon+1}{2}; 1, 1; \gamma^2; \gamma^2\right) = \sum_{k=0}^\infty \frac{\Gamma(\epsilon+2k)}{k! \Gamma(k+1)} {}_2F_1(-k, -k; 1; 1)(\gamma/2)^{2k}$ [80]. Here $F_4(a, b; c, c'; z, \xi)$ is an Appell's function. Since ${}_2F_1(-k, -k; 1, 1) = \Gamma(2k+1)/\Gamma^2(k+1)$, we obtain $g_2(\gamma) = -\sum_{k=1}^\infty \frac{\Gamma(2k)\Gamma(2k+1)}{(k!)^4} (\gamma/2)^{2k} = -\frac{1}{8} \int_0^{4\gamma^2} {}_3F_2\left(1, \frac{3}{2}, \frac{3}{2}; 2, 2; x\right) dx = -\frac{\gamma^2}{2} {}_4F_3\left(1, \frac{3}{2}, \frac{3}{2}, 1; 2, 2, 2; 4\gamma^2\right)$. An alternate expression in terms of ${}_3F_2$ can be deduced from [78, equation 18]; we thank Professor Glasser for drawing our attention to this.

As $\gamma \uparrow 1/d$, we have the asymptotic expansions

$$f_d(\gamma) = \begin{cases} (d/2\pi)^{d/2} \Gamma(1 - \frac{d}{2})(1 - d\gamma)^{(d-2)/2} + O(1) & \text{for } 0 < d < 2 \\ -\frac{1}{\pi} \log(1 - 2\gamma) + \frac{3}{\pi} \log 2 + O\left((1 - 2\gamma) \log(1 - 2\gamma)\right) & \text{for } d = 2 \\ f_* + (d/2\pi)^{d/2} \Gamma(1 - \frac{d}{2})(1 - d\gamma)^{(d-2)/2} + O(1 - d\gamma) & \text{for } 2 < d < 4 \end{cases} \quad (\text{A.15})$$

The limiting value $f_*(d) \equiv f_d(1/d)$ is infinite for $d \leq 2$ and finite for $d > 2$. It has the known exact value for $d = 3$ [81, 79]³⁴

$$f_*(3) = \frac{12}{\pi^2} (18 + 12\sqrt{2} - 10\sqrt{3} - 7\sqrt{6}) K^2[(2 - \sqrt{3})(\sqrt{3} - \sqrt{2})] \quad (\text{A.16a})$$

$$= \frac{\sqrt{6}}{32\pi^3} \Gamma\left(\frac{1}{24}\right) \Gamma\left(\frac{5}{24}\right) \Gamma\left(\frac{7}{24}\right) \Gamma\left(\frac{11}{24}\right) \quad (\text{A.16b})$$

$$= \frac{\sqrt{3} - 1}{32\pi^3} \Gamma^2\left(\frac{1}{24}\right) \Gamma^2\left(\frac{11}{24}\right) \quad (\text{A.16c})$$

$$\approx 1.51638\ 60591\ 51978 \quad (\text{A.16d})$$

and the following approximate values for higher dimensions:

$$f_*(4) \approx 1.23946\ 71218 \quad (\text{A.17})$$

$$f_*(5) \approx 1.15630\ 81248 \quad (\text{A.18})$$

$$f_*(6) \approx 1.11696\ 33732 \quad (\text{A.19})$$

As $d \rightarrow \infty$ we have the asymptotic expansion

$$f_*(d) = 1 + \frac{1}{2d} + \frac{3}{4d^2} + \frac{3}{2d^3} + \frac{15}{4d^4} + \frac{355}{32d^5} + \frac{595}{16d^6} + \dots \quad (\text{A.20})$$

The limiting slope $f'_*(d) \equiv \lim_{\gamma \uparrow 1/d} df_d(\gamma)/d\gamma$ is infinite for $d \leq 4$ and finite for $d > 4$. Its asymptotic expansion as $d \rightarrow \infty$ is

$$f'_*(d) = 1 + \frac{3}{d} + \frac{39}{4d^2} + \frac{285}{8d^3} + \frac{2325}{16d^4} + \dots \quad (\text{A.21})$$

The limiting second derivative $f''_*(d) \equiv \lim_{\gamma \uparrow 1/d} d^2 f_d(\gamma)/d\gamma^2$ is infinite for $d \leq 6$ and finite for $d > 6$. Its asymptotic expansion as $d \rightarrow \infty$ is

$$f''_*(d) = d + 9 + \frac{207}{4d} + \frac{2265}{8d^2} + \dots \quad (\text{A.22})$$

³⁴ The formula in terms of the elliptic integral is due to Watson [81]; the formula in terms of four gamma functions is due to Glasser and Zucker [79]; the reduction to a formula involving only two gamma functions is due to Borwein and Zucker [82]. See also [83] for recent extensions. (N.B.: The original paper [79] has a typographical error in the numerical prefactor, as does [84, p. 21]. The correct prefactor, given here in (A.16b), has been reported in [83], [85, p. 126] and [87, erratum].)

The limiting value $g_*(d) \equiv g_d(1/d)$ is finite in all dimensions $d > 0$. It has the exact values

$$g_*(1) = -\log 2 \approx -0.693147 \quad (\text{A.23})$$

$$g_*(2) = \frac{4G}{\pi} - 2\log 2 \approx -0.220051 \quad (\text{A.24})$$

where $G \approx 0.915966$ is Catalan's constant, and the following approximate values for higher dimensions:

$$g_*(3) \approx -0.11837\,01593 \quad (\text{A.25})$$

$$g_*(4) \approx -0.07973\,38971 \quad (\text{A.26})$$

$$g_*(5) \approx -0.06009\,70332 \quad (\text{A.27})$$

$$g_*(6) \approx -0.04827\,96878 \quad (\text{A.28})$$

Finally, as $d \rightarrow \infty$ we have the asymptotic expansion

$$g_*(d) = -\frac{1}{4d} - \frac{3}{16d^2} - \frac{7}{32d^3} - \frac{45}{128d^4} - \frac{269}{384d^5} - \frac{805}{512d^6} + \dots \quad (\text{A.29})$$

A.2 Numerical Calculation of $f_d(\gamma)$ and its Derivatives

In this section we discuss briefly how to make accurate numerical computations of $f_d(\gamma)$ and its derivatives. What is slightly tricky is to maintain accuracy when $|\gamma|$ is near $1/d$.

The function $f_d(\gamma)$ and its first and second derivatives can be written in the following convenient way:

$$f_d(\gamma) = A_0(\gamma, d) \quad (\text{A.30})$$

$$\gamma f'_d(\gamma) = A_1(\gamma, d) - A_0(\gamma, d) \quad (\text{A.31})$$

$$\gamma^2 f''_d(\gamma) = A_2(\gamma, d) - 4A_1(\gamma, d) + 2A_0(\gamma, d) \quad (\text{A.32})$$

where

$$A_k(\gamma, d) = \int_0^\infty t^k e^{-t} I_0(\gamma t)^d dt. \quad (\text{A.33})$$

For large values of t , the integrand behaves as $t^k e^{-(1-\gamma d)t}$, so that the integral converges slowly when γ is close to $1/d$. To improve the convergence, we split the interval of t -integration into two subintervals $[0, a]$ and $[a, \infty)$, where a is chosen in such a way that for $z \geq a/d$ the function $I_0(z)^d$ is well approximated by its large- z asymptotic expansion

$$I_0(z)^d \approx \frac{e^{dz}}{(2\pi z)^{d/2}} \left[1 + \frac{d}{8z} + \frac{d(d+8)}{128z^2} + \frac{d(d^2+24d+200)}{3072z^3} + O(1/z^4) \right]. \quad (\text{A.34})$$

Introducing the subtracted quantities

$$F_0(z, d) = I_0(z)^d - \frac{e^{dz}}{(2\pi z)^{d/2}} \quad (\text{A.35})$$

$$F_1(z, d) = I_0(z)^d - \frac{e^{dz}}{(2\pi z)^{d/2}} \left(1 + \frac{d}{8z}\right) \quad (\text{A.36})$$

$$F_2(z, d) = I_0(z)^d - \frac{e^{dz}}{(2\pi z)^{d/2}} \left(1 + \frac{d}{8z} + \frac{d(d+8)}{128z^2}\right) \quad (\text{A.37})$$

we can then rewrite (A.33) as

$$A_0(\gamma, d) = \int_0^a e^{-t} I_0(\gamma t)^d dt + \int_a^\infty e^{-t} F_0(\gamma t, d) dt + \frac{(1-\gamma d)^{\frac{d}{2}-1}}{(2\pi\gamma)^{\frac{d}{2}}} \Gamma\left(1 - \frac{d}{2}, a(1-\gamma d)\right) \quad (\text{A.38})$$

$$\begin{aligned} A_1(\gamma, d) &= \int_0^a t e^{-t} I_0(\gamma t)^d dt + \int_a^\infty e^{-t} t F_1(\gamma t, d) dt + \frac{(1-\gamma d)^{\frac{d}{2}-2}}{(2\pi\gamma)^{\frac{d}{2}}} \Gamma\left(2 - \frac{d}{2}, a(1-\gamma d)\right) \\ &+ \frac{d}{8\gamma} \frac{(1-\gamma d)^{\frac{d}{2}-1}}{(2\pi\gamma)^{\frac{d}{2}}} \Gamma\left(1 - \frac{d}{2}, a(1-\gamma d)\right) \end{aligned} \quad (\text{A.39})$$

$$\begin{aligned} A_2(\gamma, d) &= \int_0^a e^{-t^2} I_0(\gamma t)^d dt + \int_a^\infty e^{-t^2} F_2(\gamma t, d) dt + \frac{(1-\gamma d)^{\frac{d}{2}-3}}{(2\pi\gamma)^{\frac{d}{2}}} \Gamma\left(3 - \frac{d}{2}, a(1-\gamma d)\right) \\ &+ \frac{d}{8\gamma} \frac{(1-\gamma d)^{\frac{d}{2}-2}}{(2\pi\gamma)^{\frac{d}{2}}} \Gamma\left(2 - \frac{d}{2}, a(1-\gamma d)\right) \\ &+ \frac{d(d+8)}{128\gamma^2} \frac{(1-\gamma d)^{\frac{d}{2}-1}}{(2\pi\gamma)^{\frac{d}{2}}} \Gamma\left(1 - \frac{d}{2}, a(1-\gamma d)\right) \end{aligned} \quad (\text{A.40})$$

where

$$\Gamma(a, z) = \int_z^\infty t^{a-1} e^{-t} dt \quad (\text{A.41})$$

is the incomplete gamma-function. In particular, at $\gamma = 1/d$ we have

$$f_*(d) \equiv f_d(1/d) = \int_0^a e^{-t} I_0(t/d)^d dt + \int_a^\infty e^{-t} F_0(t/d, d) dt + \frac{2}{d-2} \left(\frac{d}{2\pi}\right)^{\frac{d}{2}} a^{1-\frac{d}{2}} \quad (\text{A.42})$$

for $d > 2$. Using the above formulae, one can compute $f_*(3) \approx 1.5163860591520$ and compare it with the exact value (A.16).

Similar techniques can be used for $g_d(\gamma)$, but they are not really needed unless d is very close to zero.

Remark. An alternative method for computing these and similar quantities to very high precision, with rigorous error bounds, is given in [86, Appendix B]. See also [87, Appendix A and erratum] for a brief summary.

B Confluent Hypergeometric Function ${}_1F_1(a; b; b\xi)$ in the Limit $b \rightarrow \infty$

B.1 Asymptotic Expansion in Powers of $1/b$ at Fixed ξ

In this appendix we shall develop an asymptotic expansion for the confluent hypergeometric function ${}_1F_1(a; b; b\xi)$ in the limit $b \rightarrow +\infty$, where a is a fixed positive real number and $\xi = x + iy$ is a fixed complex number. Our analysis will be based on the integral representation

$${}_1F_1(a; b; z) = \frac{\Gamma(b)}{\Gamma(a)\Gamma(b-a)} \int_0^1 e^{zt} t^{a-1} (1-t)^{b-a-1} dt \quad [\text{for } \text{Re } b > \text{Re } a > 0] \quad (\text{B.1})$$

combined with Laplace's method for contour integrals [88, sections 4.6–4.10]. We have

$${}_1F_1(a; b; b\xi) = C(a, b) \int_0^1 e^{bF(t)} t^{a-1} (1-t)^{-a-1} dt, \quad (\text{B.2})$$

where

$$C(a, b) = \frac{\Gamma(b)}{\Gamma(a)\Gamma(b-a)} \quad (\text{B.3})$$

$$F(t) = \xi t + \log(1-t) \quad (\text{B.4})$$

The path of integration in (B.2) runs initially along the straight line segment from $t = 0$ to $t = 1$, but we are free to deform the contour of integration in the complex t -plane. Writing $t = u + iv$, we have

$$\text{Re } F(u, v) = xu - yv + \frac{1}{2} \log[(1-u)^2 + v^2] \quad (\text{B.5a})$$

$$\text{Im } F(u, v) = xv + yu - \arctan\left(\frac{v}{1-u}\right) \quad (\text{B.5b})$$

In particular, at the endpoints we have $F(0) = 0$ and $\text{Re } F(1) = -\infty$. There is a unique saddle point $F'(t_\star) = 0$ at $t_\star = 1 - 1/\xi$, i.e.

$$u_\star = 1 - x/(x^2 + y^2) \quad (\text{B.6a})$$

$$v_\star = y/(x^2 + y^2) \quad (\text{B.6b})$$

The value of F at this saddle point is

$$F(t_\star) = \xi - 1 - \log \xi, \quad (\text{B.7})$$

and we have in particular

$$\text{Re } F(t_\star) = x - 1 - \frac{1}{2} \log(x^2 + y^2). \quad (\text{B.8})$$

For reasons that we will explain shortly, the curve $\operatorname{Re} F(t_*) = 0$ plays a special role in characterizing the asymptotic behavior of ${}_1F_1(a; b; b\xi)$ in the limit $b \rightarrow \infty$. Let us therefore denote by \mathcal{S}_- (resp. \mathcal{S}_+) the part of the curve

$$x - 1 - \frac{1}{2} \log(x^2 + y^2) = 0 \quad (\text{B.9})$$

that lies in the region $x < 1$ (resp. $x \geq 1$), and write $\mathcal{S} = \mathcal{S}_- \cup \mathcal{S}_+$ (see Figure 30).³⁵ To the left of \mathcal{S}_+ , i.e. in the region

$$\mathcal{A} \equiv \{ \xi = x + iy : x < 1 \text{ or } x - 1 - \frac{1}{2} \log(x^2 + y^2) < 0 \}, \quad (\text{B.10})$$

we shall show that ${}_1F_1(a; b; b\xi)$ has a finite limit as $b \rightarrow \infty$. To the right of \mathcal{S}_+ , i.e. in the region

$$\mathcal{B} \equiv \{ \xi = x + iy : x > 1 \text{ and } x - 1 - \frac{1}{2} \log(x^2 + y^2) > 0 \}, \quad (\text{B.11})$$

we shall show that ${}_1F_1(a; b; b\xi)$ grows exponentially as $b \rightarrow \infty$. More precisely, we shall prove the following asymptotic expansions:

Theorem B.1

(a) For $\xi \in \mathcal{A}$, we have the asymptotic expansion

$$\begin{aligned} {}_1F_1(a; b; b\xi) &= (1 - \xi)^{-a} \left\{ 1 - \frac{a(a+1)}{2} \left(\frac{\xi}{1-\xi} \right)^2 b^{-1} \right. \\ &+ \left[\frac{a(a+1)(a+2)(a+3)}{8} \left(\frac{\xi}{1-\xi} \right)^4 + \frac{2a(a+1)(a+2)}{3} \left(\frac{\xi}{1-\xi} \right)^3 + \frac{a(a+1)}{2} \left(\frac{\xi}{1-\xi} \right)^2 - 1 \right] b^{-2} \\ &\left. + O(b^{-3}) \right\} \end{aligned} \quad (\text{B.12})$$

uniformly for ξ in compact subsets of \mathcal{A} , where $(1 - \xi)^{-a}$ is defined as the principal branch (i.e. $\arg(1 - \xi) = 0$ for ξ real < 1).

(b) For $\xi \in \mathcal{B}$, we have the asymptotic expansion

$$\begin{aligned} {}_1F_1(a; b; b\xi) &= e^{b(\xi-1-\log \xi)} b^{a-\frac{1}{2}} \frac{\sqrt{2\pi}}{\Gamma(a)} \xi(\xi-1)^{a-1} \times \\ &\left[1 + \frac{1}{12b} \left(1 + \frac{12a(a-1)}{\xi-1} + \frac{6(a-1)(a-2)}{(\xi-1)^2} \right) + O(1/b^2) \right] \end{aligned} \quad (\text{B.13})$$

uniformly for ξ in compact subsets of \mathcal{B} , where $\log \xi$ and $(\xi - 1)^{a-1}$ are defined as the principal branch (i.e. $\arg \xi = \arg(\xi - 1) = 0$ for ξ real > 1).

³⁵ This curve was introduced by Szegő [89] in connection with the zeros of the partial sums of the Taylor series of e^z [that is, $s_n(z) = \sum_{k=0}^n z^k/k!$] and of the corresponding remainders $e^z - s_n(z)$. See also [90, 91, 92].

Let us first consider region \mathcal{A} , which it is convenient to subdivide as follows:

$$\mathcal{A}_1 \equiv \{\xi = x + iy: x < 1 \text{ and } x - 1 - \frac{1}{2} \log(x^2 + y^2) \geq 0\} \quad (\text{B.14a})$$

$$\mathcal{A}_2 \equiv \{\xi = x + iy: x \leq 1 \text{ and } x - 1 - \frac{1}{2} \log(x^2 + y^2) < 0\} \quad (\text{B.14b})$$

$$\mathcal{A}_3 \equiv \{\xi = x + iy: x > 1 \text{ and } x - 1 - \frac{1}{2} \log(x^2 + y^2) < 0\} \quad (\text{B.14c})$$

Consider first the region $\text{Re } \xi \leq 1$. It is easy to see that $\text{Re } F(t) < 0$ for all real $t \in (0, 1]$, so the endpoint $t = 0$ is the dominant point on the line segment of integration in (B.2). By standard theorems on Laplace-type integrals [88, section 4.6], we obtain (B.12) provided that $\xi \neq 1$. This proves (B.12) for $\xi \in \mathcal{A}_1 \cup \mathcal{A}_2$.³⁶

Let us now demonstrate that this expansion is valid in the entire region \mathcal{A} . If $\text{Re } \xi > 1$, the real line segment $0 \leq t \leq 1$ is no longer a suitable path of integration for (B.2), because we have $\text{Re } F(t) > 0$ for small $t > 0$, so that the endpoint $t = 0$ is no longer dominant. What we need to do is to find an alternate contour of integration \mathcal{C} running from $t = 0$ to $t = 1$ such that $\text{Re } F(t) < 0$ for all $t \in \mathcal{C}$ except the endpoint $t = 0$. To see that we can indeed connect the endpoints $t = 0$ and $t = 1$ by such a contour, let us look at the curve $\text{Re } F(u, v) = 0$ in the complex t -plane. Its singular points are given by the simultaneous solutions of $\text{Re } F(u, v) = 0$ and the set of equations

$$\frac{\partial \text{Re } F(u, v)}{\partial u} \equiv x + \frac{u - 1}{(u - 1)^2 + v^2} = 0 \quad (\text{B.15a})$$

$$\frac{\partial \text{Re } F(u, v)}{\partial v} \equiv -y + \frac{v}{(u - 1)^2 + v^2} = 0 \quad (\text{B.15b})$$

Now, the unique solution of (B.15) is given precisely by the saddle point (B.6); so singular points of the curve $\text{Re } F(u, v) = 0$ can occur only when $\text{Re } F(t_*) = 0$, i.e. when $\xi \in \mathcal{S}$ (and in this case the unique singular point is the saddle point of F). Therefore, as we vary ξ , the curve $\text{Re } F(u, v) = 0$ can change its topological nature only when ξ crosses \mathcal{S} . Now, no matter what the value of ξ , the point $t = 1$ lies in the region $\text{Re } F < 0$, while the point $t = 0$ lies on its boundary. And we have already shown that when $\xi \in \mathcal{A}_1 \cup \mathcal{A}_2$, the points $t = 0$ and $t = 1$ can be connected by a path (namely, the line segment $0 \leq t \leq 1$) lying entirely in the region $\text{Re } F < 0$ except for the endpoint $t = 0$. And since we can get from \mathcal{A}_2 to anywhere in \mathcal{A}_3 without crossing \mathcal{S} , it follows that for all $\xi \in \mathcal{A}_3$ there continues to exist a path \mathcal{C} from $t = 0$ to $t = 1$ lying entirely in the region $\text{Re } F < 0$ except for the endpoint $t = 0$: see Figure 31a–c. Moreover, the same path \mathcal{C} will work for some neighborhood of the initial ξ . Therefore, the endpoint $t = 0$ is again dominant, the standard theorems apply, and we obtain the same asymptotic expansion (B.12); moreover, it is valid uniformly on compact subsets of \mathcal{A} .

³⁶ We remark that in the smaller domain $|\xi| < 1$, (B.12) can alternatively be proven by expanding the series representation

$${}_1F_1(a; b; b\xi) = \sum_{k=0}^{\infty} \frac{(a)_k}{(b)_k} \frac{(b\xi)^k}{k!}$$

term-by-term in inverse powers of b . Slater [61, p. 66] mistakenly asserts that this holds for bounded ξ , while Tricomi [60, pp. 111–112] correctly states that it works for $|\xi| < 1$.

Let us now look at the case when $\xi \in \mathcal{B}$. In this case, $\operatorname{Re} F(t_\star) > 0$, so the saddle point dominates over both endpoints [namely, $\operatorname{Re} F(0) = 0$ and $\operatorname{Re} F(1) = -\infty$]. It suffices to find a path \mathcal{C} running from $t = 0$ through the saddle point t_\star and thence to $t = 1$, such that $\operatorname{Re} F(t) < \operatorname{Re} F(t_\star)$ for all $t \in \mathcal{C}$ except $t = t_\star$. Making the change of variables $\widehat{t} = \xi(1 - t)$ [valid for $\xi \neq 0$], we find that

$$F(t) - F(t_\star) = -(\widehat{t} - 1 - \log \widehat{t}), \quad (\text{B.16})$$

so the curve $\operatorname{Re} F(t) = \operatorname{Re} F(t_\star)$ is precisely a dilated and rotated version of the Szegő curve \mathcal{S} . Moreover, the image of $t = 0$ (namely, $\widehat{t} = \xi$) lies in \mathcal{B} , while the image of $t = 1$ (namely, $\widehat{t} = 0$) lies in \mathcal{A}_1 . So each of these two points can be connected to the saddle point $t = t_\star$ (whose image is $\widehat{t} = 1$) by a path whose image lies in \mathcal{B} and \mathcal{A}_1 , respectively: see Figure 32. This provides the needed path \mathcal{C} . ■

B.2 Complex Zeros of ${}_1F_1(a; b; b\xi)$ as $b \rightarrow \infty$

We can now use some general results on the limit sets of complex zeros for certain sequences of analytic functions, proved recently by one of the authors [93], to deduce from the asymptotic expansions (B.12)/(B.13) the existence of zeros of ${}_1F_1(a; b; b\xi)$ near the Szegő curve \mathcal{S}_+ for large b .

We begin with a “real” form of the theorem:

Theorem B.2 *Let D be a domain in \mathbb{C} , and let $x_0 \in D \cap \mathbb{R}$. Let (f_m) be analytic functions on D , and let (a_m) be positive real constants such that $(|f_m|^{a_m})$ are uniformly bounded on compact subsets of D . Assume further that*

- (a) *For each $x \in D \cap \mathbb{R}$, $f_m(x)$ is real and > 0 .*
- (b) *For each $x \in D \cap \mathbb{R}$, $\lim_{m \rightarrow \infty} a_m \log f_m(x) \equiv g(x)$ exists and is finite.*
- (c) *g is not real-analytic at x_0 .*

Then, for all m sufficiently large, there exist zeros z_m^ of f_m such that $\lim_{m \rightarrow \infty} z_m^* = x_0$.*

Theorem B.2 is in fact well-known to workers in mathematical statistical mechanics: it is the contrapositive of an observation going back to Yang and Lee [94] concerning the genesis of phase transitions (see e.g. [95, Theorem 4.1, p. 51]). The proof of Theorem B.2 is, in fact, a direct transcription of the intuition sketched in Section 6. We first need a standard lemma from complex analysis:

Lemma B.3 (log exp Vitali) *Let D be a connected open subset of \mathbb{C}^n , and let $\{g_m\}_{m=1}^\infty$ be a family of analytic functions on D such that*

- (a) *For each compact $C \subset D$, $\sup_m \sup_{z \in C} \operatorname{Re} g_m(z) < \infty$*

and either

(b1) For some determining set $S \subset D$, $\lim_{m \rightarrow \infty} g_m(z)$ exists for all $z \in S$

or (b2) For some $z_0 \in D$ and all multi-indices α , $\lim_{m \rightarrow \infty} (D^\alpha g_m)(z_0)$ exists.

Then g_m converges, uniformly on compact subsets of D , to an analytic function g .

We recall that $S \subset D$ is called a *determining set* for D if g analytic on D and $g \upharpoonright S \equiv 0$ implies $g \equiv 0$. For example, any real environment (i.e. a set of the form $z_0 + U$, where U is a nonempty open subset of \mathbb{R}^n) is a determining set. For $n = 1$, any set S having an accumulation point in D is a determining set. A proof of Lemma B.3 can be found in [96, p. 343]; it is a special case of a vastly more powerful result, due to Montel (1912), on normal families of analytic functions [97, 98].

PROOF OF THEOREM B.2. Suppose the contrary, i.e. suppose that there exists an $\epsilon > 0$ and an infinite sequence $m_1 < m_2 < \dots$ such that none of the functions f_{m_i} has a zero in the set $D_\epsilon = \{z \in \mathbb{C} : |z - x_0| < \epsilon\} \subset D$. Then, since D_ϵ is simply connected, $\log f_{m_i}$ is analytic in D_ϵ (we take the branch that is real on $D_\epsilon \cap \mathbb{R}$), and $g_i \equiv (1/a_{m_i}) \log f_{m_i}$ satisfies $\lim_{i \rightarrow \infty} g_i(x) = g(x)$ for $x \in D_\epsilon \cap \mathbb{R}$. Therefore, by Lemma B.3 it follows that there exists an analytic function \tilde{g} on D_ϵ that coincides with g on $D_\epsilon \cap \mathbb{R}$. But this contradicts hypothesis (c). ■

The proof of Theorem 6.1 is now an immediate consequence of (6.13) [or (B.12)/(B.13)], once we observe that ${}_1F_1(a; c; z) \leq e^{|\operatorname{Re} z|}$ and that ${}_1F_1(a; c; z) > 0$ for z real.

Let us now state without proof a “complex” analogue of (B.2):

Theorem B.4 (Sokal [93]) *Let D be a domain in \mathbb{C} , and let $z_0 \in D$. Let (f_m) be analytic functions on D , and let (a_m) be positive real constants such that $(|f_m|^{a_m})$ are uniformly bounded on compact subsets of D . Suppose that there does not exist a neighborhood $U \ni z_0$ and a function v on U that is either harmonic or else identically $-\infty$ such that $\liminf_{m \rightarrow \infty} a_m \log |f_m(z)| \leq v(z) \leq \limsup_{m \rightarrow \infty} a_m \log |f_m(z)|$ for all $z \in U$. Then, for all m sufficiently large, there exist zeros z_m^* of f_m such that $\lim_{m \rightarrow \infty} z_m^* = z_0$.*

The proof, which is not difficult, can be found in [93]; it uses elementary facts from the theory of normal families [97, 98].

We can use Theorem B.4 to deduce a vast extension of Theorem 6.1 concerning the zeros of ${}_1F_1(a; b; b\xi)$ for large b . Indeed, from the leading term of the asymptotic expansions (B.12)/(B.13), we have

$$\lim_{b \rightarrow +\infty} \frac{1}{b} \log |{}_1F_1(a; b; b\xi)| = \begin{cases} 0 & \text{for } \xi \in \mathcal{A} \\ \operatorname{Re}(\xi - 1 - \log \xi) & \text{for } \xi \in \mathcal{B} \end{cases} \quad (\text{B.17})$$

We can then apply Theorem B.4 to any point $\xi_0 \in \mathcal{S}_+$ (which is the boundary between \mathcal{A} and \mathcal{B}) to deduce that:

Theorem B.5 *Fix $a > 0$ and $\xi_0 \in \mathcal{S}_+$. Then there exist, for all sufficiently large $b > 0$, complex numbers z_b^* satisfying ${}_1F_1(a; b; z_b^*) = 0$ and $\lim_{b \rightarrow \infty} (z_b^*/b) = \xi_0$.*

To the best of our knowledge, neither Theorem B.5 nor its real specialization, Theorem 6.1, can be found in the extensive literature on confluent hypergeometric functions (see [59, 60, 61, 99, 100, 90, 91, 101, 92, 102] among many others). An old theorem of Tsvetkoff [99, Theorem 7] states that for $b > 2a$, every zero of ${}_1F_1(a; b; z)$ lies in the region $\operatorname{Re} z > b - 2a$ (see also [91, Proposition 3.2] for a slight strengthening); Theorem 6.1 shows that this is asymptotically sharp as $b \rightarrow \infty$, to leading order.

B.3 Asymptotic Expansion when $\xi = 1 + b^{-1/2}\zeta$

In Section B.1 we saw that the asymptotic expansion of ${}_1F_1(a; b; b\xi)$ changes dramatically as ξ crosses the curve \mathcal{S}_+ , and in particular on the real axis as it crosses $\xi = 1$. We would now like to look more closely at the crossover behavior in a neighborhood of the point $\xi = 1$. It turns out that the right “magnification” is $b^{1/2}$: that is, we should look for an expansion of ${}_1F_1(a; b; b\xi)$ when we take $\xi = 1 + b^{-1/2}\zeta$ with ζ fixed and finite.

Theorem B.6 *Uniformly for ζ in compact subsets of the complex plane, we have the asymptotic expansion*

$${}_1F_1(a; b; b(1 + b^{-1/2}\zeta)) = \frac{\Gamma(b)}{\Gamma(b-a)} b^{-a/2} e^{\zeta^2/4} \left[D_{-a}(-\zeta) + \frac{A_1(a, \zeta)}{b^{1/2}} + \frac{A_2(a, \zeta)}{b} + O(b^{-3/2}) \right], \quad (\text{B.18})$$

where D_ν is the parabolic cylinder function

$$D_\nu(z) = \frac{e^{-z^2/4}}{\Gamma(-\nu)} \int_0^\infty e^{-zs - s^2/2} s^{-\nu-1} ds \quad (\text{B.19})$$

and

$$A_1(a, \zeta) = a(a+1)D_{-a-1}(-\zeta) - \frac{a(a+1)(a+2)}{3}D_{-a-3}(-\zeta) \quad (\text{B.20})$$

$$A_2(a, \zeta) = \frac{a(a+1)^2(a+2)}{2}D_{-a-2}(-\zeta) - \frac{\Gamma(a+4)}{\Gamma(a)} \left(\frac{1}{4} + \frac{a+1}{3} \right) D_{-a-4}(-\zeta) + \frac{\Gamma(a+6)}{18\Gamma(a)} D_{-a-6}(-\zeta) \quad (\text{B.21})$$

Corollary B.7 *For large enough real b , ${}_1F_1(a; b; b\xi)$ has complex zeros whose asymptotic expansion is given by*

$$\xi_0 = 1 + \frac{\zeta_0}{b^{1/2}} + \frac{\alpha}{b} + \frac{\beta}{b^{3/2}} + O(1/b^2) \quad (\text{B.22})$$

where ζ_0 is any zero of $D_{-a}(-\zeta)$, and

$$\alpha = a(a+1) \frac{D_{-a-1}(-\zeta_0) - \frac{1}{3}(a+2)D_{-a-3}(-\zeta_0)}{D'_{-a}(-\zeta_0)} \quad (\text{B.23})$$

$$\begin{aligned}
\beta = & \left\{ \frac{1}{2}\alpha^2 D''_{-a}(-\zeta_0) + \alpha a(a+1) [D'_{-a-1}(-\zeta_0) - \frac{1}{3}(a+2)D'_{-a-3}(-\zeta_0)] \right. \\
& + \left[\frac{a(a+1)^2(a+2)}{2} D_{-a-2}(-\zeta_0) - \frac{\Gamma(a+4)}{\Gamma(a)} \left(\frac{1}{4} + \frac{a+1}{3} \right) D_{-a-4}(-\zeta_0) \right. \\
& \left. \left. + \frac{\Gamma(a+6)}{18\Gamma(a)} D_{-a-6}(-\zeta_0) \right] \right\} / D'_{-a}(-\zeta_0) \tag{B.24}
\end{aligned}$$

To prove Theorem B.6, we start with the integral representation (B.2)–(B.4) and set $\xi = 1 + b^{-1/2}\zeta$. Expanding

$$F(t) = \xi t + \log(1-t) = (\xi-1)t - \sum_{k=2}^{\infty} \frac{t^k}{k} \tag{B.25}$$

and making the change of variables $s = b^{1/2}t$, we can write (B.2) in the form

$$\begin{aligned}
{}_1F_1(a; b; b(1 + b^{-1/2}\zeta)) = \\
C(a, b) b^{-a/2} \int_0^{b^{1/2}} e^{-s^2/2+s\zeta} \left(1 - \frac{s}{b^{1/2}}\right)^{-a-1} s^{a-1} \exp\left[-\sum_{k=3}^{\infty} \frac{s^k}{k b^{(k-2)/2}}\right] ds. \tag{B.26}
\end{aligned}$$

The blow-up of the term $(1 - s/b^{1/2})^{-a-1}$ as $s \uparrow b^{1/2}$ is harmless, as it is more than compensated (for large $b > 0$) by the suppression contained in the $\exp[-\dots]$ factor [as can be seen by examining (B.1) as $t \uparrow 1$]. Therefore, (B.26) becomes, for large b ,

$${}_1F_1(a; b; b(1 + b^{-1/2}\zeta)) = C(a, b) b^{-a/2} \int_0^{\infty} e^{-s^2/2+s\zeta} s^{a-1} ds [1 + O(b^{-1/2})] \tag{B.27a}$$

$$= C(a, b) b^{-a/2} \Gamma(a) e^{\zeta^2/4} D_{-a}(-\zeta) [1 + O(b^{-1/2})]. \tag{B.27b}$$

The corrections in powers of $b^{-1/2}$ can be easily extracted, and we arrive at expansion (B.18). Corollary B.7 then follows using the implicit function theorem. ■

C Correlation Inequalities

In this appendix we prove some correlation inequalities for N -component σ -models with Hamiltonian of the form

$$H(\{\boldsymbol{\sigma}\}) = - \sum_{\langle xy \rangle} \mathcal{V}_{xy}(\boldsymbol{\sigma}_x \cdot \boldsymbol{\sigma}_y), \tag{C.1}$$

where each spin $\boldsymbol{\sigma}_x$ is a unit vector in \mathbb{R}^N and each \mathcal{V}_{xy} is a real-valued function on $[-1, 1]$.

C.1 Tools #1: Griffiths Inequalities for the Ising Model

Consider an Ising model consisting of finitely many spins $\varepsilon_x = \pm 1$, with Hamiltonian

$$H(\{\varepsilon\}) = - \sum_A J_A \varepsilon^A . \quad (\text{C.2})$$

Here we have used the notation $\varepsilon^A = \prod_x \varepsilon_x^{A_x}$, where $A = \{A_x\}$ is an arbitrary multi-index (i.e. a vector of non-negative integers). Of course, for the Ising model it suffices to use $A_x = 0, 1$; the sum in (C.2) runs over all such multi-indices. Thus, we have allowed quite general multi-spin interactions. Of course, magnetic fields and pair interactions are included as special cases.

We then have the following well-known inequalities:

Theorem C.1 (Griffiths' first and second inequalities) *Assume that $J_A \geq 0$ for all A . Then:*

$$\begin{aligned} \text{[G-I]} \quad & \langle \varepsilon^A \rangle \geq 0 \text{ for all } A. \\ \text{[G-II]} \quad & \langle \varepsilon^A; \varepsilon^B \rangle \equiv \langle \varepsilon^A \varepsilon^B \rangle - \langle \varepsilon^A \rangle \langle \varepsilon^B \rangle \geq 0 \text{ for all } A, B. \end{aligned}$$

Theorem C.2 (Griffiths' comparison inequality) *Assume that $J_A \geq |J'_A|$ for all A . Then*

$$\text{[G-Comp]} \quad \langle \varepsilon^A \rangle_J \geq |\langle \varepsilon^A \rangle_{J'}| \text{ for all } A.$$

Elementary proofs of (vastly generalized versions of) Theorems C.1 and C.2 can be found in [103] and [104], respectively.

C.2 Tools #2: Ginibre Inequalities for the XY Model

Next consider a classical XY (plane-rotator) model consisting of finitely many spins $\theta_x \in [0, 2\pi)$, with Hamiltonian

$$H(\{\theta\}) = - \sum_A \text{Re}(J_A e^{iA \cdot \theta}) \quad (\text{C.3a})$$

$$= - \sum_A |J_A| \cos(A \cdot \theta + \arg J_A) , \quad (\text{C.3b})$$

where the sum runs over all vectors $A = \{A_x\}$ of (signed) integers, the interactions J_A are arbitrary complex numbers, and $A \cdot \theta \equiv \sum_x A_x \theta_x$. We then have the following inequalities:

Theorem C.3 (Ginibre's first and second inequalities) *Assume that $J_A \geq 0$ for all A . Then:*

$$\text{[Ginibre-I]} \quad \langle \cos A \cdot \theta \rangle \geq 0 \text{ for all } A.$$

[Ginibre–II] $\langle \cos A \cdot \theta; \cos B \cdot \theta \rangle \equiv \langle \cos A \cdot \theta \cos B \cdot \theta \rangle - \langle \cos A \cdot \theta \rangle \langle \cos B \cdot \theta \rangle \geq 0$
for all A, B .

Theorem C.4 (Ginibre comparison inequality) *Assume that $J_A \geq |J'_A|$ for all A . Then*

[Ginibre–Comp] $\langle \cos A \cdot \theta \rangle_J \geq |\langle \cos(A \cdot \theta + \varphi_A) \rangle_{J'}|$ for all A and all (real) angles φ_A .

Proofs of (generalized versions of) Theorems C.3 and C.4 can be found [105] and [106], respectively.

C.3 Correlation Inequalities for S^{N-1} σ -Models

We now prove some correlation inequalities for N -component σ -models. Our method — which is in essence due to Fröhlich [107] — is to embed an Ising or XY model into the N -component model, and then apply the Griffiths or Ginibre comparison inequality to this embedded model (which has annealed random couplings).³⁷

We consider N -component σ -models of the type

$$H(\{\boldsymbol{\sigma}\}) = - \sum_{\langle xy \rangle} \mathcal{V}_{xy}(\boldsymbol{\sigma}_x \cdot \boldsymbol{\sigma}_y) \quad (\text{C.4})$$

(and even more general models). It is convenient to split \mathcal{V}_{xy} into its even and odd parts:

$$\mathcal{V}_{xy}^\pm(s) = \frac{\mathcal{V}_{xy}(s) \pm \mathcal{V}_{xy}(-s)}{2}. \quad (\text{C.5})$$

We begin by proving that correlations in the σ -model are bounded above by the corresponding correlations in the Ising model:

Theorem C.5 *Consider a σ -model defined by the Boltzmann-Gibbs measure $Z^{-1}e^{-H(\{\boldsymbol{\sigma}\})}d\mu(\{\boldsymbol{\sigma}\})$, where H is defined by (C.4), and $d\mu(\{\boldsymbol{\sigma}\})$ is an arbitrary nonnegative measure that is invariant under the Z_2 gauge transformations $\boldsymbol{\sigma}_x \rightarrow \eta_x \boldsymbol{\sigma}_x$ ($\eta_x = \pm 1$). Then, for any set of sites $x_1, y_1, \dots, x_n, y_n$, we have*

$$|\langle (\boldsymbol{\sigma}_{x_1} \cdot \boldsymbol{\sigma}_{y_1}) \cdots (\boldsymbol{\sigma}_{x_n} \cdot \boldsymbol{\sigma}_{y_n}) \rangle_{H,\mu}| \leq \langle \varepsilon_{x_1} \varepsilon_{y_1} \cdots \varepsilon_{x_n} \varepsilon_{y_n} \rangle_{\text{Ising}, J} \langle |\boldsymbol{\sigma}_{x_1} \cdot \boldsymbol{\sigma}_{y_1}| \cdots |\boldsymbol{\sigma}_{x_n} \cdot \boldsymbol{\sigma}_{y_n}| \rangle_{H,\mu} \quad (\text{C.6a})$$

$$\leq \langle \varepsilon_{x_1} \varepsilon_{y_1} \cdots \varepsilon_{x_n} \varepsilon_{y_n} \rangle_{\text{Ising}, J} \langle (\boldsymbol{\sigma}_{x_1} \cdot \boldsymbol{\sigma}_{y_1})^2 \cdots (\boldsymbol{\sigma}_{x_n} \cdot \boldsymbol{\sigma}_{y_n})^2 \rangle_{H,\mu}^{1/2} \quad (\text{C.6b})$$

$$\leq \langle \varepsilon_{x_1} \varepsilon_{y_1} \cdots \varepsilon_{x_n} \varepsilon_{y_n} \rangle_{\text{Ising}, J}, \quad (\text{C.6c})$$

where

$$J_{xy} = \|\mathcal{V}_{xy}^-\|_\infty \equiv \sup_{s \in [-1, 1]} |\mathcal{V}_{xy}^-(s)|. \quad (\text{C.7})$$

³⁷ A slightly weaker version of this method was applied earlier by Mack and Petkova [108]. They were apparently unaware of the Griffiths and Ginibre *comparison* inequalities, so they relied instead on the (somewhat weaker) Griffiths II and Ginibre II inequalities. To satisfy the ferromagnetism hypotheses of these latter inequalities, they had to impose a “no-vortex” (or “no-monopole”) constraint. This constraint is now seen to be optional but *not* necessary.

PROOF. The proof is based on the trivial identity

$$\int F(\{\boldsymbol{\sigma}\}) d\mu(\{\boldsymbol{\sigma}\}) = \int \int F(\{\varepsilon\boldsymbol{\sigma}\}) d\mu(\{\boldsymbol{\sigma}\}) d\nu(\{\varepsilon\}), \quad (\text{C.8})$$

where $d\nu(\{\varepsilon\})$ is normalized counting measure on the configurations of Ising spins $\varepsilon_x = \pm 1$, and F is an arbitrary function. This identity expresses the Z_2 gauge invariance of $d\mu(\{\boldsymbol{\sigma}\})$.

Without loss of generality we can assume that each \mathcal{V}_{xy} is an odd function, since the even parts of \mathcal{V}_{xy} can be absorbed into μ .

Let us apply (C.8) to $F(\{\boldsymbol{\sigma}\}) = (\boldsymbol{\sigma}_{x_1} \cdot \boldsymbol{\sigma}_{y_1}) \cdots (\boldsymbol{\sigma}_{x_n} \cdot \boldsymbol{\sigma}_{y_n}) e^{-H(\{\boldsymbol{\sigma}\})}$:

$$\begin{aligned} & \int (\boldsymbol{\sigma}_{x_1} \cdot \boldsymbol{\sigma}_{y_1}) \cdots (\boldsymbol{\sigma}_{x_n} \cdot \boldsymbol{\sigma}_{y_n}) e^{-H(\{\boldsymbol{\sigma}\})} d\mu(\{\boldsymbol{\sigma}\}) \\ &= \int \int \varepsilon_{x_1} \varepsilon_{y_1} \cdots \varepsilon_{x_n} \varepsilon_{y_n} (\boldsymbol{\sigma}_{x_1} \cdot \boldsymbol{\sigma}_{y_1}) \cdots (\boldsymbol{\sigma}_{x_n} \cdot \boldsymbol{\sigma}_{y_n}) e^{-H(\{\varepsilon\boldsymbol{\sigma}\})} d\mu(\{\boldsymbol{\sigma}\}) d\nu(\{\varepsilon\}) \\ &= \int d\mu(\{\boldsymbol{\sigma}\}) (\boldsymbol{\sigma}_{x_1} \cdot \boldsymbol{\sigma}_{y_1}) \cdots (\boldsymbol{\sigma}_{x_n} \cdot \boldsymbol{\sigma}_{y_n}) \int \varepsilon_{x_1} \varepsilon_{y_1} \cdots \varepsilon_{x_n} \varepsilon_{y_n} \prod_{\langle xy \rangle} e^{\varepsilon_x \varepsilon_y \mathcal{V}_{xy}^-(\boldsymbol{\sigma}_x \cdot \boldsymbol{\sigma}_y)} d\nu(\{\varepsilon\}) \end{aligned} \quad (\text{C.9})$$

We now perform the integration over $\{\varepsilon\}$; by the Griffiths comparison inequality (Theorem C.2) we have

$$\begin{aligned} & \left| \int \varepsilon_{x_1} \varepsilon_{y_1} \cdots \varepsilon_{x_n} \varepsilon_{y_n} \prod_{\langle xy \rangle} e^{\varepsilon_x \varepsilon_y \mathcal{V}_{xy}^-(\boldsymbol{\sigma}_x \cdot \boldsymbol{\sigma}_y)} d\nu(\{\varepsilon\}) \right| \\ & \leq \langle \varepsilon_{x_1} \varepsilon_{y_1} \cdots \varepsilon_{x_n} \varepsilon_{y_n} \rangle_{\text{Ising}, J} \int \prod_{\langle xy \rangle} e^{\varepsilon_x \varepsilon_y \mathcal{V}_{xy}^-(\boldsymbol{\sigma}_x \cdot \boldsymbol{\sigma}_y)} d\nu(\{\varepsilon\}). \end{aligned} \quad (\text{C.10})$$

It follows that

$$\begin{aligned} & \left| \int (\boldsymbol{\sigma}_{x_1} \cdot \boldsymbol{\sigma}_{y_1}) \cdots (\boldsymbol{\sigma}_{x_n} \cdot \boldsymbol{\sigma}_{y_n}) e^{-H(\{\boldsymbol{\sigma}\})} d\mu(\{\boldsymbol{\sigma}\}) \right| \\ & \leq \langle \varepsilon_{x_1} \varepsilon_{y_1} \cdots \varepsilon_{x_n} \varepsilon_{y_n} \rangle_{\text{Ising}, J} \int d\mu(\{\boldsymbol{\sigma}\}) |(\boldsymbol{\sigma}_{x_1} \cdot \boldsymbol{\sigma}_{y_1}) \cdots (\boldsymbol{\sigma}_{x_n} \cdot \boldsymbol{\sigma}_{y_n})| \int \prod_{\langle xy \rangle} e^{\varepsilon_x \varepsilon_y \mathcal{V}_{xy}^-(\boldsymbol{\sigma}_x \cdot \boldsymbol{\sigma}_y)} d\nu(\{\varepsilon\}) \\ & = \langle \varepsilon_{x_1} \varepsilon_{y_1} \cdots \varepsilon_{x_n} \varepsilon_{y_n} \rangle_{\text{Ising}, J} \int |(\boldsymbol{\sigma}_{x_1} \cdot \boldsymbol{\sigma}_{y_1}) \cdots (\boldsymbol{\sigma}_{x_n} \cdot \boldsymbol{\sigma}_{y_n})| e^{-H(\{\boldsymbol{\sigma}\})} d\mu(\{\boldsymbol{\sigma}\}). \end{aligned} \quad (\text{C.11})$$

The rest follows from the Schwarz inequality together with the trivial bound $|\boldsymbol{\sigma}| \leq 1$. ■

Corollary C.6 *For the mixed isovector/isotensor model*

$$H = - \sum_{\langle xy \rangle} \left[J_{xy} \boldsymbol{\sigma}_x \cdot \boldsymbol{\sigma}_y + \frac{K_{xy}}{2} (\boldsymbol{\sigma}_x \cdot \boldsymbol{\sigma}_y)^2 \right], \quad (\text{C.12})$$

we have

$$|\langle (\boldsymbol{\sigma}_{x_1} \cdot \boldsymbol{\sigma}_{y_1}) \cdots (\boldsymbol{\sigma}_{x_n} \cdot \boldsymbol{\sigma}_{y_n}) \rangle_{J, K}| \leq \langle \varepsilon_{x_1} \varepsilon_{y_1} \cdots \varepsilon_{x_n} \varepsilon_{y_n} \rangle_{\text{Ising}, |J|}. \quad (\text{C.13})$$

Remarks. 1. The bound of Theorem C.5 and Corollary C.6 holds for arbitrary products $\prod(\boldsymbol{\sigma}_{x_i} \cdot \boldsymbol{\sigma}_{y_i})$, but it is only of interest for *isovector* correlation functions. For *isotensor* correlation functions (i.e. those in which each spin $\boldsymbol{\sigma}_x$ appears an *even* number of times), the corresponding Ising-model correlation is 1, and the bound is trivial.

2. The only restriction on the measure μ is that it be Z_2 -gauge-invariant. An interesting family of examples is given by

$$d\mu(\{\boldsymbol{\sigma}\}) = \exp \left[\beta_P \sum_{\mathcal{S}} \prod_{\langle xy \rangle \in \mathcal{S}} \text{sgn}(\boldsymbol{\sigma}_x \cdot \boldsymbol{\sigma}_y) \right] \prod_x d\Omega(\boldsymbol{\sigma}_x) \quad (\text{C.14})$$

where the sum runs over plaquettes \mathcal{S} . For $\beta_P = 0$, this is the ordinary σ -model. For $\beta_P \rightarrow +\infty$, this is the no-vortex σ -model [108, 109], in which the constraint $\prod_{\langle xy \rangle \in \mathcal{S}} \boldsymbol{\sigma}_x \cdot \boldsymbol{\sigma}_y \geq 0$ is imposed for every plaquette \mathcal{S} .

3. This proof is based on the embedding $(\varepsilon, \boldsymbol{\sigma}) \mapsto \varepsilon \boldsymbol{\sigma}$. More general embeddings could be considered, i.e. $(\varepsilon, \boldsymbol{\sigma}) \mapsto (I - P)\boldsymbol{\sigma} + \varepsilon P \boldsymbol{\sigma}$ where P is any orthogonal projection in \mathbb{R}^N . (If $\text{rank } P = 1$, this is the Wolff embedding [28, 29]; if $\text{rank } P = k$, this is the codimension- k embedding discussed in [31]; if $\text{rank } P = N$, it is the embedding used above.) We do not know whether embeddings with $\text{rank } P < N$ might be useful for proving correlation inequalities. We note, however, that the Wolff embedding has been employed for analytic purposes (rigorous lower bounds on the correlation function via a Fortuin-Kasteleyn representation) by Patrascioiu and Seiler [110] and Aizenman [111].

Next we consider bounds relating the N -component σ -model to an XY model. For simplicity we consider first an ordinary N -vector model

$$H(\{\boldsymbol{\sigma}\}) = - \sum_{\langle xy \rangle} J'_{xy} \boldsymbol{\sigma}_x \cdot \boldsymbol{\sigma}_y, \quad (\text{C.15})$$

and compare it to an XY model

$$H(\{\theta\}) = - \sum_{\langle xy \rangle} J_{xy} \cos(\theta_x - \theta_y). \quad (\text{C.16})$$

Theorem C.7 Consider an N -vector model defined by the Boltzmann-Gibbs measure $Z^{-1} e^{-H(\{\boldsymbol{\sigma}\})} d\mu(\{\boldsymbol{\sigma}\})$, where H is defined by (C.15) and $d\mu(\{\boldsymbol{\sigma}\}) = \prod_x d\Omega(\boldsymbol{\sigma}_x)$. Consider for comparison an XY model defined by the Boltzmann-Gibbs measure $Z^{-1} e^{-H(\{\theta\})} d\nu(\{\theta\})$, where H is defined by (C.16) and $d\nu(\{\theta\}) = \prod_x d\theta_x$. Assume that $|J'_{xy}| \leq J_{xy}$ for all x, y .

Then

$$|\langle \boldsymbol{\sigma}_x \cdot \boldsymbol{\sigma}_y \rangle_{N, J'}| \leq \langle \cos(\theta_x - \theta_y) \rangle_{XY, J} \quad (\text{C.17})$$

and

$$0 \leq \langle (\boldsymbol{\sigma}_x \cdot \boldsymbol{\sigma}_y)^2 \rangle_{N, J'} \leq \frac{1}{N} + \frac{(N-1)(N+2)}{N [2N - (N-2) \langle \cos 2(\theta_x - \theta_y) \rangle_{XY, J}]} \langle \cos 2(\theta_x - \theta_y) \rangle_{XY, J} \quad (\text{C.18a})$$

$$\leq \frac{1}{N} + \left(1 - \frac{1}{N}\right) \langle \cos 2(\theta_x - \theta_y) \rangle_{XY, J}. \quad (\text{C.18b})$$

PROOF. Let $R(\theta) \in SO(N)$ be the rotation through an angle θ in the 1–2 plane. We will employ an XY embedding $(\theta_x, \boldsymbol{\sigma}_x) \mapsto R(\theta_x)\boldsymbol{\sigma}_x$. The proof is based on the trivial identity

$$\int F(\{\boldsymbol{\sigma}\}) d\mu(\{\boldsymbol{\sigma}\}) = \int \int F(\{R(\theta)\boldsymbol{\sigma}\}) d\mu(\{\boldsymbol{\sigma}\}) d\nu(\{\theta\}), \quad (\text{C.19})$$

where $d\mu(\{\boldsymbol{\sigma}\})$ is uniform measure on the product of spheres, $d\nu(\{\theta\})$ is uniform measure on the product of circles, and F is an arbitrary function.

Define $\boldsymbol{\sigma}_x^\parallel = (\sigma_x^{(1)}, \sigma_x^{(2)})$ and $\boldsymbol{\sigma}_x^\perp = (\sigma_x^{(3)}, \dots, \sigma_x^{(N)})$. Let us apply (C.19) to $F(\{\boldsymbol{\sigma}\}) = (\boldsymbol{\sigma}_x^\parallel \cdot \boldsymbol{\sigma}_y^\parallel) e^{-H(\{\boldsymbol{\sigma}\})}$:

$$\begin{aligned} & \int (\boldsymbol{\sigma}_x^\parallel \cdot \boldsymbol{\sigma}_y^\parallel) e^{-H(\{\boldsymbol{\sigma}\})} d\mu(\{\boldsymbol{\sigma}\}) \\ &= \int \int \cos[\theta_x - \theta_y + \angle(\boldsymbol{\sigma}_x^\parallel, \boldsymbol{\sigma}_y^\parallel)] (1 - \boldsymbol{\sigma}_x^{\perp 2})^{1/2} (1 - \boldsymbol{\sigma}_y^{\perp 2})^{1/2} e^{-H(\{R(\theta)\boldsymbol{\sigma}\})} d\mu(\{\boldsymbol{\sigma}\}) d\nu(\{\theta\}) \end{aligned} \quad (\text{C.20})$$

where $\angle(\boldsymbol{\sigma}_x^\parallel, \boldsymbol{\sigma}_y^\parallel)$ denotes the angle between $\boldsymbol{\sigma}_x^\parallel$ and $\boldsymbol{\sigma}_y^\parallel$. Note that $H(\{R(\theta)\boldsymbol{\sigma}\})$, considered as a function of $\{\theta\}$ for fixed $\{\boldsymbol{\sigma}\}$, is an XY model with couplings $\tilde{J}_{xy} = J'_{xy} |\boldsymbol{\sigma}_x^\parallel| |\boldsymbol{\sigma}_y^\parallel| e^{i\angle(\boldsymbol{\sigma}_x^\parallel, \boldsymbol{\sigma}_y^\parallel)}$. Since $|\tilde{J}_{xy}| \leq |J'_{xy}| \leq J_{xy}$, we can perform the integration over $\{\theta\}$, using the Ginibre comparison inequality (Theorem C.4) to obtain an upper bound:

$$\begin{aligned} & \left| \int \cos[\theta_x - \theta_y + \angle(\boldsymbol{\sigma}_x^\parallel, \boldsymbol{\sigma}_y^\parallel)] e^{-H(\{R(\theta)\boldsymbol{\sigma}\})} d\nu(\{\theta\}) \right| \\ & \leq \langle \cos(\theta_x - \theta_y) \rangle_{XY, J} \int e^{-H(\{R(\theta)\boldsymbol{\sigma}\})} d\nu(\{\theta\}). \end{aligned} \quad (\text{C.21})$$

It follows that

$$\begin{aligned} & \left| \int (\boldsymbol{\sigma}_x^\parallel \cdot \boldsymbol{\sigma}_y^\parallel) e^{-H(\{\boldsymbol{\sigma}\})} d\mu(\{\boldsymbol{\sigma}\}) \right| \\ & \leq \langle \cos(\theta_x - \theta_y) \rangle_{XY, J} \int \int (1 - \boldsymbol{\sigma}_x^{\perp 2})^{1/2} (1 - \boldsymbol{\sigma}_y^{\perp 2})^{1/2} e^{-H(\{R(\theta)\boldsymbol{\sigma}\})} d\mu(\{\boldsymbol{\sigma}\}) d\nu(\{\theta\}) \\ & = \langle \cos(\theta_x - \theta_y) \rangle_{XY, J} \int (1 - \boldsymbol{\sigma}_x^{\perp 2})^{1/2} (1 - \boldsymbol{\sigma}_y^{\perp 2})^{1/2} e^{-H(\{\boldsymbol{\sigma}\})} d\mu(\{\boldsymbol{\sigma}\}). \end{aligned} \quad (\text{C.22})$$

In terms of normalized quantities, this says that

$$|\langle \boldsymbol{\sigma}_x^\parallel \cdot \boldsymbol{\sigma}_y^\parallel \rangle_{N, J'}| \leq \langle \cos(\theta_x - \theta_y) \rangle_{XY, J} \left\langle (1 - \boldsymbol{\sigma}_x^{\perp 2})^{1/2} (1 - \boldsymbol{\sigma}_y^{\perp 2})^{1/2} \right\rangle_{N, J'}. \quad (\text{C.23})$$

Now we use the inequality $ab \leq \frac{1}{2}(a^2 + b^2)$ together with global $O(N)$ invariance to conclude that

$$\begin{aligned} \left\langle (1 - \boldsymbol{\sigma}_x^{\perp 2})^{1/2} (1 - \boldsymbol{\sigma}_y^{\perp 2})^{1/2} \right\rangle & \leq \frac{1}{2} \left[\langle 1 - \boldsymbol{\sigma}_x^{\perp 2} \rangle + \langle 1 - \boldsymbol{\sigma}_y^{\perp 2} \rangle \right] \\ & = \frac{2}{N}. \end{aligned} \quad (\text{C.24})$$

Hence

$$|\langle \boldsymbol{\sigma}_x^\parallel \cdot \boldsymbol{\sigma}_y^\parallel \rangle_{N,J'}| \leq \frac{2}{N} \langle \cos(\theta_x - \theta_y) \rangle_{XY,J}. \quad (\text{C.25})$$

Using $O(N)$ invariance again in the form $\langle \boldsymbol{\sigma}_x \cdot \boldsymbol{\sigma}_y \rangle = (N/2) \langle \boldsymbol{\sigma}_x^\parallel \cdot \boldsymbol{\sigma}_y^\parallel \rangle$, we complete the proof of (C.17).

Next let us apply (C.19) to $F(\{\boldsymbol{\sigma}\}) = (\boldsymbol{\sigma}_x^\parallel \cdot \boldsymbol{\sigma}_y^\parallel)^2 e^{-H(\{\boldsymbol{\sigma}\})}$. By the same steps as before, we show that

$$\langle (\boldsymbol{\sigma}_x^\parallel \cdot \boldsymbol{\sigma}_y^\parallel)^2 \rangle_{N,J'} \leq \langle \cos^2(\theta_x - \theta_y) \rangle_{XY,J} \left\langle (1 - \boldsymbol{\sigma}_x^{\perp 2})(1 - \boldsymbol{\sigma}_y^{\perp 2}) \right\rangle_{N,J'}. \quad (\text{C.26})$$

Now we exploit $O(N)$ invariance in the form of identities

$$\langle T_x^{(\alpha\beta)} \rangle = 0 \quad (\text{C.27a})$$

$$\langle T_x^{(\alpha\beta)} T_y^{(\kappa\lambda)} \rangle = \frac{1}{N^2 + N - 2} (\delta^{\alpha\kappa} \delta^{\beta\lambda} + \delta^{\alpha\lambda} \delta^{\beta\kappa} - \frac{2}{N} \delta^{\alpha\beta} \delta^{\kappa\lambda}) G_T(x, y) \quad (\text{C.27b})$$

where the isotensor field $T_x^{(\alpha\beta)}$ is defined in (2.7). After some algebra we obtain

$$\langle (\boldsymbol{\sigma}_x^\parallel \cdot \boldsymbol{\sigma}_y^\parallel)^2 \rangle_{N,J'} = \frac{2}{N^2} + \frac{6N - 4}{N(N^2 + N - 2)} G_T(x, y) \quad (\text{C.28a})$$

$$\langle \boldsymbol{\sigma}_x^{\perp 2} \rangle = \langle \boldsymbol{\sigma}_y^{\perp 2} \rangle = \frac{N - 2}{N} \quad (\text{C.28b})$$

$$\langle \boldsymbol{\sigma}_x^{\perp 2} \boldsymbol{\sigma}_y^{\perp 2} \rangle = \left(\frac{N - 2}{N} \right)^2 + \frac{4N - 8}{N(N^2 + N - 2)} G_T(x, y) \quad (\text{C.28c})$$

so that (C.26) can be written as

$$\frac{2}{N^2} + \frac{6N - 4}{N(N^2 + N - 2)} G_T(x, y) \leq \frac{1}{2} (1 + \gamma_{xy}) \left[\frac{4}{N^2} + \frac{4N - 8}{N(N^2 + N - 2)} G_T(x, y) \right] \quad (\text{C.29})$$

where $\gamma_{xy} \equiv \langle \cos 2(\theta_x - \theta_y) \rangle_{XY,J}$. The bounds (C.18) follow by simple algebra. ■

Remarks. 1. Note that the additive term $1/N$ in (C.18) is just what is needed to give the (properly truncated) isotensor correlation function, i.e.

$$G_T(x, y)_{N,J'} \leq \left(1 - \frac{1}{N} \right) \langle \cos 2(\theta_x - \theta_y) \rangle_{XY,J}. \quad (\text{C.30})$$

2. A partially alternate proof of Theorem C.7 can be based on the parametrization $\boldsymbol{\sigma}_x = \left((1 - \boldsymbol{\sigma}_x^{\perp 2})^{1/2} \cos \theta_x, (1 - \boldsymbol{\sigma}_x^{\perp 2})^{1/2} \sin \theta_x, \boldsymbol{\sigma}_x^\parallel \right)$. Thus, θ_x is here the polar coordinate of $\boldsymbol{\sigma}_x^\parallel$ (whereas it was previously an *additional* rotation applied to $\boldsymbol{\sigma}_x^\parallel$). Under the identification $\boldsymbol{\sigma}_x \leftrightarrow (\theta_x, \boldsymbol{\sigma}_x^\perp)$, the uniform measure $d\mu(\{\boldsymbol{\sigma}\})$ becomes $d\nu(\{\theta\}) d\tilde{\mu}(\{\boldsymbol{\sigma}^\perp\})$ for a suitable measure $\tilde{\mu}$ (whose form is of no interest to us). Now the Hamiltonian $H(\{\boldsymbol{\sigma}\})$, considered as a function of $\{\theta\}$ with $\{\boldsymbol{\sigma}^\perp\}$ fixed, has couplings $\hat{J}_{xy} = J'_{xy} (1 - \boldsymbol{\sigma}_x^{\perp 2})^{1/2} (1 - \boldsymbol{\sigma}_y^{\perp 2})^{1/2}$, and

so is *ferromagnetic* if the original model is (i.e. if $J'_{xy} \geq 0$). The remainder of the proof is as before, but in the ferromagnetic case we can now use the Ginibre II inequality rather than the stronger Ginibre comparison inequality. However, the first proof has the advantage that it generalizes readily to *any* σ -model whose invariance group contains a $U(1)$ subgroup, e.g. to principal chiral models.

2. One could consider different embeddings of XY spins into N -vector spins, e.g. different one-parameter subgroups $R(\theta) \in SO(N)$. We do not know whether such embeddings might be useful for proving correlation inequalities.

Finally, let us consider the N -component mixed isovector/isotensor model

$$H(\{\boldsymbol{\sigma}\}) = - \sum_{\langle xy \rangle} [J'_{xy} \boldsymbol{\sigma}_x \cdot \boldsymbol{\sigma}_y + \frac{1}{2} K'_{xy} (\boldsymbol{\sigma}_x \cdot \boldsymbol{\sigma}_y)^2] , \quad (\text{C.31})$$

and compare it to a generalized XY model

$$H(\{\theta\}) = - \sum_{\langle xy \rangle} [J_{xy} \cos(\theta_x - \theta_y) + K_{xy} \cos 2(\theta_x - \theta_y)] . \quad (\text{C.32})$$

Theorem C.8 Consider an N -component mixed isovector/isotensor model defined by the Boltzmann-Gibbs measure $Z^{-1} e^{-H(\{\boldsymbol{\sigma}\})} d\mu(\{\boldsymbol{\sigma}\})$, where H is defined by (C.31), and $d\mu(\{\boldsymbol{\sigma}\}) = \prod_x d\Omega(\boldsymbol{\sigma}_x)$. Consider for comparison a generalized XY model defined by the Boltzmann-Gibbs measure $Z^{-1} e^{-H(\{\theta\})} d\nu(\{\theta\})$, where H is defined by (C.32), and $d\nu(\{\boldsymbol{\sigma}\}) = \prod_x d\theta_x$. Assume that

$$\left\{ \begin{array}{ll} |J'_{xy}| & \text{if } |K'_{xy}| \leq |J'_{xy}| \\ \frac{1}{4} |K'_{xy}| \left(1 + \frac{|J'_{xy}|}{|K'_{xy}|}\right)^2 & \text{if } |K'_{xy}| > |J'_{xy}| \end{array} \right\} \leq J_{xy} \quad (\text{C.33})$$

and

$$\frac{1}{4} |K'_{xy}| \leq K_{xy} \quad (\text{C.34})$$

for all x, y . Then inequalities (C.17) and (C.18) hold for $\langle \cdot \rangle_{N, J', K'}$ and $\langle \cdot \rangle_{XY, J, K}$.

Remark. The left-hand side of (C.33) is bounded above by $|J'_{xy}| + \frac{1}{4} |K'_{xy}|$. So one can get a simpler (but weaker) version of the theorem by using this formula in the hypothesis.

PROOF. The proof is identical to that of Theorem C.7. We find that $H(\{R(\theta)\boldsymbol{\sigma}\})$, considered as a function of $\{\theta\}$ for fixed $\{\boldsymbol{\sigma}\}$, is a generalized XY model with couplings

$$\tilde{J}_{xy} = (J'_{xy} + K'_{xy} \boldsymbol{\sigma}_x^\perp \cdot \boldsymbol{\sigma}_y^\perp) |\boldsymbol{\sigma}_x^\parallel| |\boldsymbol{\sigma}_y^\parallel| e^{i\angle(\boldsymbol{\sigma}_x^\parallel, \boldsymbol{\sigma}_y^\parallel)} \quad (\text{C.35a})$$

$$\tilde{K}_{xy} = \frac{1}{4} K'_{xy} |\boldsymbol{\sigma}_x^\parallel|^2 |\boldsymbol{\sigma}_y^\parallel|^2 e^{2i\angle(\boldsymbol{\sigma}_x^\parallel, \boldsymbol{\sigma}_y^\parallel)} \quad (\text{C.35b})$$

By straightforward calculus we see that $|\tilde{J}_{xy}| \leq$ the left-hand side of (C.33). So we can use Ginibre comparison inequality (Theorem C.4) as before. The rest of the proof concerns the treatment of the various *observables* (as opposed to *Hamiltonians*), and so is unchanged. ■

Acknowledgments

We wish to thank Paolo Butera, Sergio Caracciolo, Hervé Kunz, Andrea Pelissetto and Paolo Rossi for many helpful discussions, and Larry Glasser for correspondence. In particular, it was Paolo Butera who pointed out to one of us (A.D.S.), nearly a decade ago, that the $N = \infty$ phase transition in RP^{N-1} models occurs also in dimension $d = 1$ — a comment that directly inspired the present work. This research was supported in part by U.S. National Science Foundation grants PHY-9520978 and PHY-9900769. It was also aided by the gracious hospitality of the Scuola Normale Superiore.

References

- [1] S. Hikami and T. Maskawa, Prog. Theor. Phys. **67**, 1038 (1982).
- [2] N. Magnoli and F. Ravanini, Z. Phys. C **34**, 43 (1987).
- [3] K. Ohno, H.-O. Carmesin, H. Kawamura and Y. Okabe, Phys. Rev. B **42**, 10360 (1990).
- [4] H. Kunz and G. Zumbach, J. Phys. A **22**, L1043 (1989).
- [5] H. Kunz and G. Zumbach, Phys. Lett. B **257**, 299 (1991).
- [6] H. Kunz and G. Zumbach, Phys. Rev. B **46**, 662 (1992).
- [7] H. Kunz and G. Zumbach, J. Phys. A **25**, 6155 (1992).
- [8] P. Butera and M. Comi, Phys. Rev. B **46**, 11141 (1992), hep-lat/9205027.
- [9] S. Caracciolo, R.G. Edwards, A. Pelissetto and A.D. Sokal, Nucl. Phys. B (Proc. Suppl.) **26**, 595 (1992), hep-lat/9201003.
- [10] S. Caracciolo, R.G. Edwards, A. Pelissetto and A.D. Sokal, Nucl. Phys. B (Proc. Suppl.) **30**, 815 (1993), hep-lat/9212012.
- [11] S. Caracciolo, R.G. Edwards, A. Pelissetto and A.D. Sokal, Phys. Rev. Lett. **71**, 3906 (1993), hep-lat/9307022.
- [12] S. Caracciolo and A. Pelissetto, $1/N$ expansion for mixed $O(N) - RP^{N-1}$ σ -models, unpublished manuscript (1995).
- [13] M. Hasenbusch, Phys. Rev. D **53**, 3445 (1996), hep-lat/9507008.
- [14] F. Niedermayer, P. Weisz and D.-S. Shin, Phys. Rev. D **53**, 5918 (1996).
- [15] S. M. Catterall, M. Hasenbusch, R. R. Horgan and R. Renken, Phys. Rev. D **58**, 074510 (1998), hep-lat/9801032.
- [16] S. Caracciolo, R.G. Edwards, A. Pelissetto and A.D. Sokal, unpublished work (1991–95).

- [17] P. DiVecchia, R. Musto, F. Nicodemi, R. Pettorino and P. Rossi, Nucl. Phys. B **235**[FS11], 478 (1984).
- [18] M. Hasenbusch and S. Meyer, Phys. Rev. Lett. **68**, 435 (1992).
- [19] K. Jansen and U.-J. Wiese, Nucl. Phys. B **370**, 762 (1992).
- [20] A.C. Irving and C. Michael, Nucl. Phys. B **371**, 521 (1992).
- [21] U. Wolff, Phys. Lett. B **284**, 94 (1992), hep-lat/9205001.
- [22] M. Campostrini, P. Rossi and E. Vicari, Phys. Rev. D **46**, 2647 (1992).
- [23] M. Campostrini, P. Rossi and E. Vicari, Phys. Rev. D **46**, 4643 (1992), hep-lat/9207032.
- [24] M. Campostrini and P. Rossi, Riv. Nuovo Cim. **16**, no. 6, 1 (1993).
- [25] E. Gava, R. Jengo and C. Omero, Nucl. Phys. B **168**, 465 (1980).
- [26] J. Goodman and A.D. Sokal, Phys. Rev. D **40**, 2035 (1989).
- [27] T. Mendes, A. Pelissetto and A.D. Sokal, Nucl. Phys. B **477**, 203 (1996), hep-lat/9604015.
- [28] U. Wolff, Phys. Rev. Lett. **62**, 361 (1989).
- [29] U. Wolff, Nucl. Phys. B **334**, 581 (1990).
- [30] S. Caracciolo, R.G. Edwards, A. Pelissetto and A.D. Sokal, Nucl. Phys. B (Proc. Suppl.) **20**, 72 (1991).
- [31] S. Caracciolo, R.G. Edwards, A. Pelissetto and A.D. Sokal, Nucl. Phys. B **403**, 475 (1993), hep-lat/9205005.
- [32] G. Lasher, Phys. Rev. A **5**, 1350 (1972).
- [33] P.A. Lebwohl and G. Lasher, Phys. Rev. A **6**, 426 (1972).
- [34] G. Kohring and R.E. Shrock, Nucl. Phys. B **285**[FS19], 504 (1987).
- [35] T.J. Krieger and H.M James, J. Chem. Phys. **22**, 796 (1954).
- [36] Lin Lei, Mol. Cryst. Liq. Cryst. **146**, 41 (1987).
- [37] K.M. Leung and Lin Lei, Mol. Cryst. Liq. Cryst. **146**, 71 (1987).
- [38] F. Biscarini, C. Zannoni, C. Chiccoli and P. Pasini, Molec. Phys. **73**, 439 (1991).
- [39] M. Oku and R. Abe, Prog. Theor. Phys. **67**, 118 (1982).
- [40] M. Oku, Prog. Theor. Phys. **68**, 2176 (1982).
- [41] P. Butera, private communication (1991).

- [42] R.L. Dobrushin, *Commun. Math. Phys.* **32**, 269 (1973).
- [43] M. Cassandro and E. Olivieri, *Commun. Math. Phys.* **80**, 255 (1981).
- [44] B. Simon, *The Statistical Mechanics of Lattice Gases*, Volume I (Princeton University Press, Princeton NJ, 1993).
- [45] S. Elitzur, *Phys. Rev. D* **12**, 3978 (1975).
- [46] L.L. Liu and R.I. Joseph, *J. Phys. Chem. Solids* **33**, 451 (1972).
- [47] M.F. Thorpe and M. Blume, *Phys. Rev. B* **5**, 1961 (1972).
- [48] A. Cucchieri, T. Mendes, A. Pelissetto and A.D. Sokal, *J. Stat. Phys.* **86**, 581 (1997), hep-lat/9509021.
- [49] E. Seiler and K. Yildirim, *J. Math. Phys.* **38**, 4872 (1997), hep-lat/9609030.
- [50] M. Hasenbusch and R. R. Horgan, *Phys. Rev. D* **60**, 037503 (1999), hep-lat/9812013.
- [51] W. Celmaster and F. Green, *Phys. Rev. Lett.* **50**, 1556 (1983).
- [52] N. Angelescu and V.A. Zagrebnov, *J. Phys. A: Math. Gen.* **15**, L639 (1982).
- [53] A. Tanaka and T. Idogaki, *J. Phys. Soc. Japan* **67**, 604 (1998).
- [54] M. Campbell and L. Chayes, *J. Phys. A: Math. Gen.* **32**, 8881 (1999).
- [55] P.G. de Gennes and J. Prost, *The Physics of Liquid Crystals*, 2nd ed. (Clarendon Press, Oxford, 1993).
- [56] P.M. Chaikin and T.C. Lubsenky, *Principles of Condensed Matter Physics* (Cambridge University Press, Cambridge, 1995).
- [57] A.D. Sokal, Comment on the $N \rightarrow \infty$ limit for N -vector and related models, unpublished manuscript (1992).
- [58] L.G. Yaffe, *Rev. Mod. Phys.* **54**, 407 (1982).
- [59] H. Buchholz, *Die Konfluente Hypergeometrische Funktion* (Springer-Verlag, Berlin–Heidelberg, 1952). English translation: *The Confluent Hypergeometric Function* (Springer-Verlag, New York, 1969).
- [60] F. Tricomi, *Funzioni Ipergeometriche Confluenti* (Edizioni Cremonese, Roma, 1954).
- [61] L.J. Slater, *Confluent Hypergeometric Functions* (Cambridge Univ. Press, Cambridge, 1960).
- [62] P. Appell and J. Kampé de Fériet, *Fonctions Hypergéométriques et Hypersphériques: Polynômes d’Hermite* (Gauthier-Villars, Paris, 1926).

- [63] H. Exton, *Multiple Hypergeometric Functions and Applications* (Ellis Horwood, Chichester, 1976).
- [64] H.M. Srivastava and P.W. Karlsson, *Multiple Gaussian Hypergeometric Series* (Ellis Horwood, Chichester, 1985).
- [65] G.N. Watson, *A Treatise on the Theory of Bessel Functions*, 2nd ed. (Cambridge University Press, Cambridge, 1944).
- [66] E.H. Lieb and A.D. Sokal, *Commun. Math. Phys.* **80**, 153 (1981).
- [67] C.M. Newman, *Proc. Amer. Math. Soc.* **61**, 245 (1976).
- [68] M. Abramowitz and I.A. Stegun, *Handbook of Mathematical Functions* (U.S. Government Printing Office, Washington, D.C., 1970). Reprinted by Dover, New York.
- [69] N.D. Mermin, *J. Math. Phys.* **8**, 1061 (1967).
- [70] R.L. Dobrushin and S.B. Shlosman, *Commun. Math. Phys.* **42**, 31 (1975).
- [71] C.-E. Pfister, *Commun. Math. Phys.* **79**, 181 (1981).
- [72] O.A. McBryan and T. Spencer, *Commun. Math. Phys.* **53**, 299 (1977).
- [73] J. Fröhlich, B. Simon and T. Spencer, *Commun. Math. Phys.* **50**, 79 (1976).
- [74] J. Fröhlich and T. Spencer, in *New Developments in Quantum Field Theory and Statistical Mechanics (Cargèse 1976)*, ed. M. Lévy and P. Mitter (Plenum, New York–London, 1977), pp. 79–130.
- [75] J. Fröhlich, R. Israel, E.H. Lieb and B. Simon, *Commun. Math. Phys.* **62**, 1 (1978).
- [76] R.B. Israel, *Convexity in the Theory of Lattice Gases* (Princeton University Press, Princeton NJ, 1979).
- [77] G.S. Joyce, *J. Phys. A* **5**, L65 (1972).
- [78] M.L. Glasser, *J. Res. Nat. Bur. Stand. B* **80**, 313 (1976).
- [79] M.L. Glasser and I.J. Zucker, *Proc. Natl. Acad. Sci. USA* **74**, 1800 (1977).
- [80] A.P. Prudnikov, Yu.A. Brychkov and O.I. Marichev, *Integraly i ryady. Specialnye funktsii* (Nauka, Moscow, 1983). English translation: *Integrals and Series. Vol. 2: Special Functions* (Gordon & Breach, New York, 1988).
- [81] G.N. Watson, *Quart. J. Math. (Oxford)* **10**, 266 (1939).
- [82] J.M. Borwein and I.J. Zucker, *IMA J. Numer. Anal.* **12**, 519 (1992).
- [83] M.L. Glasser and J. Boersma, *J. Phys. A: Math. Gen.* **33**, 5017 (2000).

- [84] C. Itzykson and J.-M. Drouffe, *Statistical Field Theory*, vol. 1 (Cambridge University Press, Cambridge–New York, 1989).
- [85] P.G. Doyle and J.L. Snell, *Random Walks and Electric Networks* (Mathematical Association of America, Washington, 1984).
- [86] T. Hara and G. Slade, *Rev. Math. Phys.* **4**, 235 (1992).
- [87] T. Hara, G. Slade and A.D. Sokal, *J. Stat. Phys.* **72**, 479 (1993); **78**, 1187 (E) (1995); hep-lat/9302003.
- [88] F.W.J. Olver, *Asymptotics and Special Functions* (Academic Press, San Diego, 1974).
- [89] G. Szegő, *Sitzungsber. Berlin Math. Ges.* **23**, 50 (1924). Reprinted in G. Szegő, *Collected Papers*, vol. 1, edited by R. Askey (Birkhäuser, Boston, 1982).
- [90] E.B. Saff and R.S. Varga, *SIAM J. Math. Anal.* **7**, 344 (1976).
- [91] E.B. Saff and R.S. Varga, *Numer. Math.* **30**, 241 (1978).
- [92] I.E. Pritsker and R.S. Varga, *Trans. Amer. Math. Soc.* **349**, 4085 (1997).
- [93] A.D. Sokal, Chromatic roots are dense in the whole complex plane, in preparation.
- [94] C.N. Yang and T.D. Lee, *Phys. Rev.* **87**, 404 (1952).
- [95] R.B. Griffiths, in C. Domb and M.S. Green (editors), *Phase Transitions and Critical Phenomena*, vol. 1, pp. 7–109 (Academic Press, London–New York, 1972).
- [96] B. Simon, *The $P(\varphi)_2$ Euclidean (Quantum) Field Theory* (Princeton Univ. Press, Princeton, NJ, 1974).
- [97] P. Montel, *Leçons sur les familles normales de fonctions analytiques et leurs applications* (Gauthier-Villars, Paris, 1927). Reprinted by Chelsea Publishing Co., New York, 1974.
- [98] J.L. Schiff, *Normal Families* (Springer-Verlag, New York, 1993).
- [99] G.E. Tsvetkoff, *C.R. (Doklady) Acad. Sci. URSS (N.S.)* **32**, 10 (1941).
- [100] N.D. Kazarinoff, *J. Math. Mech.* **6**, 341 (1957).
- [101] N.M. Temme, *J. Inst. Maths. Applics.* **22**, 215 (1978).
- [102] T.S. Norfolk, *J. Math. Anal. Appl.* **218**, 421 (1998).
- [103] G.S. Sylvester, *J. Stat. Phys.* **15**, 327 (1976).
- [104] D. Szász, *J. Stat. Phys.* **19**, 453 (1978).
- [105] J. Ginibre, *Commun. Math. Phys.* **16**, 310 (1970).
- [106] A. Messenger, S. Miracle-Solé and C.-E. Pfister, *Commun. Math. Phys.* **58**, 19 (1978).

- [107] J. Fröhlich, Phys. Lett. B **83**, 195 (1979).
- [108] G. Mack and V.B. Petkova, Ann. Phys. **123**, 442 (1979).
- [109] A. Patrascioiu and E. Seiler, The difference between abelian and non-abelian models: fact and fancy, Max-Planck-Institut preprint MPI-Ph/91-88 (1991), math-ph/9903038.
- [110] A. Patrascioiu and E. Seiler, J. Stat. Phys. **69**, 573 (1992).
- [111] M. Aizenman, J. Stat. Phys. **77**, 351 (1994).

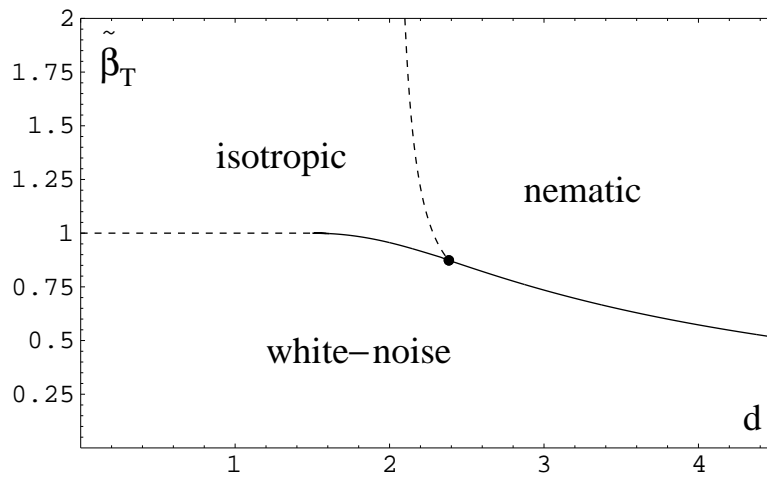


Figure 1: Phase diagram of the RP^{N-1} model at $N = \infty$ in the $(\tilde{\beta}_T, d)$ -plane. Transition from white-noise phase to isotropic phase is second-order for $0 < d \leq 3/2$ and first-order for $3/2 < d < d_* \approx 2.38403$. Transition from isotropic phase to nematic ordered phase is second-order for $2 < d < d_*$. Transition from white-noise phase to nematic ordered phase is first-order for $d \geq d_*$.

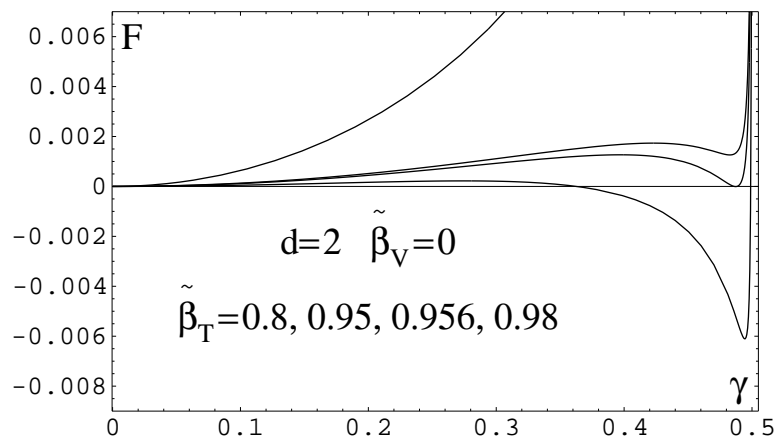
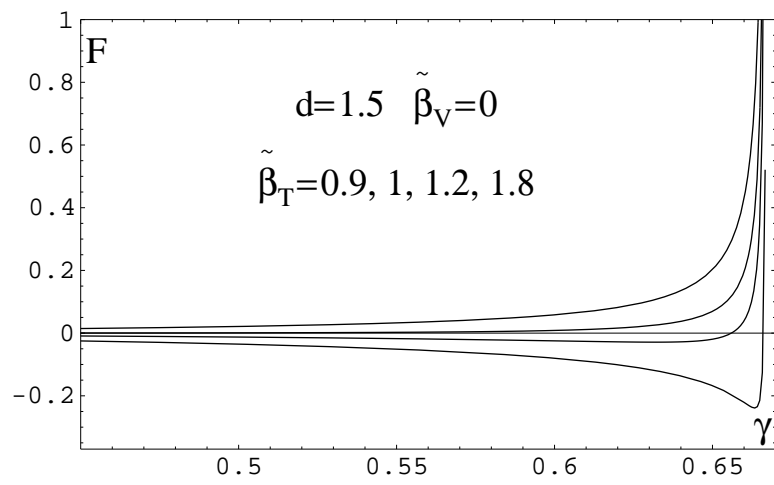
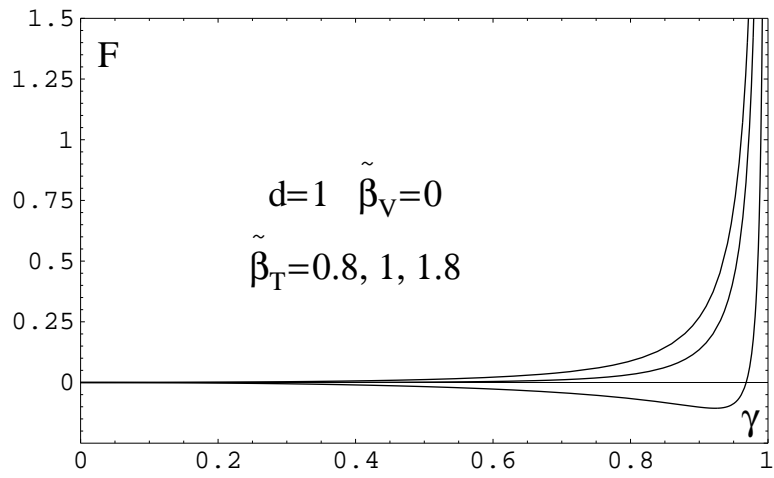


Figure 2: $\mathcal{F}_0(\gamma)$ versus γ for various values of $\tilde{\beta}_T$, for (a) $d = 1$, (b) $d = 3/2$, (c) $d = 2$. Since $\mathcal{F}_0(\gamma) = \mathcal{F}_0(-\gamma)$, we show only $\gamma \geq 0$.

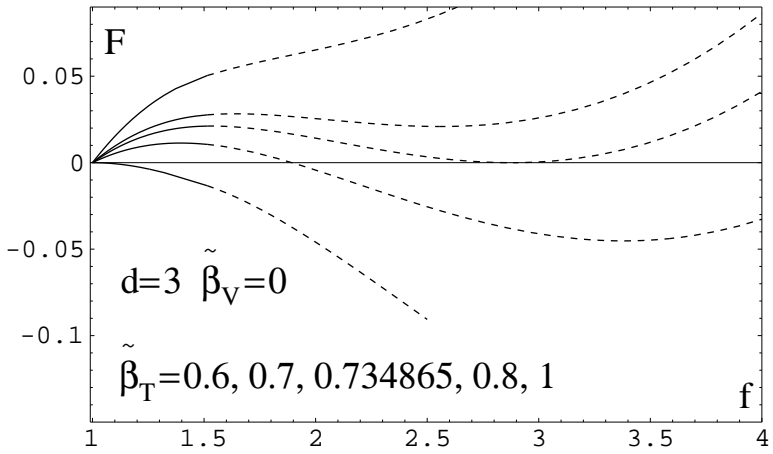
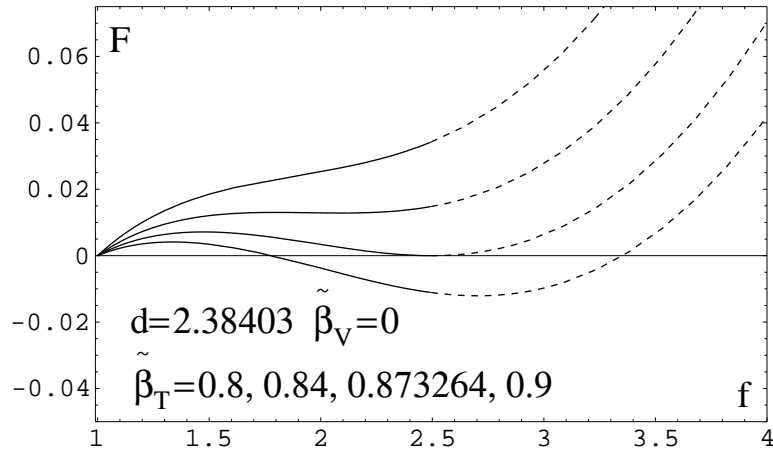
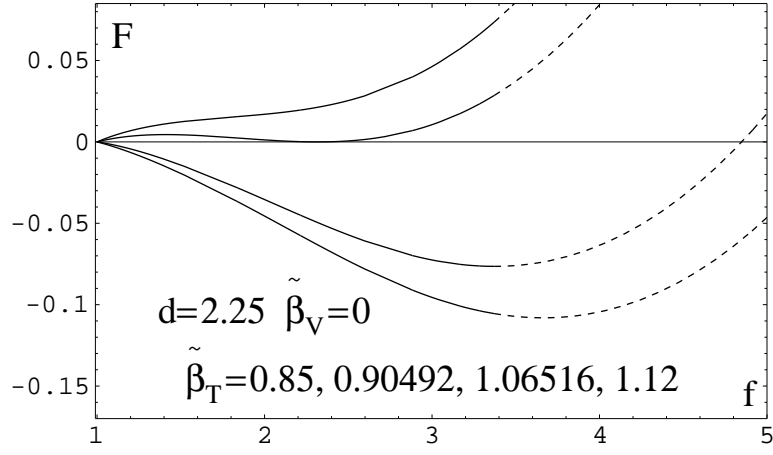


Figure 3: $\mathcal{F}_0(\gamma)$ (solid curve) and $\mathcal{F}_{0^*}(f)$ (dashed curve) plotted versus f for various values of $\tilde{\beta}_T$, for (a) $d = 9/4$, (b) $d = d_* \approx 2.38403$, (c) $d = 3$. The junction between the solid and dashed curves corresponds to $\gamma = 1/d$, $f = f_*$.

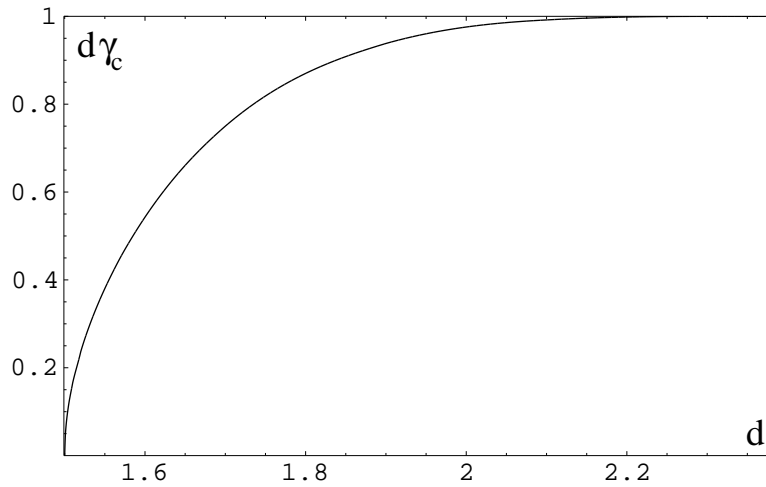


Figure 4: $d\gamma_c$ plotted versus d for $3/2 \leq d \leq d_* \approx 2.38403$. Here γ_c is the γ value at the first-order phase transition of the RP^∞ model [see (4.6)]; it tends to zero as $d \downarrow 3/2$ and to $1/d$ as $d \uparrow d_*$.

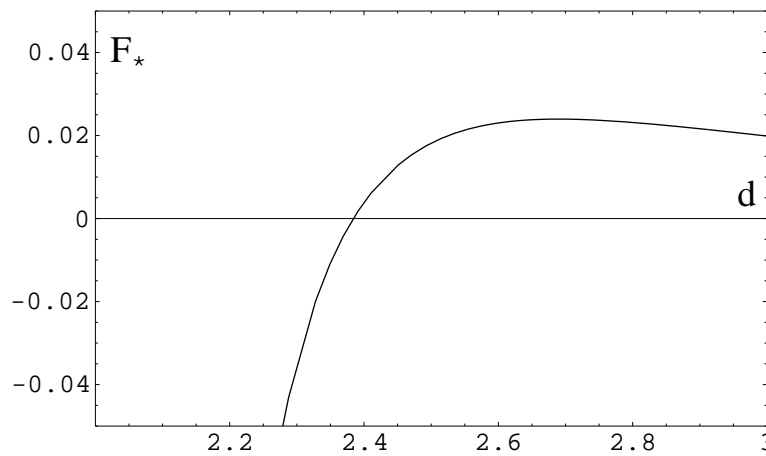


Figure 5: $\mathcal{F}_* \equiv -(f_* - 1)/4 + (\log f_* + g_*)/2$ plotted versus d . We have $\mathcal{F}_* = 0$ at the dimension $d_* \approx 2.38403$.

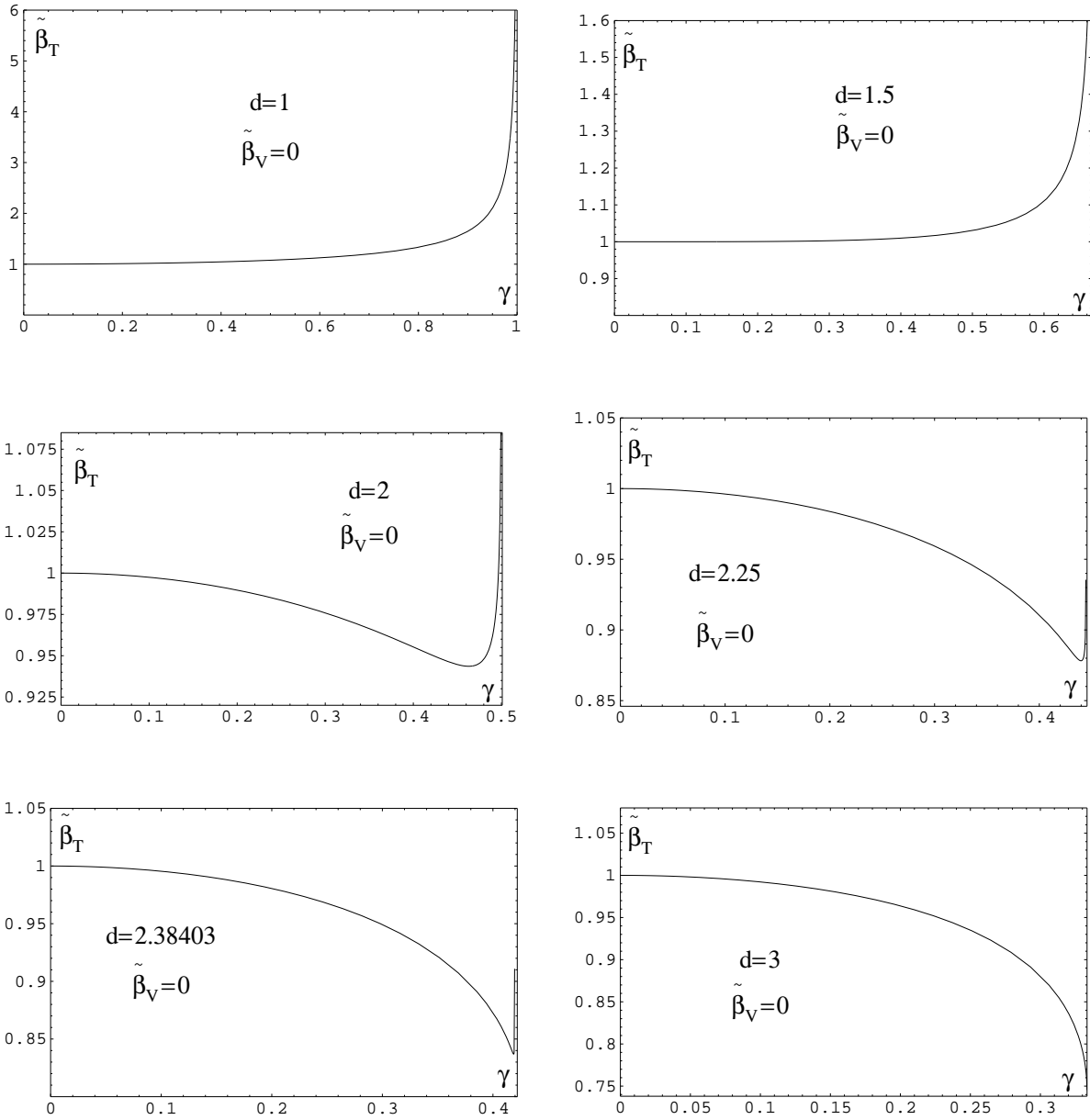


Figure 6: $\tilde{\beta}_T$ versus γ at $\tilde{\beta}_V = 0$, for (a) $d = 1$, (b) $d = 3/2$, (c) $d = 2$, (d) $d = 9/4$, (e) $d = d_* \approx 2.38403$, (f) $d = 3$. For $3/2 < d < \bar{d} \approx 2.55031$, $\tilde{\beta}_T$ reaches a minimum at $\gamma = \gamma_{cusp}(d)$.

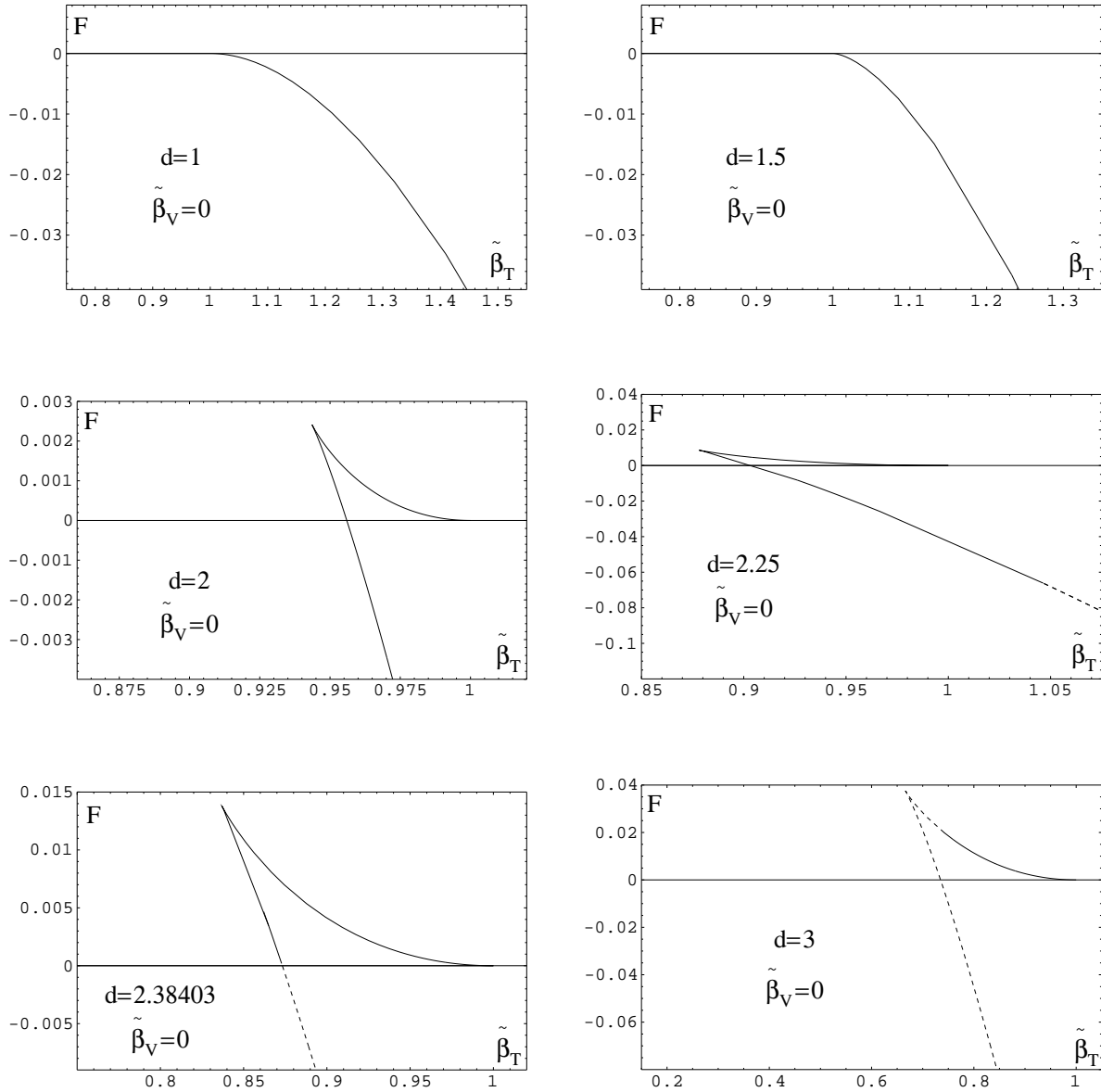


Figure 7: Free energy \overline{F} versus $\tilde{\beta}_T$ at $\tilde{\beta}_V = 0$, for (a) $d = 1$, (b) $d = 3/2$, (c) $d = 2$, (d) $d = 9/4$, (e) $d = d_* \approx 2.38403$, (f) $d = 3$. In (d)–(f), the dashed curve corresponds to the condensate phase.

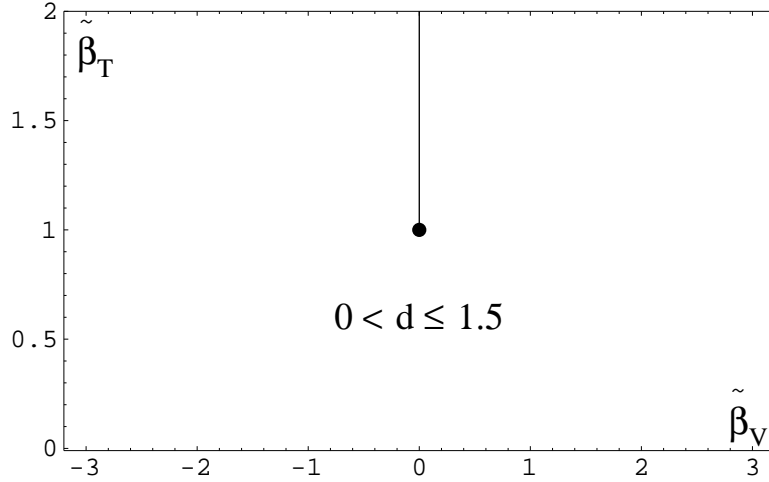


Figure 8: Phase diagram in the $(\tilde{\beta}_V, \tilde{\beta}_T)$ -plane for dimensions $0 < d \leq 3/2$. There is a second-order transition at $(\tilde{\beta}_V, \tilde{\beta}_T) = (0, 1)$ and a line of first-order transitions at $\tilde{\beta}_V = 0$, $\tilde{\beta}_T > 1$.

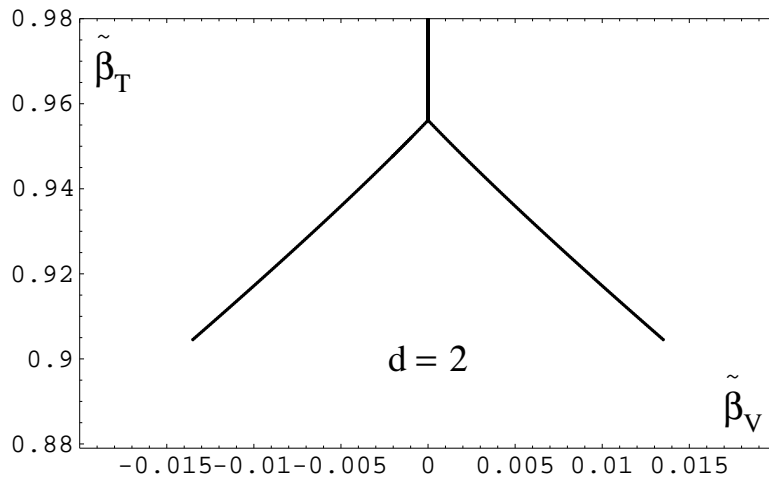


Figure 9: Phase diagram in the $(\tilde{\beta}_V, \tilde{\beta}_T)$ -plane for dimensions $3/2 < d \leq 2$, shown here for the case $d = 2$. The first-order transition curves $\tilde{\beta}_{T,c}(\tilde{\beta}_V)$ are almost straight lines but are in fact slightly convex. In $d = 2$, the triple point lies at $(\tilde{\beta}_V, \tilde{\beta}_T) \approx (0, 0.956)$ and $\gamma_c \approx 0.487$, while the endpoints of the first-order transition curves lie at $(\pm\tilde{\beta}_{V,e}, \tilde{\beta}_{T,e}) \approx (\pm 0.0134, 0.905)$ and $\gamma_e \approx 0.411$.

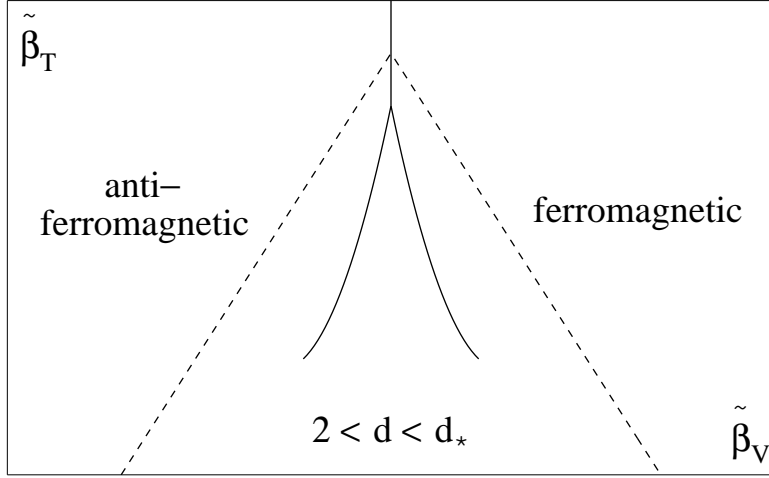


Figure 10: Phase diagram in the $(\tilde{\beta}_V, \tilde{\beta}_T)$ -plane for dimensions $2 < d < d_* \approx 2.38403$. In addition to the first-order transitions present for $3/2 < d \leq 2$ at $\tilde{\beta}_{T,c}(\tilde{\beta}_V)$, there is an additional pair of second-order transition lines (dashed) at $\tilde{\beta}_{T,c'}(\tilde{\beta}_V)$ given by (5.1). The phase at the upper right (resp. upper left) of the diagram exhibits ferromagnetic (resp. antiferromagnetic) long-range order.

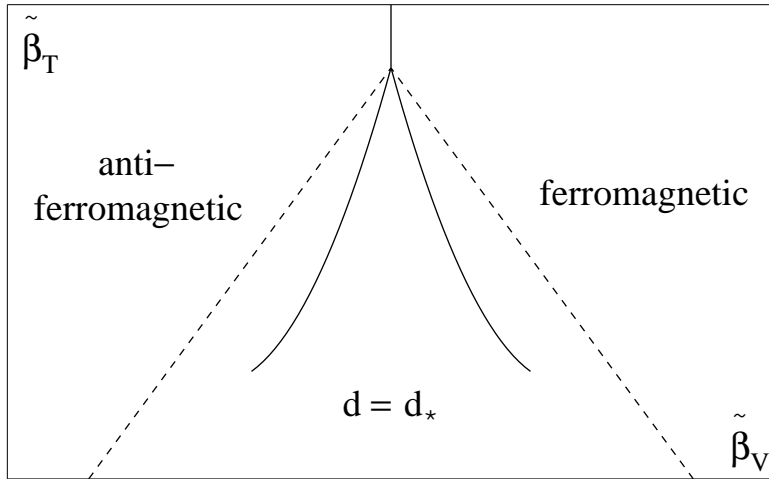


Figure 11: Phase diagram in the $(\tilde{\beta}_V, \tilde{\beta}_T)$ -plane for dimension $d = d_* \approx 2.38403$. The two transitions coincide at $\tilde{\beta}_V = 0$. The phase at the upper right (resp. upper left) of the diagram exhibits ferromagnetic (resp. antiferromagnetic) long-range order.

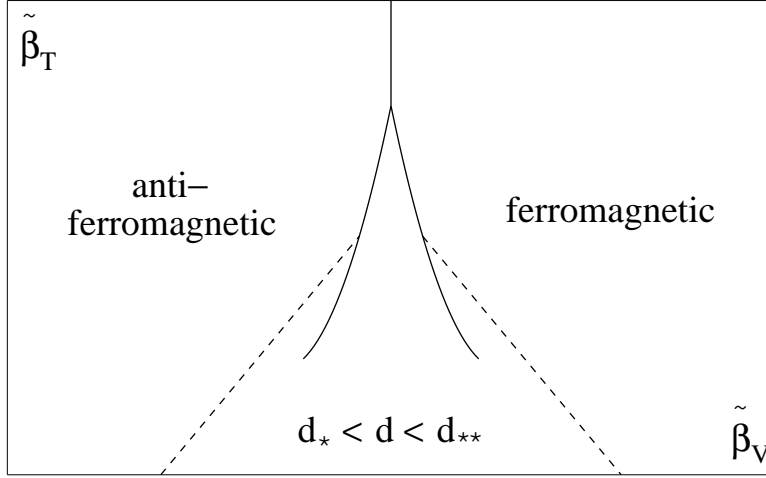


Figure 12: Phase diagram in the $(\tilde{\beta}_V, \tilde{\beta}_T)$ -plane for dimensions $d_* \approx 2.38403 < d < d_{**} = 3$. Second-order transitions (dashed lines) occur only where they lie above the first-order transition curves; this occurs for $|\tilde{\beta}_V| > \tilde{\beta}_{V,cc'}$. The phase at the upper right (resp. upper left) of the diagram exhibits ferromagnetic (resp. antiferromagnetic) long-range order.

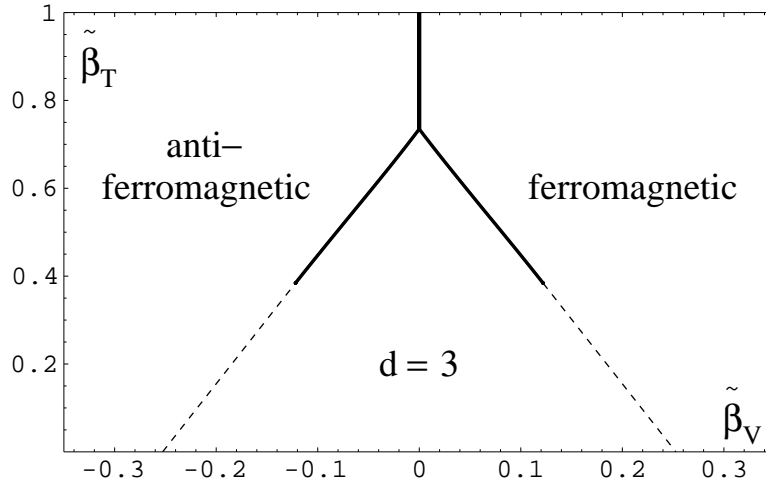


Figure 13: Phase diagram in $(\tilde{\beta}_V, \tilde{\beta}_T)$ -plane for $d \geq d_{**} = 3$, shown here for the case $d = 3$. The first-order transition curves $\tilde{\beta}_{T,c}(\tilde{\beta}_V)$ are almost straight lines but are in fact slightly convex. In $d = 3$, the triple point lies at $(\tilde{\beta}_V, \tilde{\beta}_T) \approx (0, 0.73487)$, while the endpoints of the first-order transition curves lie at $(\tilde{\beta}_{V,e}, \tilde{\beta}_{T,e}) = (\pm f_*(3)[2 - f_*(3)]/6, f_*(3)^2/6) \approx (\pm 0.122224, 0.383238)$. The phase at the upper right (resp. upper left) of the diagram exhibits ferromagnetic (resp. antiferromagnetic) long-range order.

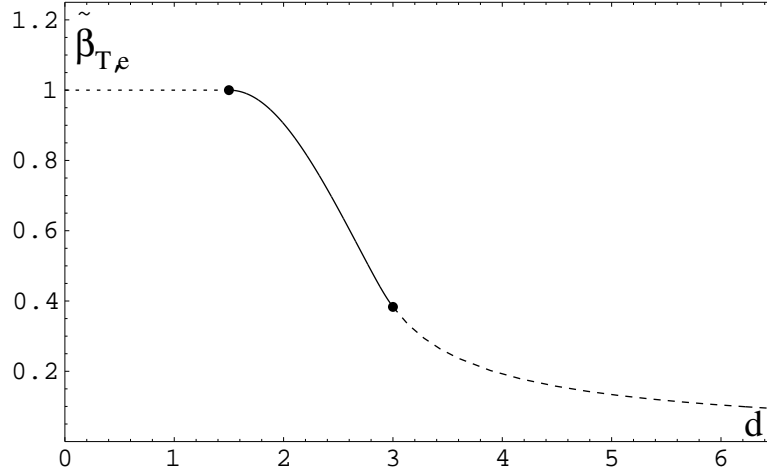


Figure 14: Coordinate $\tilde{\beta}_{T,e}$ of the endpoint of the first-order transition curve, as function of dimension d . For $d \geq d_{**} = 3$ it is given by $\tilde{\beta}_{T,e} = f_*^2/2d$ (dashed line) and tends to zero as $d \rightarrow \infty$.

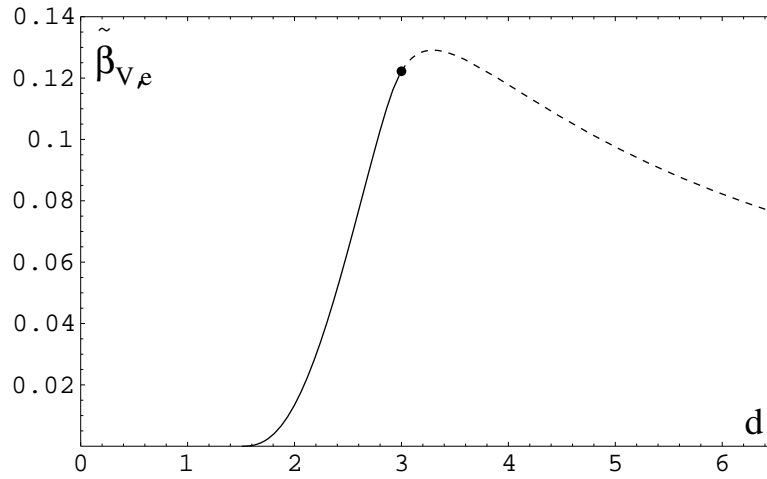


Figure 15: Coordinate $\tilde{\beta}_{V,e}$ of the endpoint of the first-order transition curve, as function of dimension d . For $d \geq d_{**} = 3$ it is given by $\tilde{\beta}_{V,e} = \tilde{\beta}_{V,2} = f_*(2 - f_*)/2d$ (dashed line) and tends to zero as $d \rightarrow \infty$.

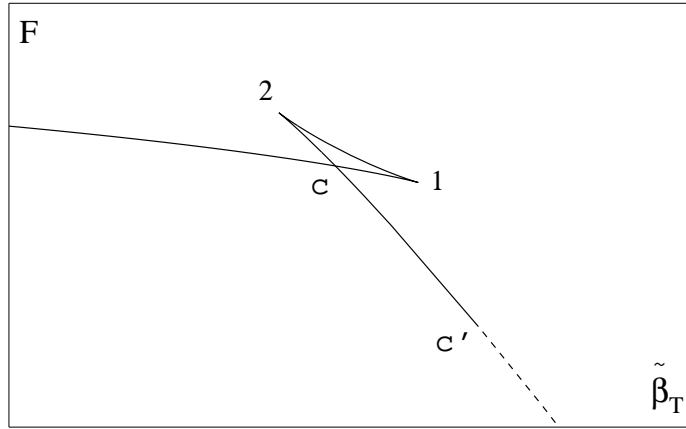


Figure 16: “Notations guide” for the parametric plots of $\overline{\mathcal{F}}$ versus $\tilde{\beta}_T$. Points 1 and 2 are, respectively, the local maximum and minimum of $\tilde{\beta}_T$ versus f . Point c is the first-order transition at $\tilde{\beta}_{T,c}(\tilde{\beta}_V)$. Point c' is the second-order normal-to-condensate transition at $f = f_*$. The condensate phase $f \geq f_*$ is shown as a dashed line.

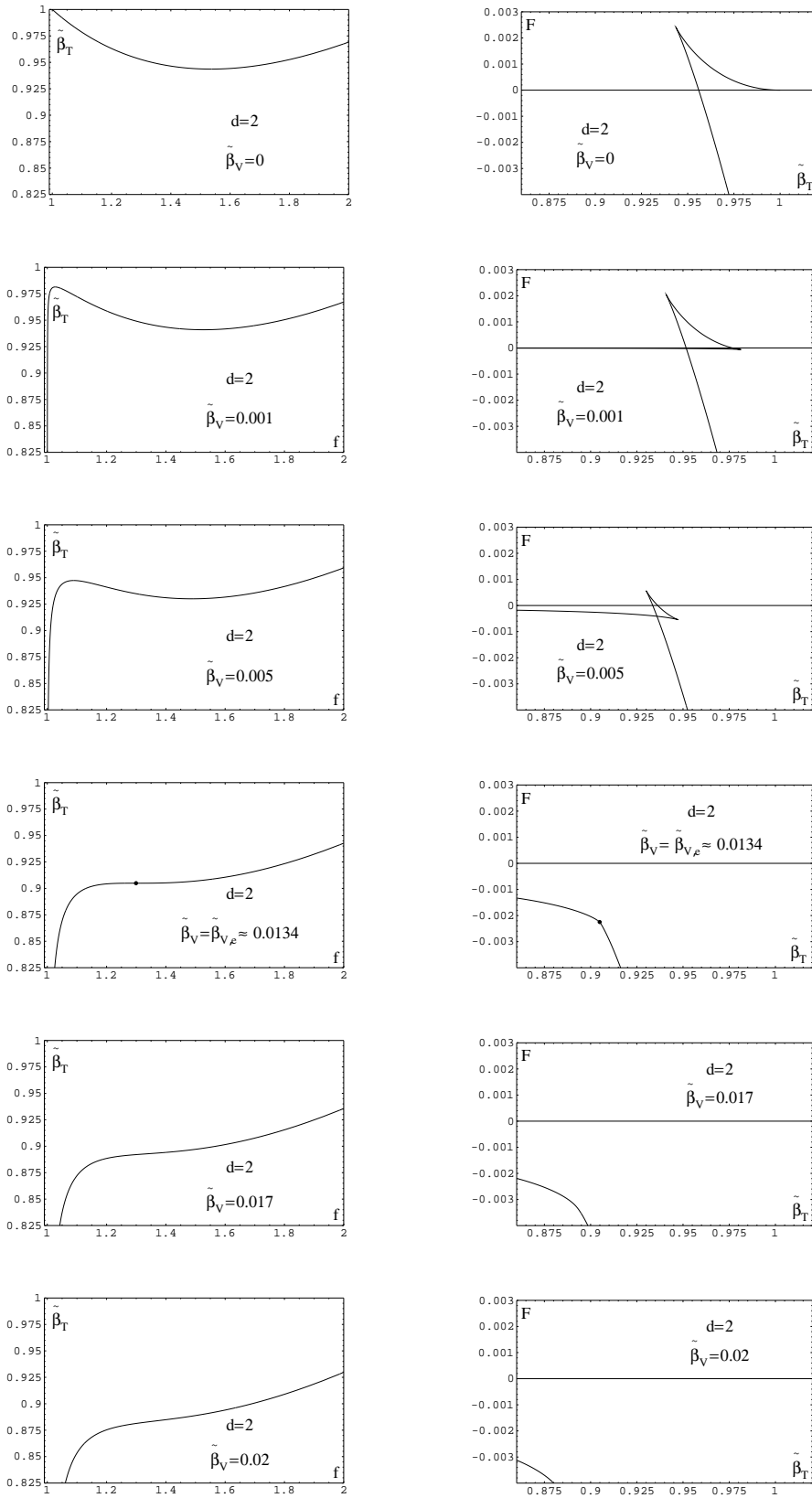


Figure 17: $\tilde{\beta}_T$ versus f , and $\bar{\mathcal{F}}$ versus $\tilde{\beta}_T$, for $d = 2$ at (a) $\tilde{\beta}_V = 0$, (b) $\tilde{\beta}_V = 0.001$, (c) $\tilde{\beta}_V = 0.005$, (d) $\tilde{\beta}_V = \tilde{\beta}_{V,e} \approx 0.0134$ [the dot indicates the endpoint $(\tilde{\beta}_{V,e}, \tilde{\beta}_{T,e})$], (e) $\tilde{\beta}_V = 0.017$, (f) $\tilde{\beta}_V = 0.02$.

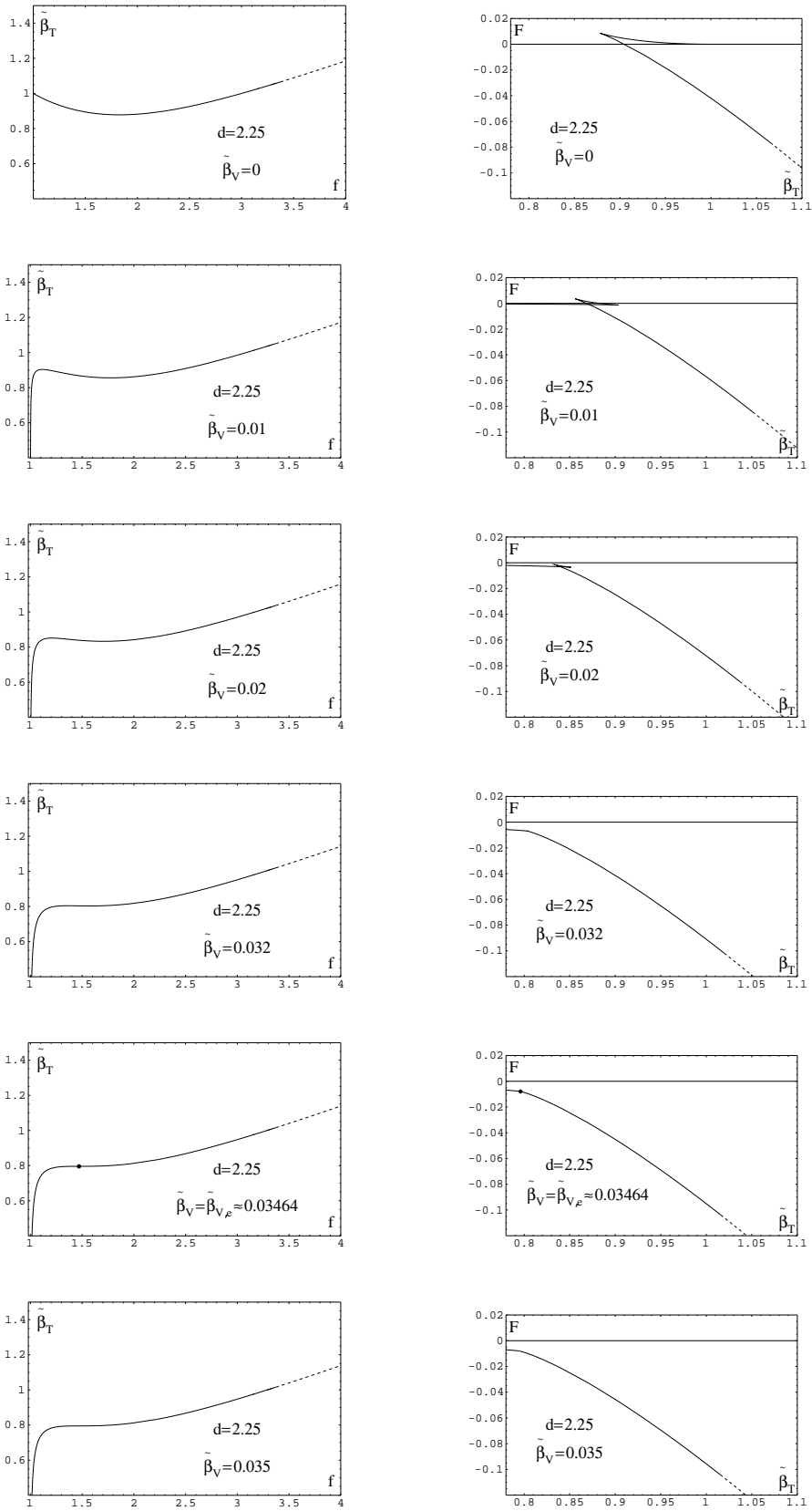


Figure 18: $\tilde{\beta}_T$ versus f , and \bar{F} versus $\tilde{\beta}_T$, for $d = 2.25$ at (a) $\tilde{\beta}_V = 0$, (b) $\tilde{\beta}_V = 0.01$, (c) $\tilde{\beta}_V = 0.02$, (d) $\tilde{\beta}_V = 0.032$, (e) $\tilde{\beta}_V = \tilde{\beta}_{V,e} \approx 0.03464$ (note that $\tilde{\beta}_{T,e} \approx 0.795978$ and $\gamma_e \approx 0.416596$), (f) $\tilde{\beta}_V = 0.035$.

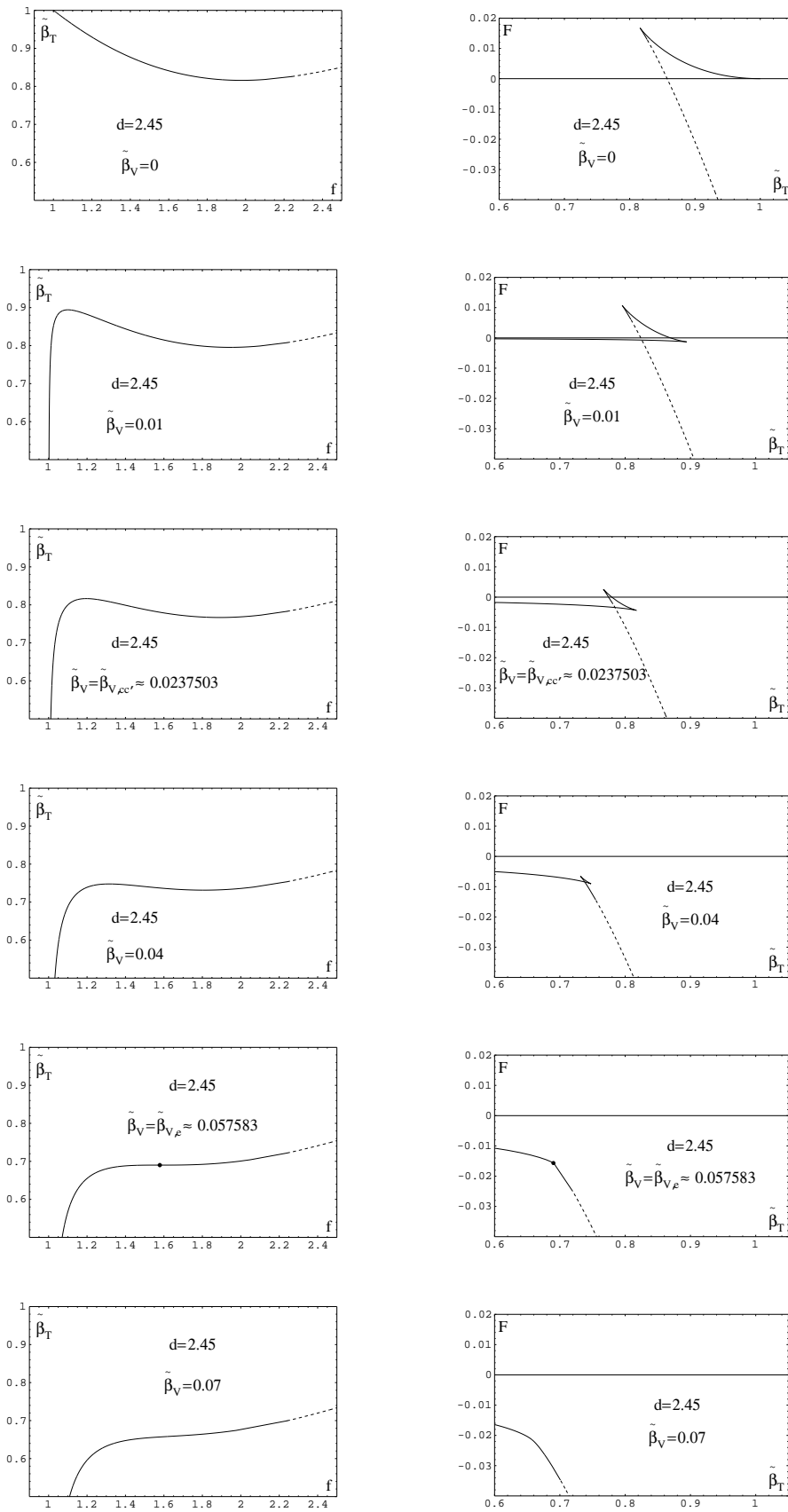


Figure 19: $\tilde{\beta}_T$ versus f , and \tilde{F} versus $\tilde{\beta}_T$, for $d = 2.45$ at (a) $\tilde{\beta}_V = 0$, (b) $\tilde{\beta}_V = 0.01$, (c) $\tilde{\beta}_V = \tilde{\beta}_{V,cc'} \approx 0.0237503$, (d) $\tilde{\beta}_V = 0.04$, (e) $\tilde{\beta}_V = \tilde{\beta}_{V,e} \approx 0.057583$ (note that $\tilde{\beta}_{T,e} \approx 0.69010393$ and $\gamma_e \approx 0.399979$), (f) $\tilde{\beta}_V = 0.07$.

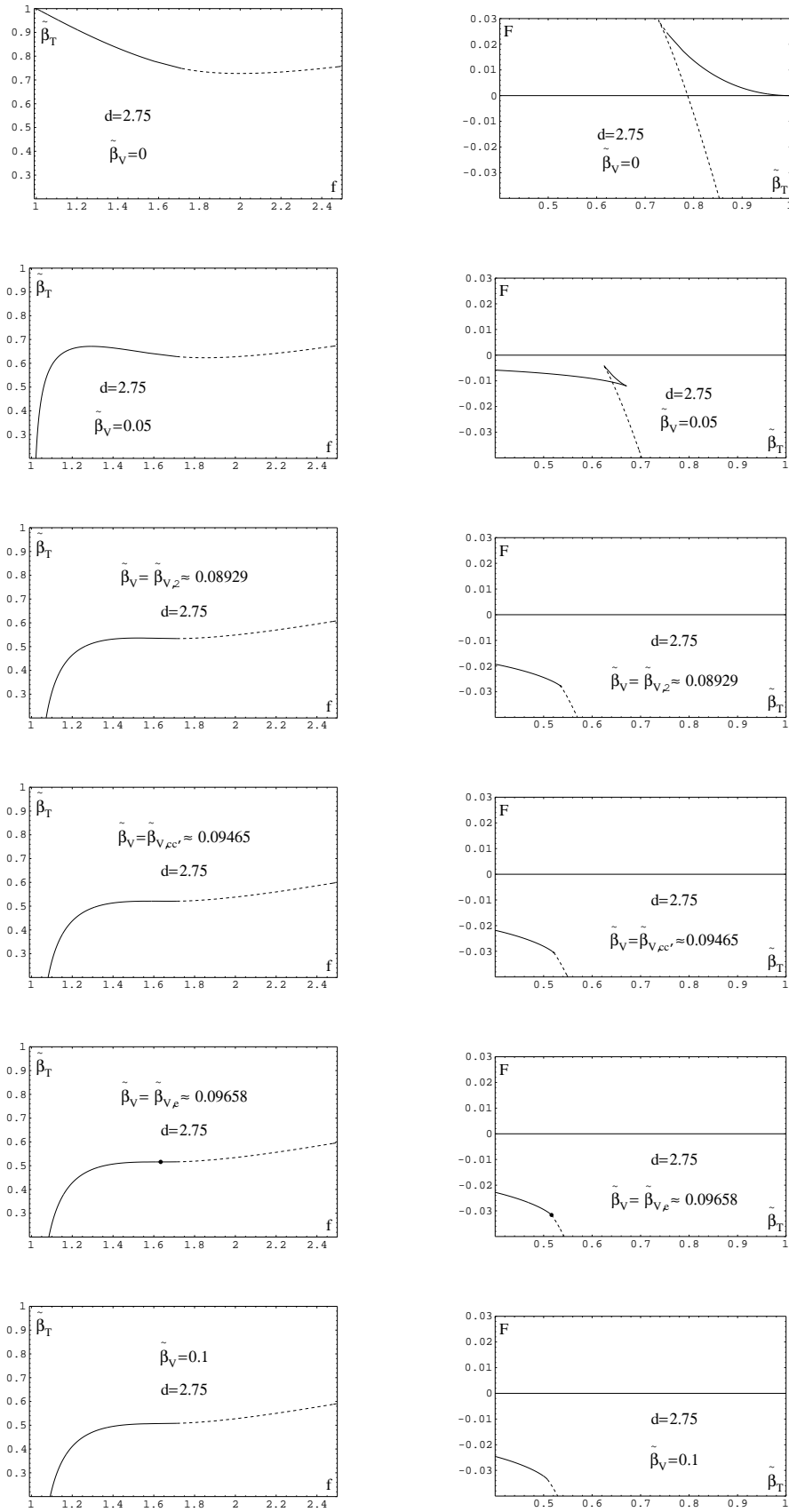


Figure 20: $\tilde{\beta}_T$ versus f , and \bar{F} versus $\tilde{\beta}_T$, for $d = 2.75$ at (a) $\tilde{\beta}_V = 0$, (b) $\tilde{\beta}_V = 0.05$, (c) $\tilde{\beta}_V = \tilde{\beta}_{V,2} \approx 0.0892914$ (d) $\tilde{\beta}_V = \tilde{\beta}_{V,cc'} \approx 0.0946534$, (e) $\tilde{\beta}_V = \tilde{\beta}_{V,e} \approx 0.0965845$ (note that $\tilde{\beta}_{T,e} \approx 0.5158930$ and $\gamma_e \approx 0.363383$), (f) $\tilde{\beta}_V = 0.1$.

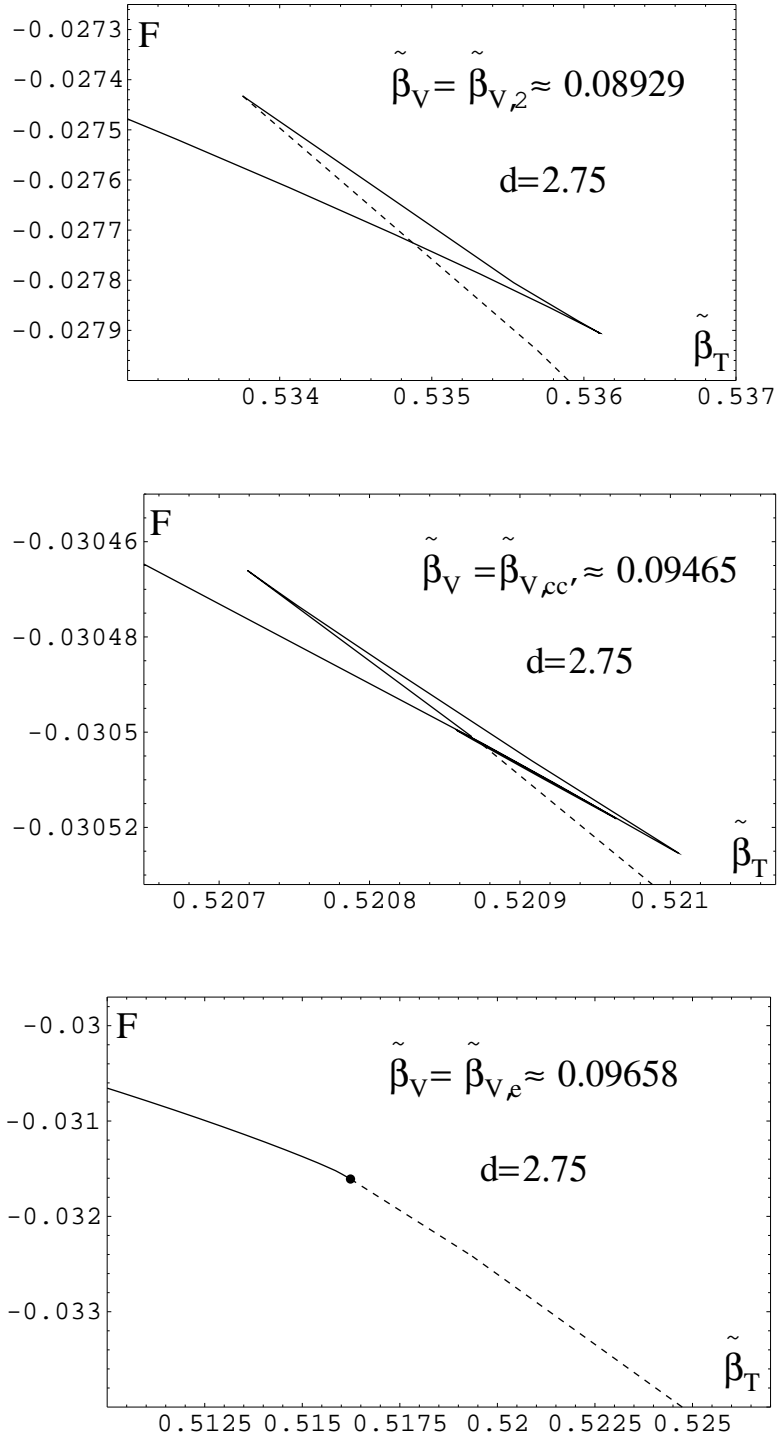


Figure 21: Blow-ups of the parametric plots for $d = 2.75$. (a) At $\tilde{\beta}_V = \tilde{\beta}_{V,2} \approx 0.08929$, points c' and 2 coincide. (b) At $\tilde{\beta}_V = \tilde{\beta}_{V,cc'} \approx 0.09465$, points c' and c coincide. (c) At $\tilde{\beta}_V = \tilde{\beta}_{V,e} \approx 0.09658$, the “triangle” disappears; this occurs within the normal phase.

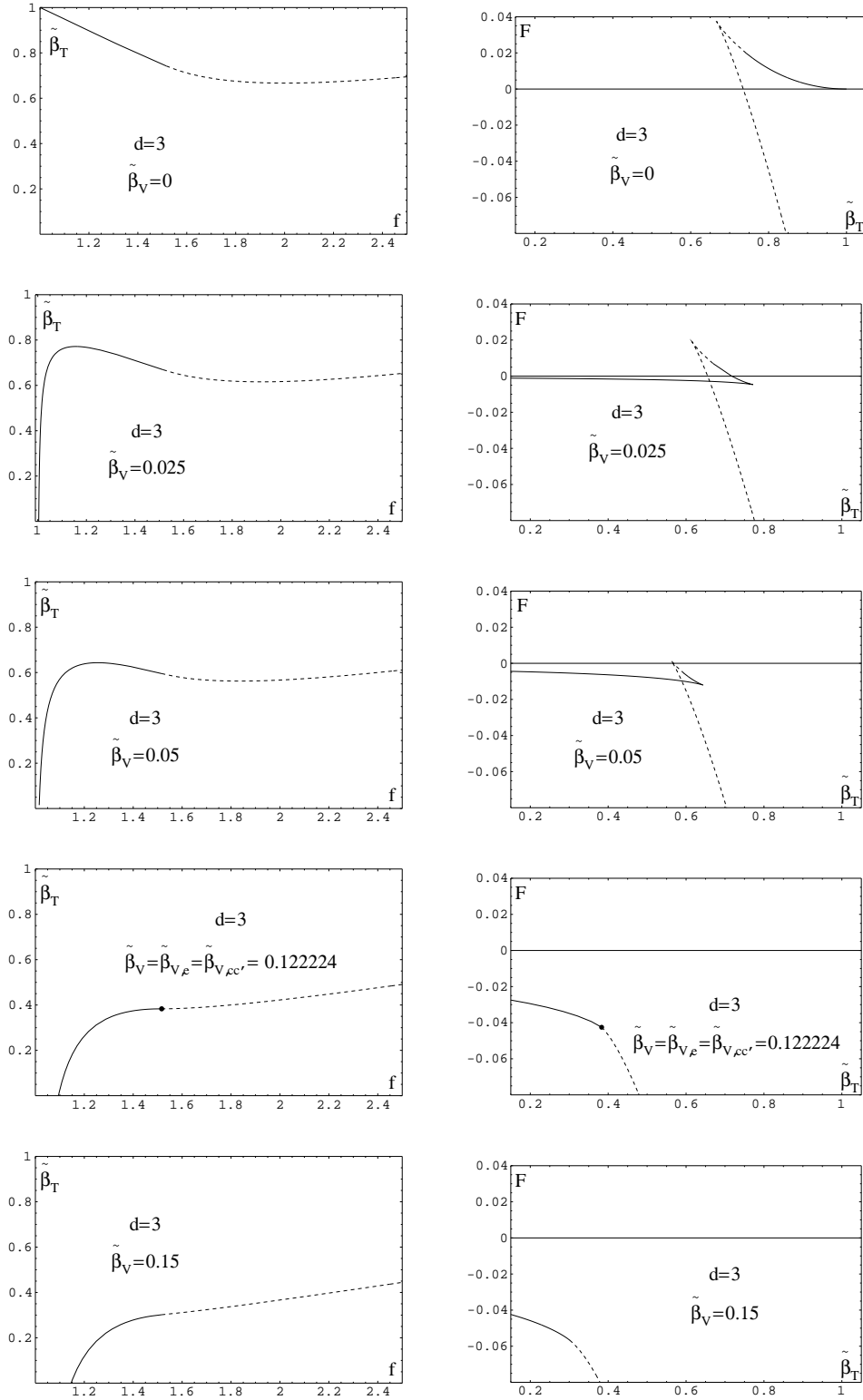


Figure 22: $\tilde{\beta}_T$ versus f , and $\bar{\mathcal{F}}$ versus $\tilde{\beta}_T$, for $d = 3$ at (a) $\tilde{\beta}_V = 0$, (b) $\tilde{\beta}_V = 0.025$, (c) $\tilde{\beta}_V = 0.05$, (d) $\tilde{\beta}_V = \tilde{\beta}_{V,2} = \tilde{\beta}_{V,cc'} = \tilde{\beta}_{V,e} \approx 0.122224$, (e) $\tilde{\beta}_V = 0.15$.

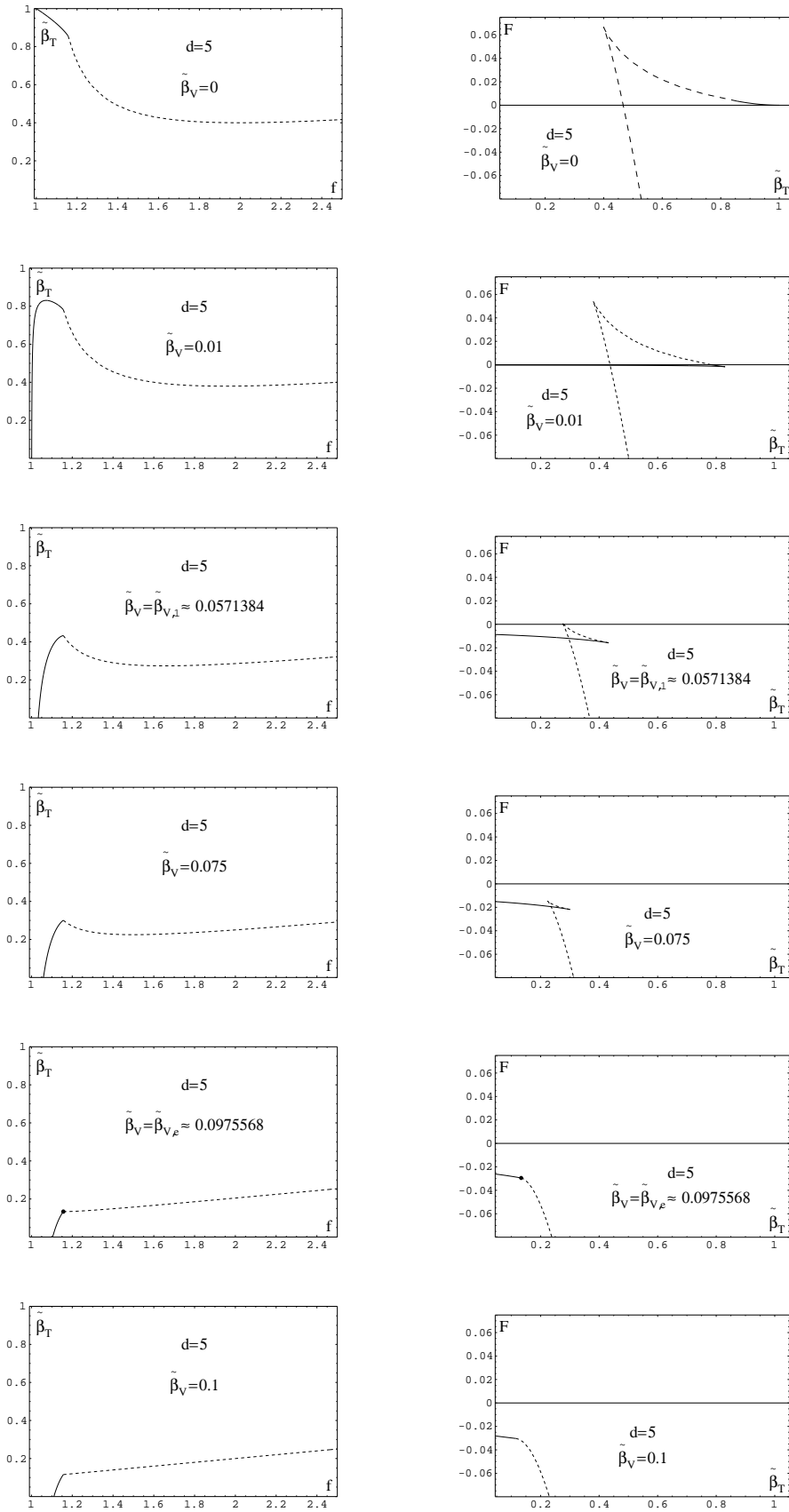


Figure 23: $\tilde{\beta}_T$ versus f , and \tilde{F} versus $\tilde{\beta}_T$, for $d = 5$ at (a) $\tilde{\beta}_V = 0$, (b) $\tilde{\beta}_V = 0.01$, (c) $\tilde{\beta}_V = \tilde{\beta}_{V,1} \approx 0.0571384$, (d) $\tilde{\beta}_V = 0.075$, (e) $\tilde{\beta}_V = \tilde{\beta}_{V,2} = \tilde{\beta}_{V,cc'} = \tilde{\beta}_{V,e} \approx 0.0975568$, (f) $\tilde{\beta}_V = 0.1$.

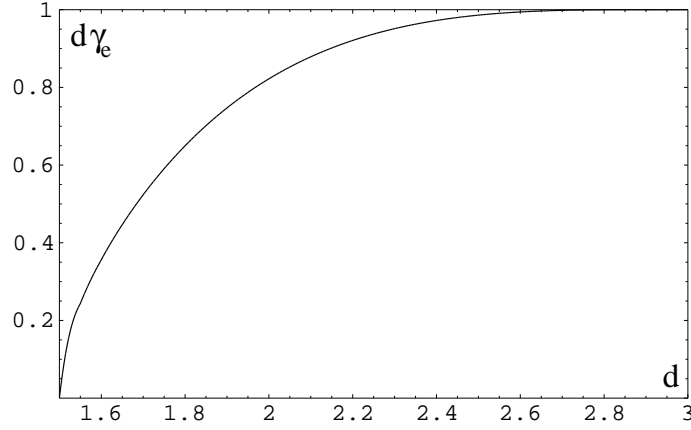


Figure 24: $d\gamma_e$ plotted versus d for $3/2 \leq d \leq d_{**} = 3$.

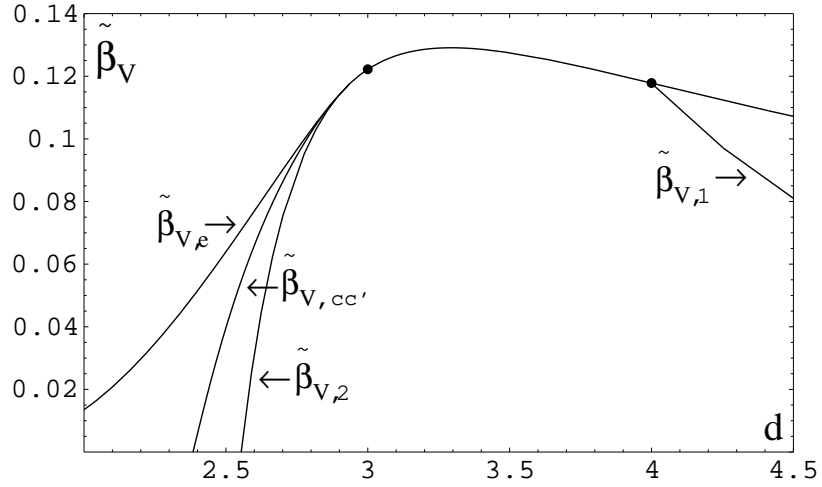


Figure 25: $\tilde{\beta}_{V,e}$, $\tilde{\beta}_{V,cc'}$, $\tilde{\beta}_{V,2}$ and $\tilde{\beta}_{V,1}$ as functions of dimension d . The curve $\tilde{\beta}_{V,e}$ smoothly reaches 0 at $d = 3/2$; the curve $\tilde{\beta}_{V,cc'}$ hits 0 at $d = d_* \approx 2.38403$; the curve $\tilde{\beta}_{V,2} = f_*(2 - f_*)/(2d)$ hits 0 at $d = \bar{d} \approx 2.55391$; the curves $\tilde{\beta}_{V,e}$, $\tilde{\beta}_{V,cc'}$ and $\tilde{\beta}_{V,2}$ all merge at $d = d_{**} = 3$; the curve $\tilde{\beta}_{V,1}$ branches off the $\tilde{\beta}_{V,e} = \tilde{\beta}_{V,cc'} = \tilde{\beta}_{V,2}$ curve at $d = 4$, and then approaches zero as $d \rightarrow \infty$.

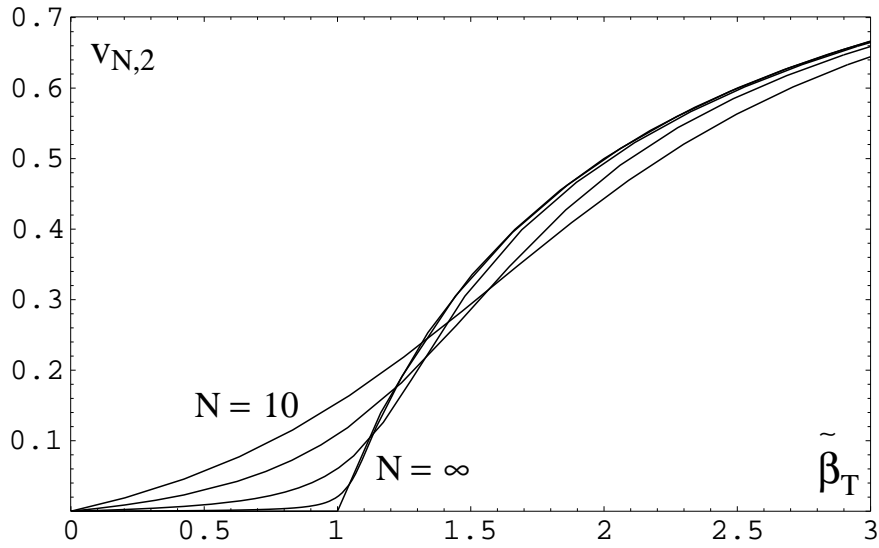
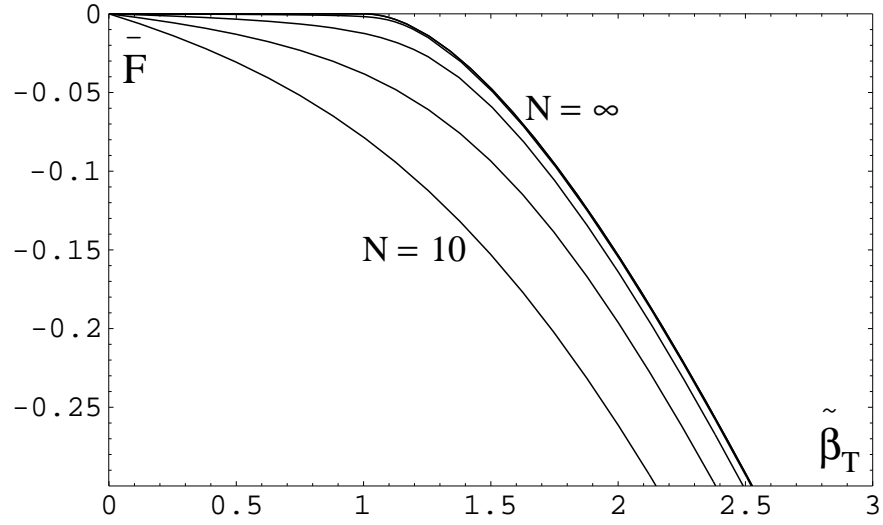


Figure 26: Approach to the $N = \infty$ limit in the one-dimensional RP^{N-1} model: curves shown are $N = 10, 25, 100, 1000, \infty$. (a) Free energy $\bar{F}(\tilde{\beta}) = -(1/N) \log \mathcal{Z}_N(N\tilde{\beta})$. (b) Correlation decay rate $v_{N,2} = e^{-m_T}$ where m_T is the isotensor mass gap.

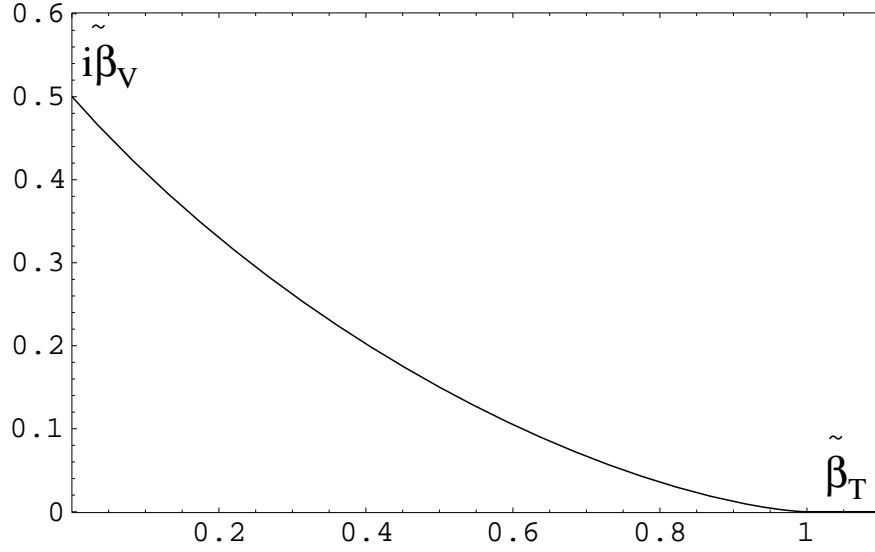


Figure 27: Magnitude of the first imaginary zero of $\mathcal{Z}_N(N\tilde{\beta}_V, N\tilde{\beta}_T)$ in the limit $N \rightarrow \infty$, as a function of $\tilde{\beta}_T$.

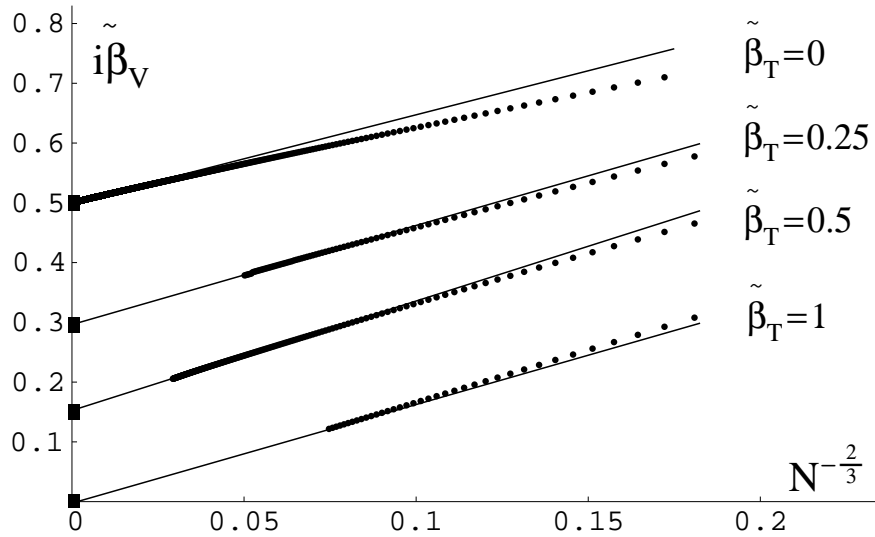


Figure 28: Magnitude of the first imaginary zero of $\mathcal{Z}_N(N\tilde{\beta}_V, N\tilde{\beta}_T)$ plotted versus $N^{-2/3}$, for $\tilde{\beta}_T = 0, 1/4, 1/2, 1$. Solid box indicates the exact limiting value (7.22) for $N = \infty$. Slope of straight line is given by a best fit to the data for $N \gtrsim 50$, except for $\tilde{\beta}_T = 0$, when it is given by the exact asymptotic formula (see footnote 29).

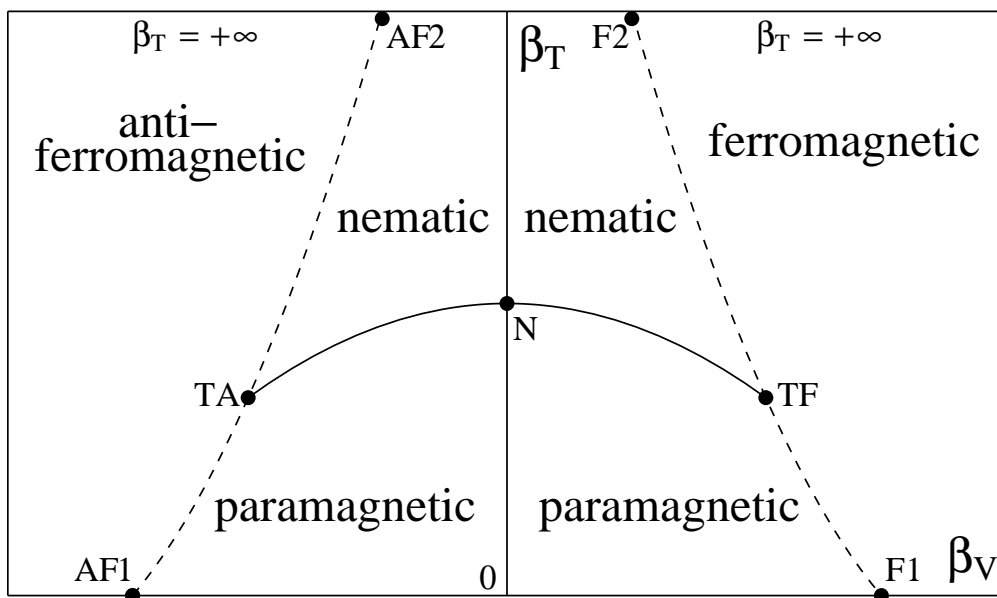


Figure 29: Conjectured phase diagram in the (β_V, β_T) -plane for the mixed isovector/isotensor model with $2 < N < \infty$ in dimension $d > 2$. First-order transitions are shown as solid lines, and second-order transitions as dashed lines.

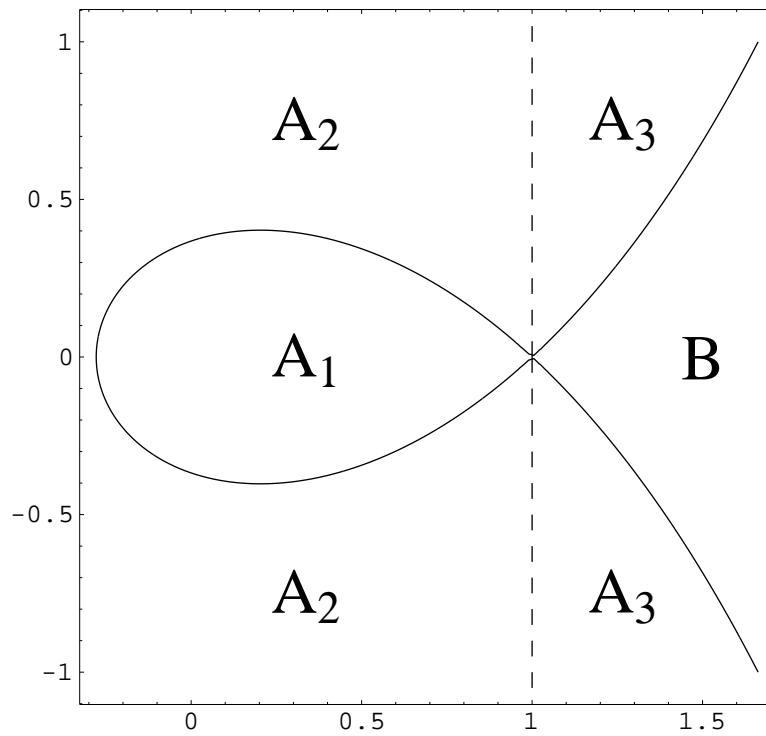


Figure 30: Szegő curve $x^2 + y^2 = e^{2(x-1)}$ in the complex $\xi = x + iy$ plane: we denote by \mathcal{S}_- (resp. \mathcal{S}_+) the part of this curve at $x < 1$ (resp. $x \geq 1$). The regions \mathcal{A}_1 , \mathcal{A}_2 , \mathcal{A}_3 and \mathcal{B} are indicated.

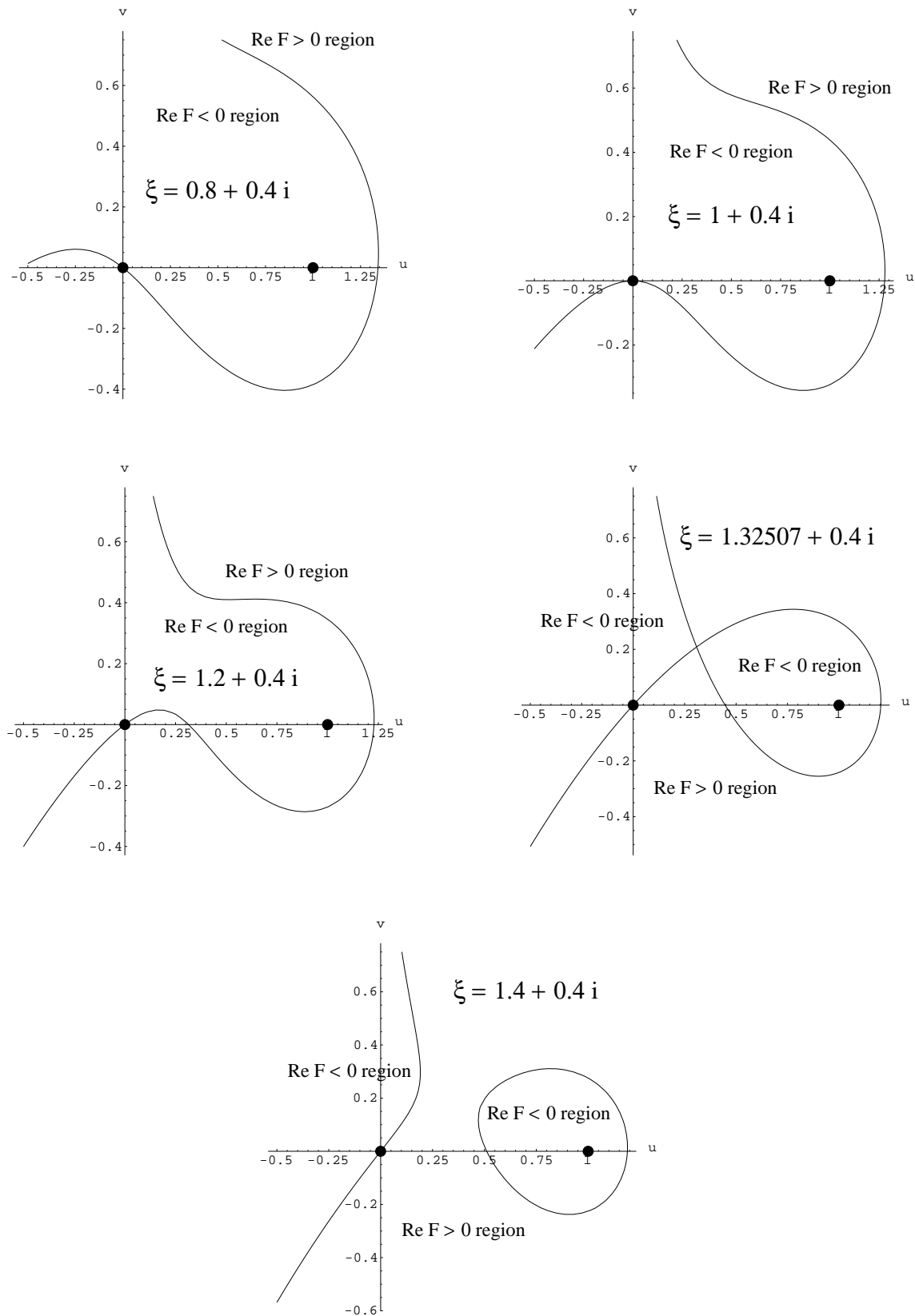


Figure 31: Curve $\text{Re } F(t) = 0$ in the complex $t = u + iv$ plane, for (a) $\xi \in \mathcal{A}_2$, (b) ξ on the boundary between \mathcal{A}_2 and \mathcal{A}_3 , (c) $\xi \in \mathcal{A}_3$, (d) $\xi \in \mathcal{S}_+$, (e) $\xi \in \mathcal{B}$. The points $t = 0$ and $t = 1$ can be connected by a path lying in the region $\text{Re } F < 0$ whenever $t \in \mathcal{A}$, but not otherwise.

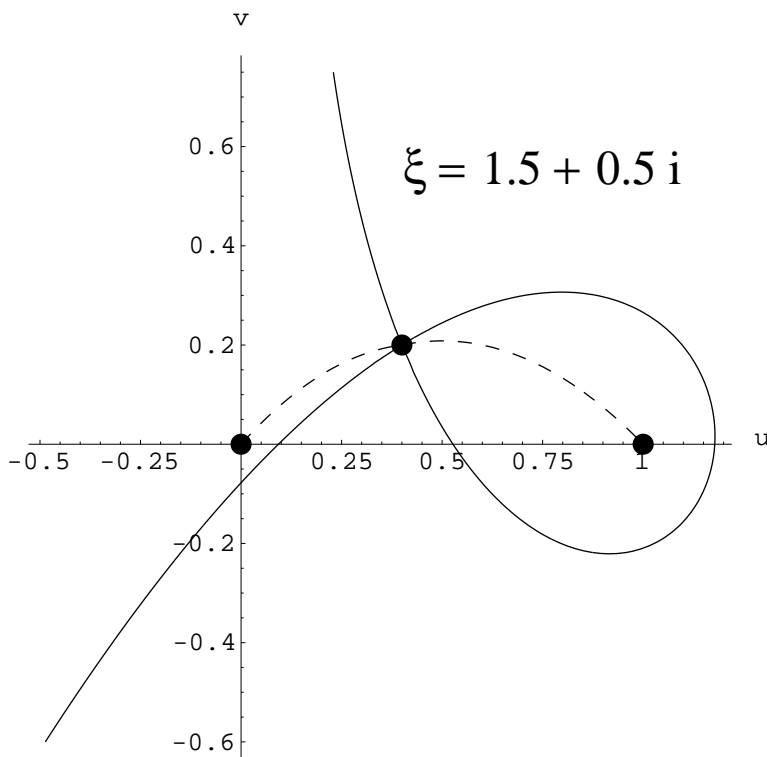


Figure 32: Curve $\text{Re} F(t) = \text{Re} F(t_*)$ in the complex $t = u + iv$ plane, for a point $\xi \in \mathcal{B}$. One possible path \mathcal{C} is shown in dashes: it runs from $t = 0$ to the saddle point t_* and thence to $t = 1$, staying entirely in the region $\text{Re} F(t) < \text{Re} F(t_*)$ except at $t = t_*$.

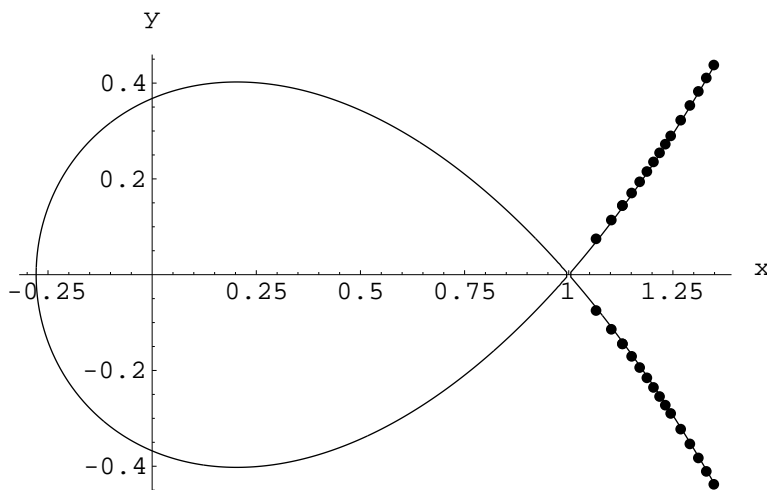


Figure 33: Szegő curve $x^2 + y^2 = e^{2(x-1)}$ together with some zeros of ${}_1F_1(a; b; b(x + iy))$ for $a = 1/2$, $b = 1000$. Note the accumulation of zeros densely on \mathcal{S}_+ .